

REPUBLIQUE ALGERIENNE DEMOCRATIQUE ET POPULAIRE  
MINISTERE DE L'ENSEIGNEMENT SUPERIEUR ET DE LA RECHERCHE  
SCIENTIFIQUE  
UNIVERSITE M'HAMED BOUGARA-BOUMERDES



Institut de Génie Electrique Electronique

## Thèse de Doctorat

Présentée par

**SMAILI Nessrine**

Filière : Génie électrique et Electrotechnique  
Option: Télécommunication

---

### Development of Pilot Symbols Contamination Mitigation Techniques in Massive MIMO/mmWave Systems

---

**Devant le jury :**

GUESSOUM	abderrezak	Prof	Univ.Blida	Président
DAHIMANE	Abdelhakim	Prof	IGEE/UMBB	Examineur
FERGANI	Lamia	MCA	USTHB/Alger	Examineur
AZRAR	Arab	Prof	IGEE/UMBB	Rapporteur
DJEDDOU	Mustapha	MCA	EMP/Alger	Co-Rapporteur

Année Universitaire : 2018/2019

*To the memory of my father.*

*To my mother.*

*To my husband and my son.*

*To my brothers and sisters.*

*To all my family.*

*To all my friends.*

*To any one who ever thought me any thing.*

*I dedicate this work.*

## *Acknowledgments*

My first acknowledgments are addressed to my supervisor, Dr. Djeddou Mustapha, who was also my master thesis advisor. I have no words to express how much I owe to him, both regarding my education and my master. He is not only an excellent researcher and teacher, he is one of the very few person I ever met that was able to make me feel comfortable in the work I have done until now, fully understanding my needs not only in the academic field.

Together with him, I would like to thank Prof. Azrar Arab, who was on my side during all of my three years as doctorate student, there is no way to count the enormous number of times he gave me his support and we fruitfully discussed about my work and my studies.

# Table of Contents

<b>Symbols and Notations</b>	<b>vii</b>
<b>Acronyms</b>	<b>ix</b>
<b>Table of Contents</b>	<b>xiii</b>
<b>List of figures</b>	<b>xiv</b>
<b>Abstract</b>	<b>1</b>
<b>General Introduction</b>	<b>2</b>
<b>I Generalities</b>	<b>6</b>
I.1 Introduction . . . . .	7
I.2 Evolution of mobile communication . . . . .	7
I.3 Why is there a need for 5G? . . . . .	11
I.4 Multiple access techniques for 5G . . . . .	12
I.5 The possible architecture of 5G systems . . . . .	13
I.5.1 Higher spectral efficiency . . . . .	14
I.5.1.1 Massive MIMO system . . . . .	14
I.5.1.2 Cooperation and coordination . . . . .	17
I.5.2 Higher cell density . . . . .	18
I.5.3 More spectrum . . . . .	19
I.5.3.1 MmWave cellular system . . . . .	20
I.5.4 5G: A concentration of new paradigms and innovative technologies .	24
I.6 Modulation technique for 5G . . . . .	25
I.7 Research challenges for 5G . . . . .	27

<b>II Residual self interference mitigation for FD Massive MIMO</b>	<b>29</b>
II.1 Introduction . . . . .	30
II.2 Full-duplex communications . . . . .	30
II.3 Multiuser MIMO communications . . . . .	32
II.4 Multiple access technique . . . . .	32
II.4.1 Orthogonal multiple access (OMA) techniques . . . . .	33
II.4.2 Non-Orthogonal multiple access (NOMA) technique . . . . .	33
II.4.3 Multiple access IDMA technique . . . . .	35
II.5 MIMO-OFDM-IDMA system model . . . . .	36
II.6 Residual self interference (RSI) suppression . . . . .	39
II.6.1 LS estimator . . . . .	39
II.6.2 SOBI estimator . . . . .	40
II.7 Simulation results . . . . .	42
<b>III Channel precoding in Massive MIMO System</b>	<b>46</b>
III.1 Introduction . . . . .	47
III.2 Precoding in Massive MIMO . . . . .	47
III.3 System Model: multi-cell downlink . . . . .	49
III.4 Proposed beamforming scheme . . . . .	52
III.4.1 Mathematics of oblique projection (OP) . . . . .	52
III.4.2 Application of oblique projection to our problem . . . . .	53
III.4.3 Oblique projection zero forcing beamformer . . . . .	54
III.4.4 Achievable rate . . . . .	56
III.5 Simulation results . . . . .	57
<b>IV Parameter Channel Estimation For Pilot Contamination Mitigation in Massive MIMO System</b>	<b>60</b>
IV.1 Introduction . . . . .	61
IV.2 Pilot contamination in Massive MIMO . . . . .	61
IV.2.1 Channel estimation and pilot contamination definition . . . . .	61
IV.2.2 Channel estimation without pilot contamination . . . . .	64
IV.2.2.1 System model . . . . .	64
IV.2.2.2 Parameters channel estimation . . . . .	65
IV.2.2.3 Cramer-rao bound derivation . . . . .	72

IV.2.3	Channel estimation with pilot contamination . . . . .	74
IV.2.3.1	System model . . . . .	74
IV.2.3.2	The geometric channel model . . . . .	75
IV.3	Proposed beamspace unitary (BU-ESPRIT) parameter channel estimation .	77
IV.4	Simulation results . . . . .	83
<b>V</b>	<b>Pilot contamination mitigation for mmWave Massive MIMO</b>	<b>87</b>
V.1	Introduction . . . . .	88
V.2	Channel estimation in mmwave . . . . .	88
V.3	Data model and pilot contamination problem for single path . . . . .	91
V.3.1	Proposed solution strategy . . . . .	93
V.3.1.1	Conventional array transmission . . . . .	95
V.3.1.2	Antenna subset transmission (AST) . . . . .	96
V.3.2	Signal to interference ratio derivation . . . . .	99
V.3.3	Simulation results . . . . .	101
	<b>CONCLUSION</b>	<b>105</b>
	<b>Bibliographie</b>	<b>111</b>

# Symbols and Notations

In this theses, we will denote matrices and vectors with bold face type, using capital letters for matrices and lower case letters for vectors. The notations  $(.)^T$  and  $(.)^H$  stand for the transpose and Hermitian transpose, respectively.

$(.)^T$	Transposition operator.
$(.)^*$	Complex conjugate.
$(.)^H$	Hermitian operation.
$(.)^\dagger$	The pseudo-inverse operation.
$Tr(.)$	Trace operation.
$vec(\mathbf{A})$	Vector column obtained by stacking columns of the matrix $\mathbf{A}$
$\mathbf{A} \circ \mathbf{B}$	Khatri-Rao product, Kronecker product by column of $\mathbf{A}$ and $\mathbf{B}$ . For the matrix $\mathbf{A}$ $N \times M$ and the matrix $\mathbf{B}$ $N \times M$ , it is defined by the matrix $NK \times M$ $\mathbf{A} \circ \mathbf{B} = [\mathbf{a}_1 \otimes \mathbf{b}_1 \cdots \mathbf{a}_N \otimes \mathbf{b}_N]$ Where $\mathbf{a}_k$ is here $k^{ème}$ column of $\mathbf{A}$ .
$\mathbf{A} \odot \mathbf{B}$	Hadamard product, multiplication element by element.
$\mathbf{A} \otimes \mathbf{B}$	Kronecker product of matrix $\mathbf{A}$ $N \times M$ and the matrix $\mathbf{B}$ $K \times L$ defined by the matrix $NK \times ML$ $\mathbf{A} \otimes \mathbf{B} = \begin{bmatrix} a_{11}\mathbf{B} & \cdots & a_{1M}\mathbf{B} \\ \vdots & \ddots & \vdots \\ a_{N1}\mathbf{B} & \cdots & a_{NM}\mathbf{B} \end{bmatrix}.$
$\hat{\theta}$	Estimated parameter $\theta$ .
$\mathbf{I}_m$	Identity matrix $m \times m$ . The index $m$ is often omitted.
$diag(\mathbf{A})$	Vector column containing the diagonal elements of the matrix $\mathbf{A}$ .
$diag(a_1, \dots, a_K)$	Diagonal matrix $K \times K$ whose diagonal elements are $a_1$ to $a_k$ .
$\ \mathbf{A}\ _F$	The Frobenius norm of matrix, defined by $\ \mathbf{A}\ _F^2 = Tr(\mathbf{A}\mathbf{A}^H)$ .

$[\mathbf{A}]_{ij}$ ou $a_{ij}$	The $(i, j)^{th}$ element of the matrix $\mathbf{A}$ .
$\arg \min_x f(x)$	L'argument manimisant la fonction $f(x)$ par rapport à $x$ .
$\mathbf{E}[\cdot]$	Mathematical expectation of a random variable..
$\mathbf{Re}[\cdot]$	The real matrix part.
$\mathbf{Im}[\cdot]$	The imaginary matrix part.



# Acronyms

2D-UESPRIT	2 Dimension Unitary Estimation of Signal Parameters via Rotational Invariance Techniques
3GPP	3rd Generation Partnership Project
3GPPSCM	3rd Generation Partnership Project Spatial Channel Model
3GPP2	3rd Generation Partnership Project 2
5G	Fifth generation
ABF	Analog Beamforming
ADC	Analog to Digital Converter
AOA	Angle of Arrival
AOD	Angle of Departure
BS	Base Station
BU-ESPRIT	Beamspace Unitary Estimation of Signal Parameters via Rotational Invariance Techniques
BER	Bit Error Rate
CRB	Cramer Rao Bound
CDMA	Code Division Multiple Access
CDMA 2000	Code Division Multiple Access 2000
CSI	channel state information
DAC	Digital to Analog Converter
DBF	Digital Beamforming
DFT	Discrete Fourier Transform
D2D	Device to Device
EDGE	Enhanced Data Rate for GSM Evolution
ETSI	European Telecommunications Standards Institute
ESPRIT	Estimation of Signal Parameters via Rotational Invariance Techniques
FBA	Forward Backward Averaging

FBMC	Filter Bank Multi Carrier
FDD	Frequency Division Duplexing
FD-MIMO	Full duplex MIMO
FFT	Fast Fourier Transform
UFMC	Universal Filtred Multi Carrier
F-OFDM	Filtred Orthogonal Frequency Division Multiplexing
GFDM	Generalised Frequency Division Multiplexing
GSM	Global System for Mobile Communication
GPRS	General Packet Radio Service
HSDPA	High Speed Downlink Packet Access
HSUPA	High Speed Uplink Packet Access
HSPA	High Speed Packet Access
i.i.d.	independent and identically distributed
IEEE	Institute of Electrical and Electronics Engineers
ISI	Inter Symbol Interference
IFFT	Inverse Fast Fourier Transform
IMT-2000	International Mobile Telecommunications for the year 2000
IoT	internet of things
IS-95	Interim Standard 95
ITU	International Telecommunication Union
IMT-Advenced	International Mobile Telecommunication Advanced
LNA	Low Noise Amplifier
LOS	Line Of Sight
MU-MIMO	Multi User Multiple Input and Multiple Output
MIMO	Multiple Input and Multiple Output
MS	Mobile Station
MMS	Multimedia Messaging Service
M2M	Machine to Machine
MRC	maximum ration combining
MRT	maximum ratio transmission
MSE	MeaN Square Error
MMSE	minimum mean-squared error
MSS	Mobile Satellite Service

NLOS	Non Line Of Sight
NIST	National Institute of Standards and Technology
NYU WIRELESS	New York University WIRELESS
OFDM	Orthogonal Frequency Division Multiplexing
PAPR	Peak to Average Power Ratio
PDP	Power Delay Profile
PSK	Phase Shift Keying
QPSK	Quadrature Phase Shift Keying
RF	Radio Frequency
SINR	signal-to-interference-plus-noise ratio
SIR	signal-to-interference ratio
SISO	single-input single-output
SMS	Short Message Service
SVD	Singular Value Decomposition
SNR	Signal to Noise Ratio
SDMA	Space Division Multiple Access
SU-MIMO	single-user MIMO
TDD	Time Division Duplexing
TD-SCDMA	Time Division Synchronous Code Division Multiple Access
TTI	Transmission Time Interval
TX	transmitter
UHD	Ultra High Denition
ULA	Uniform linear array
UMTS	Universal Mobile Telecommunications System
ùVGA	Variable Gain Amplifier
WCDMA	Wideband Code Division Multiple Access
WiGig	Wireless Gigabit
ZF	Zero Forcing

# List of Figures

I.1	Evolution of mobile technologies. . . . .	7
I.2	Evolution of communication mobile . . . . .	10
I.3	Data rate comparison of the fifth generation with the third and fourth generations. . . . .	12
I.4	TDD vs FDD modes. . . . .	12
I.5	TDD transmission protocol. . . . .	13
I.6	Options for improving the system capacity. . . . .	14
I.7	Massive MIMO. . . . .	15
I.8	Coordinated transmission from multiple base stations. . . . .	17
I.9	Cooperation types. . . . .	18
I.10	Network composed of a macro cell and several small cell. . . . .	19
I.11	Massive MIMO vs mmWave system . . . . .	21
I.12	The possible architecture of mmwave systems. . . . .	21
I.13	Analogue and digital beamforming. . . . .	23
I.14	Blok diagram of hybrid beamforming applied in mmwave system. . . . .	23
I.15	GFDM implementation . . . . .	26
II.1	FD scenarios . . . . .	31
II.2	HD MU-MIMO system model. . . . .	32
II.3	The milestones of multiple access technologies. . . . .	35
II.4	A IDMA-OFDM FD Massive MIMO system model. . . . .	36
II.5	OFDM-IDMA system structure of the transmitter/receiver. . . . .	37
II.6	A IDMA-OFDM FD Massive MIMO system model. . . . .	37
II.7	Architecture of the separator block . . . . .	41
II.8	Flowchart of second order blind identification (SOBI) . . . . .	41
II.9	The BER comparison performance for different schemes. . . . .	43

II.10	The BER comparison performance for different antenna configuration. . .	44
II.11	Impact of the SIR on the BER performance of FD-MU-MIMO-IDMA . . .	45
III.1	Downlink scheme: base station with $N_t$ antenna communicating with $P$ users . . . . .	50
III.2	Oblique subspace projection geometry . . . . .	53
III.3	Average sum rate with $N = 50$ transmit antennas in the presence of $K = 20$ and $K = 30$ users as a function of the average SNR . . . . .	58
III.4	Average sum rates for different transmit antenna configurations and $K =$ $20$ users as a function of the average SNR . . . . .	58
IV.1	Illustration of massive MIMO system with pilot contamination problem in multi-cells. . . . .	63
IV.2	MSE of estimated angles . . . . .	84
IV.3	MSE of estimated path losses . . . . .	84
IV.4	MSE of estimated angles for BU-ESPRIT . . . . .	85
IV.5	MSE of estimated path losses for BU-ESPRIT . . . . .	85
IV.6	BER performance under different BS-MS distance . . . . .	86
V.1	Pilot contamination problem illustration. . . . .	91
V.2	Antenna selection pattern for a uniform linear array: black antennas co- herently co-phased to combine at BS, black and red antennas co-phased to destructively combine at BS. . . . .	94
V.3	Successive antenna beam patterns using randomization (a and b) and conventional radiation (c) . . . . .	95
V.4	Ratio $Fa$ versus $M_{sub}$ , $M_t = 100$ and $\theta_i = 22^\circ$ . . . . .	100
V.5	Signal to interference ratio (SIR) versus $M_t$ and $M_{sub}$ . $\theta_i = 70^\circ$ and $\theta_j = 160^\circ$	101
V.6	Spectral efficiency (SE) comparison with $M_t = 64$ . . . . .	103
V.7	Spectral efficiency (SE) comparison with $M_t = 128$ . . . . .	104
V.8	Spectral efficiency (SE) comparison with $M_t = 256$ . . . . .	104
V.9	Spectral efficiency (SE) for different values of $M_{sub}$ with a fixed ratio $M_t/M_{sub} = 4$ . . . . .	105
V.10	Spectral efficiency (SE) for different values of $M_{sub}$ with a fixed value $M_t$ .	105

# List of Tables

II.1	Simulation parameters. . . . .	43
III.1	Simulation parameters for massive MIMO system . . . . .	57

## Abstract

Millimeter waves and Massive MIMO are considered an enabling keys for future 5G cellular systems. Our work is subjected towards the two problems in such systems, that are Interference signal and pilot contamination (PC). We propose to incorporate oblique projection (OP) with conventional ZF beamforming in the downlink of a massive MIMO communication system. Resulting beamformer uses OP spaces to separate the received signal into two subspaces: the one pertaining to the desired user signal and the other to interference signals, thus achieving a high degree of interference suppression. For the PC problem, we propose a scheme based on beamspace unitary ESPRIT (BU-ESPRIT) algorithm for the parameter channel estimation to combat the PC in massive MIMO system, and the incorporation of AST in mmwave massive MIMO system to cancel out the interfering signals.

**Key words:** 5G, Massive MIMO, mmwave, PC, BU-ESPRIT, AST

## Résumé:

Les ondes millimétriques et Massive MIMO sont considérées comme un élément clé dans les futurs systèmes cellulaires 5G. Notre travail est soumis aux deux problèmes de tels systèmes, d'interférence de signal et la contamination des pilotes (PC). Nous proposons d'incorporer la projection oblique (OP) avec la formation de faisceau ZF classique dans la liaison descendante d'un système de communication MIMO massif. Le beamformer résultant utilise des espaces OP pour séparer le signal reçu en deux sous-espaces : l'un se rapportant au signal utilisateur souhaité et l'autre aux signaux de brouillage, permettant ainsi d'obtenir un degré élevé de suppression des interférences. Pour le problème de PC, nous proposons un schéma basé sur l'algorithme ESPRIT (BU-ESPRIT) unitaire d'espace-faisceau pour l'estimation de canal paramétrique pour lutter contre le PC dans un système MIMO massif, aussi nous proposons d'incorporer antenna subset transmission (AST) dans un système MIMO massif à ondes millimétriques pour annuler les signaux brouilleurs.

**Key words:** 5G, Massive MIMO, mmwave, PC, BU-ESPRIT, AST.

## ملخص

تعتبر لموجات الملمترية و MIMO الضخمة بمثابة مفاتيح تمكين للأنظمة الخلوية المستقبلية الجيل الخامس (5G). يخضع عملنا تجاه مشكلتين في هذه الأنظمة، وهما التداخل إشارة والتلوث التجريبي. نقترح دمج الإسقاط المائل مع حزمة ZF التقليدية في الوصلة الهابطة لنظام اتصالات MIMO الهائل. يستخدم منظم الشعاع الناتج مسافات الإسقاط المائل لفصل الإشارة المستقبلية في فضاءين فرعيين: الإشارة المتعلقة بإشارة المستخدم المرغوبة والأخرى لإشارات التداخل، وبالتالي تحقيق درجة عالية من قمع التداخل. بالنسبة لمشكلة التداخل إشارات، نقترح مخططاً يستند إلى خوارزمية (BU-ESPRIT) أحادية الحزمة لتقدير قناة المعلمة لمحاربة التداخل إشارة في نظام MIMO الضخم، ودمج مجموعة انتقال الهوائي في هذا النظام ذو الموجات الملمترية لإلغاء إشارات التداخل.

**كلمات مفتاحية:** الجيل الخامس، الموجات الملمترية، MIMO الضخمة، التداخل إشارة، الإسقاط المائل، BU-ESPRIT

# INTRODUCTION



## Introduction

Wireless communication refers to the transmission of signals across a wireless medium. Unlike wired communications, wireless has to deal with environmental challenges such as fading and noise, with the addition of bandwidth and transmit power constraints. The fifth generation completes wireless communication with almost no limitation. Its goals include improving spectral efficiency and services, lowering cost and making uses of new spectrum. To meet these needs, many approaches are active research areas. Among these techniques, we cite millimeter wave, small cell densification, and massive MIMO paradigm. While the first approach pushes towards getting more spectrum by working in the non-exploited millimeter bands, the second one relies on network densification by integrating small to femtocells thus deploying more infrastructure to get more active users per area. The third approach involves the incorporation of a considerable number of antennas at the transmit and receive sides with the associated signal processing. In recent years, the variety of current and future wireless applications demand high data rates, larger network capacity, better energy efficiency, higher spectral efficiency and more mobility. These exigences are even more important for the wireless communication beyond 4G (B4G) and 5G. A promising technologies such as, full duplex, non orthogonal division multiple access (NOMA), and orthogonal frequency division multiple access (OFDM), have been strongly recommended for such purpose for future wireless systems. While the idea behind the first technology, is based on the idea of using the full-duplex communication that allows simultaneous transmission and reception of data in the same frequency band and thus increasing the system spectral efficiency up to two times [1] compared to the half duplex (HD) transmission scheme. Indeed, the promised gains by FD technology is harmed by the self-interference (SI) problem caused by the base station itself. The third technology named NOMA, has recently been recognized as a key multiple access technique due to its higher spectrum efficiency than traditional orthogonal multiple access (OMA) [2]. Where the allocation of users with various power levels depending on their channel conditions, known as power domain. However, when various users are allocated with different codes, and are then incorporated into the same time-frequency resources, it is named code domain. Interleave-division multiple access (IDMA) can be considered as NOMA scheme with code domain multiplexing. The last technology named OFDM, is adopted on physical layer modulation scheme, which has proven to be very efficient for the wireless communication system.

Designing channel estimation (CE) based on pilot sequence with exploiting the sparsity of the channel is an important issue for mmWave Massive MIMO. Prior work has focused on hybrid beamforming design for multiuser channels and does not tackle the inter-cell interference problem. However, inter-cell interference in mmWave systems may be less severe due to signal blockage by urban objects. Furthermore, as next-generation networks are expected to have ultra-dense small cells, the dramatic shortening of inter-cell distances will reduce the blockage density in channels, resulting in sparse or even line-of-sight (LoS) interference channels. Hence, this problem becomes more critical in the presence of pilot contamination (PC). It is shown that channel estimation in massive MIMO multi-cell system hampered by the pilot contamination effect, constitutes a major bottleneck for overall performance [3]. This problem is a famous challenging issue that channel estimation suffer from. PC is defined by re-using the same band of frequencies with different factors among the cells. Moreover, the same orthogonal pilot sequences are re-used possibly and multiplied by an orthogonal transformation among the cells. Hence, the base station coherently combines signals from terminals in other cells. Recently, pilot contamination issue has attracted a great attention from the research community. In this thesis, we address various problem named pilot contamination for channel estimation in mmwave massive MIMO, residual self interference for full duplex system and interference mitigation in massive MIMO system.

Our work is subjected towards the problem of parameter estimation of channel transmission of millimeter waves and massive MIMO systems that can be used in future fifth generation system. We are interested in the study of possible techniques for estimation of the millimeter band channel with and without inter-cell interference during the estimation phase (pilot contamination).

This thesis report is subdivided into fifth organized chapters in the following way:

- In the first chapter we give the fundamentals of wireless communications, spanning the different generations of mobile communications, modulation and multiple access techniques, the possible architecture and research challenges for 5G.
- In the second chapter we discuss the presence of self interference (SI) in full duplex (FD) created by the Base Station (BS), that severely hampers the performance of communication system, in addition to multiple access interference (MAI). Then we propose a new scheme based on NOMA-OFDM in Massive MIMO to tackle such impairments. Moreover, blind channel estimator is used to provide channel state

estimation.

- The third chapter is reserved to talk about the mitigation of interference, which is considered as an ubiquitous problem in wireless communication systems for which a number of signal processing techniques have been developed. This problem is made more critical in massive MIMO systems. We propose to incorporate oblique projection (OP) with conventional ZF beamforming in the downlink of a massive MIMO communication system and investigate the achievable data rate at the reception. Resulting beamformer uses oblique projection spaces to separate the received signal into two subspaces: the one pertaining to the desired user signal and the other to interference signals, thus achieving a high degree of interference suppression. Then, we finish with presenting simulation results.
- In the fourth chapter, we define the pilot contamination problem that appears in Multicell Massive MIMO systems then we discuss pilot contamination (PC) problem. Then, we propose a scheme based on beamspace unitary ESPRIT (BU-ESPRIT) algorithm for the parameter channel estimation to combat the pilot contamination in massive MIMO system. Finally, simulation results and their comments are given.
- In the last chapter, we address the problem of PC that beamforming can suffer due to the sidelobe signals [4]. The main contribution lies in the innovative systematic design of the analog beamformer precoder based on antenna subset transmission (AST) in mmWave massive MIMO cellular system. Herein, the main idea of incorporating the AST is to cancel out the interfering signals by randomization in contaminated direction and keeping intact the transmission via the main lobe. Finally, we comment our simulation results.
- Finally, a general conclusion that encompasses the main aspects addressed in this thesis.

# Chapter I

## **GENERALITIES**









## I.1 Introduction

Wireless communication has invaded nowadays all the fields and aspects of modern life. A lot of examples illustrate the growth in the use of these technologies, among them the introduction of the android operating system and the iPhone, the ebook readers such as the iPad, and the social networking using facebook. We observe that the demand for wireless data communication has developed significantly in these last years; leading to the new needs in terms of cellular data traffic with high data rates and increased level of security, which have become an essential part of everyday life.

In this chapter, we give brief introduction about the evolution of mobile communication. The specification of the 5G is given according to the various research initiatives on the subject. Afterward, multiple access techniques for 5G are presented. At the end of the chapter, we mention some challenges that represent possible research and development topics.

## I.2 Evolution of mobile communication

As we have moved from one wireless generation to the next, consumers and the economy have benefited from ever-increasing connection speeds and capabilities as seen in Fig. I.1. In this section, a brief overview of the history of wireless communication systems is presented.

1G	2G	3G	4G	5G
1981	1992	2001	2010	2020(?)
2 Kbps	64 Kbps	2 Mbps	100 Mbps	10 Gbps
Basic voice service using analog protocols	Designed primarily for voice using the digital standards (GSM/CDMA)	First mobile broadband utilizing IP protocols (WCDMA / CDMA2000)	True mobile broadband on a unified standard (LTE)	'Tactile Internet' with service-aware devices and fiber-like speeds
				?
				?
THE	NEED	FOR	THE	SPEED

*Figure I.1* — Evolution of mobile technologies.

### 1. **1G: First generation networks:**

The main technology of this first generation mobile system was encompassing FDMA/FDD protocols and analog FM. AMPS was the first U.S. cellular telephone system and was deployed in Chicago in 1983.

### 2. **2G: Second generation networks**

The difference between the first and second generations is the introduction of digital modulation techniques using either the combination TDMA/FDD or CDMA/FDD. The 2G systems introduced three popular TDMA standards and one popular CDMA standard in the market. These are as follows:

- **TDMA/FDD standards**

- GSM: GSM standard was the first digital mobile system utilizing the 900 MHz frequency band that is introduced by group special mobile (GSM) . In its early version, the initial GSM had a particular amount of resources such as 200 KHz radio channels, 8 full-rate or 16 half-rate TDMA channels per carrier, encryption of speech, low speed data services and support for SMS for which it gained quick popularity.
- IS-136 : Known also as north American digital cellular (NADC) system. The objective of using this system was mainly to increase the capacity over the earlier analog (AMPS) system by utilizing 3 full-rate TDMA users over each 30 KHz channel.
- PDC: This technology aimed at improving the spectrum utilization and was created as a counterpart of NADC system in Japan.

- **CDMA/FDD Standard IS-95** : The IS-95 standard, known as CDMA/One, uses 64 orthogonal coded users and code-words are transmitted simultaneously on each of the 1.25 MHz channels. This standard provides many services such as: short messaging service, slotted paging, over-the-air activation (meaning the mobile can be activated by the service provider without any third party intervention), enhanced mobile station identities etc.

### 3. **2.5G mobile networks:**

2.5G standard is developed to support modern internet applications thereby making 2G standards more advanced and compatible with the requirements of

increased data rates. The most used services in this standard are:

- Supporting higher data rate transmission for web browsing.
- Supporting e-mail traffic.
- Enabling location-based mobile service.

The main technologies were relying on 2.5G systems were: wireless application protocol (WAP), general packet radio service (GPRS), high speed circuit switched data (HSCSD), enhanced data rates for GSM evolution (EDGE),..etc.

#### 4. **3G: Third generation networks:**

3G networks were developed to obtain more data rates and high speed for internet and video access. Based on IMT-2000 proposal launched by international telecommunication union (ITU), a set of technical requirements were defined in 1997 [5], and can be summarized as:

- High data rates: 144 kbps in all environments and 2 Mbps in low-mobility and indoor environments,
- Symmetrical and asymmetrical data transmission,
- Circuit-switched and packet-switched-based services,
- Speech quality comparable to wire-line quality,
- Improved spectral efficiency,
- Several simultaneous services to end users for multimedia services,
- Global roaming,
- Open architecture for the rapid introduction of new services and technology.

Universal mobile telecommunications System (UMTS), based on WCDMA and operating at 2.1GHz [6], was defined by the third partnership project (3GPP) organization and it is considered as the most popular technology in third generation standard.

#### 5. **4G: Fourth generation networks:**

things (IoT) are amongst the drivers of this growth, as well as wearable and automotive connectivity. In response to that, 4G is a concept of inter-operability

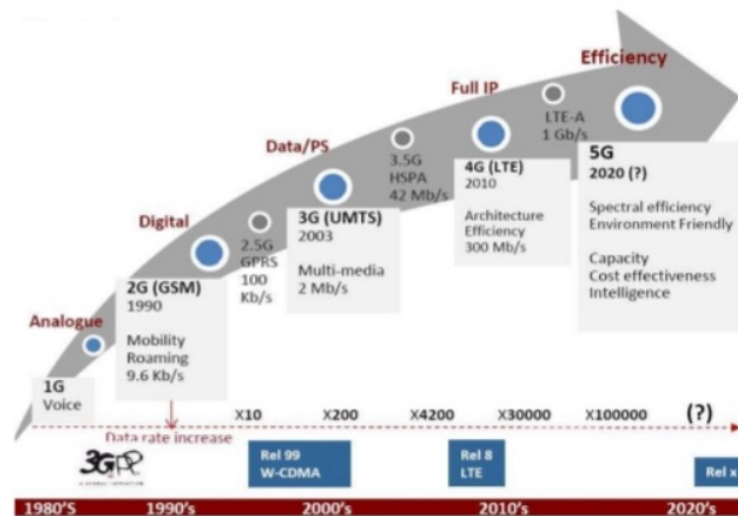


Figure I.2 — Evolution of communication mobile

between different sorts of networks, which is all about high speed data transfer such as 0-100MBPS of either the server or the data receiver set is moving at a speed of 60 Km/h. If the server and the receiver are stationary, the data transfer would be a minimum of 1GBPS.

4G is the next generation wireless networks that will replace 3G networks sometimes in future. In other context, 4G is simply an initiative by academic, to move beyond the limitations and problems of 3G which is having trouble getting deployed and meeting its promised performance and throughput.

These days in 3G we can access the internet through our mobile phone with the help of various technologies, like Wi-Fi, Wi-Max, GPRS, EDGE, WAP and Wi-Bro. But the problem is that if you are accessing the internet through your mobile phone within the help of any of these technologies and you move to place where inter-operability between different networks obtains, you are stuck. If you are using 4G, you can access the net through any of the aforesaid technologies even while moving from one place to another.

## 6. 5G: Five generation Networks:

Fifth generation standard is a promising enhancement that is not employed yet, but is intended to increase the throughput, by utilizing the limited and available spectrum bandwidth that will be from "3 to 300 GHz". Hence, there will be a big challenge for the design and the techniques which will be implemented to avoid to



deal with any issue in the future related to the limitation in data transmission traffic with respect to the user demands (Fig.I.1).

### I.3 Why is there a need for 5G?

Fifth generation standard is developed to ensure a very high transmitting data traffic and to remove some limitations encompassed in the generations mentioned above. The following are the requirements summarizing the major differences between expected 5G and other generations [7]:

- More possible interoperability and compatibility between the current global operators and their equipments.
- Improved and innovative data coding and modulation techniques, which include filter bank multi carrier methods within the schemes.
- Feasible use of millimeter wave frequencies.
- One common used platform to make 5G standard more practical for all sorts of radio access technologies.
- Better coverage with an increased throughput at cell edge. Multiple concurrent data transfer paths.
- Possible to 1Gbps and higher data rates in mobility.
- More robust; better cognitive radio/SDR Security.
- Higher system level spectral efficiency.
- World wide wireless web (WWWW), wireless-based web applications that include full multimedia capability beyond 4G speeds.
- More applications combined with artificial intelligent (AI) provided by artificial sensors.

As a baseline, fifth generation network systems will provide gigabit data rate services regardless of the user's location as shown in Fig.I.3

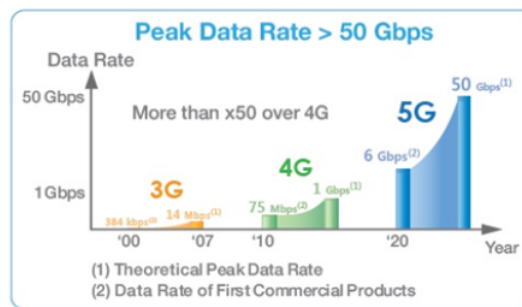


*Figure I.3* — Data rate comparison of the fifth generation with the third and fourth generations.

#### I.4 Multiple access techniques for 5G

In this section, we discuss briefly the various techniques available for duplexing. Traditionally, frequency division duplexing (FDD) or time division duplexing (TDD) are used in cellular networks (Fig.I.4).

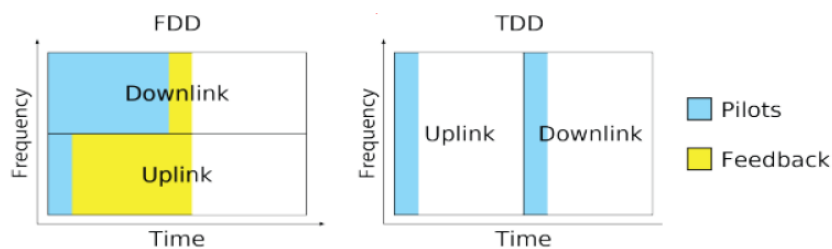


*Figure I.4* — TDD vs FDD modes.

Legacy macrocell networks are mostly deploying paired FDD spectrum. Code domain can also be utilized for duplexing. Therein, code division duplexing (CDD) is introduced as a smart codes based duplexing mechanism. CDD can be considered as a full-duplex scheme where the self-interference is mitigated through code set correlation properties optimization. The main advantages of TDD over FDD as [8]:

- Channel reciprocity.
- Dynamic traffic allocation/traffic asymmetry.
- Higher frequency diversity
- Unpaired band allocation
- Lower hardware cost.

For multi-user massive MIMO systems, the number of estimated channels by the BS is proportional to number of antennas. It is then more reasonable to carry out this operation at the level of BS where computing power is available. This is one of the reasons why a massive MIMO system is not currently viable only with a TDD access mode. In TDD massive MIMO systems, CSI estimates are obtained using channel reciprocity and Uplink (UL) training. TDD is considered as more suitable for massive MIMO operations since it implies that channel estimation needs to be performed in only one direction, and then can be used in both directions. The TDD protocol is illustrated in Fig.I.5. It is assumed that the channel is constant during the coherence interval ( $T$ ) which is  $T$  symbols. This advantage cannot be overlooked since it means that training overhead scales only with the number of users. Nevertheless, owing to the limited coherence interval, the training dimension is restricted and the same pilot sequences need to be reused which results in pilot contamination [9, 10].

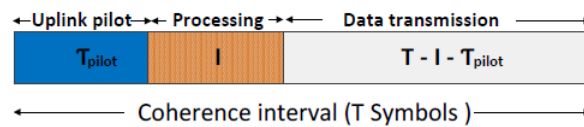


*Figure I.5* — TDD transmission protocol.

## I.5 The possible architecture of 5G systems

Cellular communication are undergoing resurgence of research interest with the development of the fifth generation (5G) cellular system; and the requirements for such systems are not yet totally agreed upon, but essentially industry and research communities want them to be a thousands times better in some dimensions than the old system in order to support the exponentially rising demand for physical layer throughput. To feed these needs, there are three approaches [11, 12, 13] as depicted in Fig.I.6. While the first approach pushes towards getting more spectrum by working in the not exploited millimeter bands [13, 14], the second one relies on network densification by integrating small to femto cells thus deploying more infrastructure to get more active users per area [15]. The third approach, on the other hand, involves the incorporation of a considerable number of antennas at the transmit and receive sides with the associated signal processing at the two sides.

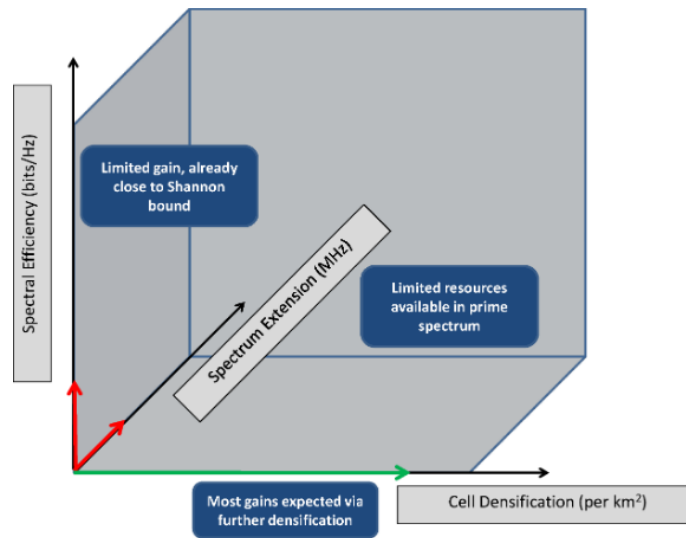


*Figure I.6* — Options for improving the system capacity.

### I.5.1 Higher spectral efficiency

The arguably largest and most active field of research in the question of improving throughput is concerned with improving spectral efficiency [16]. Cellular networks nowadays are first and foremost limited by intra cell, and especially, inter cell interference [17, 18]. This situation will also worsen, as modern cellular networks will need to serve a multitude of users, using the same time/frequency resources for increased spectrum efficiency.

#### I.5.1.1 Massive MIMO system

Massive MIMO takes its origin from point-to-point multiple-input multiple-output (MIMO) systems (Fig.I.7), which have then evolved into multi-user MIMO to give birth afterwards to the Massive MIMO architectures. Massive MIMO, originally introduced in [9, 19]. These later have been proposed as an ultimate solution for 5G wireless systems after research works have appraised and proven their great usefulness [20, 21, 22].

Massive MIMO systems hold other names within the research community such as argos [23], large scale MIMO [24]. Merging the benefits of adopting very large number of antennas at the base station (BS) and multi-user MIMO (MU-MIMO) technology, high degrees of freedom are offered which enable a large number of user devices to be simultaneously served at the same set of time-frequency resources. This is quite advantageous provided that the inter-user interference is efficiently reduced.

The main benefits of Massive MIMO systems can be summarized as follows:

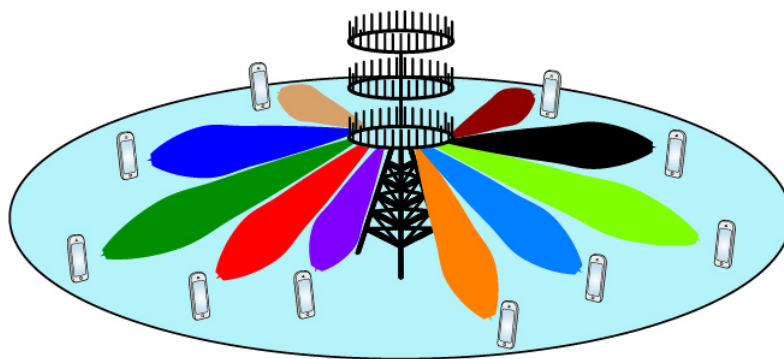


*Figure I.7* — Massive MIMO.

- **High spectral efficiency (SE) gain:**

Massive MIMO inherits the conventional MU-MIMO gains but on a massive scale, as its name specifies. As a matter of fact, with  $M$  BS antennas serving  $K$  single antenna users, a diversity of order  $M$  together with a multiplexing gain of  $\min(M, K)$  are achieved. These parameters can be tuned in order to further improve SE and achieve higher communication resilience.

- **High energy efficiency (EE) gain:**

In recent years networks energy efficiency has become one of the key factors due to environmental and economical effects. Whereas energy efficiency (EE) of wireless network has become the foremost figure of merit due to environmental, economical and operational concerns [25]. Energy efficiency has an important role in mobile communication on device side. Furthermore, increasing energy efficiency imposed a longer battery life. One of the main issues for the future mobile networks is to reduce power consumption. Most power consumption of cellular networks comes from base stations (BS) because they consume more than 60 % of the power. Therefore it is very important to reduce power consumption in BS.

- **Simple processing:**

Massive MIMO employs simple yet efficient signal processing schemes (linear precoding and decoding in the DL and UL, respectively). Indeed, the large number of BS antennas reduces the complexity of mitigating the impact of small scale fading and additive noise. In addition, when the number of antennas is sufficiently large, the resulting channel hardening further simplifies signal processing.

- **Increased robustness and reliability :**

The large number of BS antennas procures more diversity. This results in better link reliability and higher rate. In addition, as the number of antennas increases, additive noise, small scale fading, and intra- cell interference are bound to vanish.

- **Cost reduction in radio frequency (RF) power components:**

Massive MIMO employs coherent processing which allows to reduce the radiated power. This enables to use low cost radio frequency (RF) amplifiers in the milli-Watt range.

However, there always exists a compromise between achievable performance and complexity. The interesting gains of Massive MIMO come with their share of challenges [26]:

- **Pilot contamination:**

As the BS relies on the UL channel estimation for CSIT acquisition, in a multi-cell scenario, it is unavoidable to reuse the UL pilot from one cell to another, since the maximum number of orthogonal pilot sequences is upper-bounded by the duration of the coherence interval divided by the channel delay spread. Pilot reuse lead to the fact that the UL channel estimation for one UE is contaminated by UEs in other cells sharing the same UL pilot sequences. Pilot contamination constitutes an ultimate limit on performance when  $M$  becomes large. Pilot contamination is an important topic and will be the focus of this thesis and we propose pilot contamination mitigation schemes.

- **Fast and distributed coherent signal processing:**

With the increase of network capacity, the massive MIMO BS has to process a huge amount of data in real time. This is very challenging in system implementation . Designing signal processing algorithms with low complexity and the possibility to distribute the calculation to different modules in the system is another important question.

- **Channel reciprocity calibration:**To fully exploit the potential of the large number of antennas, BS needs to have accurate CSI. Massive MIMO relies on the channel reciprocity in TDD to acquire the DL CSI based on UL channel

estimation. However, as the transmit and receive hardware in transceivers are not symmetric, reciprocity calibration is essential for CSIT acquisition.

- **User scheduling:**

Massive MIMO is envisaged to handle a large number of connected devices. With the 5G requirements of high density connection, user scheduling is of paramount importance. In addition, when the same time-frequency resources are used.

There are many other challenges, such as designing the system against hardware impairments, characterizing massive MIMO channel, building up massive MIMO with low cost hardware, reducing the baseband processing power consumption, system operation with no or limited CSI, enabling massive MIMO in FDD, etc.

Research efforts in recent years have greatly pushed the frontier of the study of massive MIMO and many solutions were proposed to address these various challenges with different approaches.

### I.5.1.2 Cooperation and coordination

The official umbrella term for most cooperation (Fig.I.9) and coordination (Fig.I.8) techniques is coordinated multipoint transmission and reception (CoMP) [27]. The idea

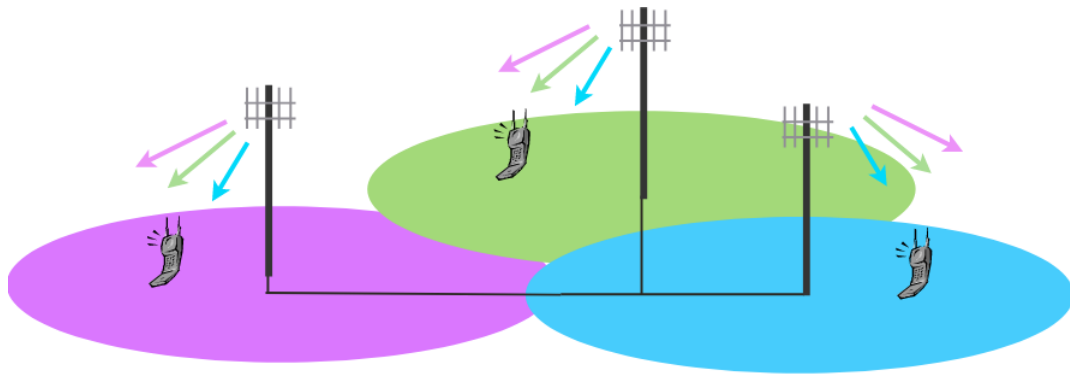


*Figure I.8* — Coordinated transmission from multiple base stations.

is to coordinate between all transmitters and receivers of all cells of a heterogeneous network as best as possible, with the (as of yet unattainable) goal of forming one big (network) MIMO system, that obeys the single user MIMO capacity scaling law [28, 29]. This cooperation can be done explicitly (for example by back-haul links) or implicitly (for example by sensing). In any case, CoMP can drastically reduce the inter cell interference and, to some extent, intra cell interference by serving certain users

employing out-of-cell antennas. Due to the large amount of possibilities for cooperation and coordination, one often introduces many sub-categories of CoMP: First, we recognize that distributed antenna systems (DAS) fall into the scope of CoMP, but only diffusely describes a system in which the antennas are spatially distributed and connected to each other. Coordinated scheduling (CS) avoids interference by each BS only scheduling users whose channels do (almost) not interfere with each other (inter and intra cell). Coordinated beamforming (CBF) [30] assumes that all BSs precode in such a

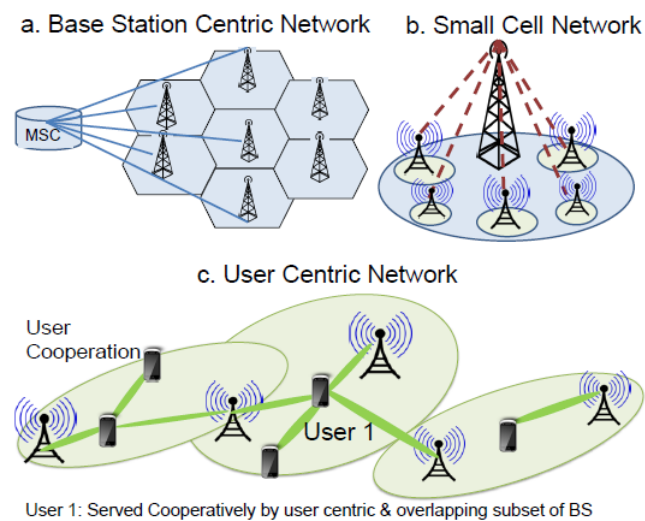


*Figure I.9* — Cooperation types.

way that the currently scheduled other cell users are not impeded. One truly cooperative scheme is transmission point selection (TPS) where all BS cooperatively only serve one user; the "best" one. The final scheme is joint transmission (JT) / network MIMO. This is the system described in the beginning, that tries to form one large single cell multi user MIMO system. It requires that all BS are directly connected to each other, are centrally controlled, and transmit the shared data to all users simultaneously [27, 28].

### I.5.2 Higher cell density

Historically, shrinking cell sizes (i.e., increasing cell density) has been the single most successful technique in satisfying demand for network capacity [31]. This is physically intuitive, as transmitters and receivers are spatially closer (i.e., reduced path-loss, less reflections/fading). Also, more density means that more cells can be fit in the same space. Interestingly, simple densification increases interference and signal power proportionally as the cells move closer together. This is most intuitively understood in a



simple homogeneous propagation environment (e.g., line of sight). Here, both the interference power and signal power increase proportionally with shrinking distances, i.e., the SIR will more or less stay the same [32]. Thus, the spectral efficiency stays the same in first order approximation. However, the increased spatial reuse gives a higher area throughput [33]. In any case, the induced interference from neighbouring cells increases, if the denser cells serve more user terminals (UTs). The classical way to counter inter cell interference is to use different frequencies in cells that are close together (frequency reuse factor larger than one) [34]. Yet, this reduces the spectral

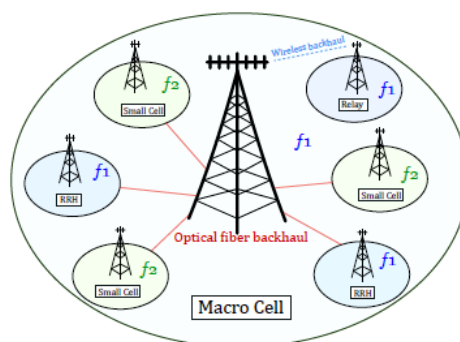


*Figure I.10* — Network composed of a macro cell and several small cell.

efficiency, thus limiting the overall achievable gain. The modern version of cell densification is often described in the framework of small cells (SCs)[34]. Here, a heterogeneous architecture is envisioned, in which the classical large macro cells are exploited for certain tasks (i.e., mobility management), but one offloads as much traffic as possible to smaller cells existing in the same environment. This means that an arbitrary quantity of small, self-organizing outdoor/indoor cells are deployed either by the operator or by the consumer to provide high capacity, low power and cheap localized network access. The mix of macro cells and SCs will affect the spectral efficiency in each cell, in particular if the SCs are consumer deployed. Such densification will also require a backhaul able to support these high debit, these links being illustrated in Fig.I.10 between the macro cell and small cells, remote radio head (RRH) and relays.

### I.5.3 More spectrum

The most obvious solution to increase throughput is to use more frequency spectrum. This is on the one hand the easiest approach, as doubling the used spectrum in the 300MHz to 3000MHz band instantly doubles the throughput, without too much (if any)

technical problems or research (assuming the overall transmit power can also be doubled). On the other hand, spectrum is heavily regulated in the sub-10GHz range, since this straightforward solution appeals to all operators. Hence, this is a very costly and a fundamentally demand limited possibility. Depending on the geographic region in question, around 1 GHz of frequency spectrum might already be allocated to wireless data services, thus limiting the realistic gains from this approach to a ( $2\times$ -  $3\times$ ) improvement. Curiously, this regulation also aggravates the observation that large parts of the available spectrum are not used most of the time. This fact gives rise to the idea of the cognitive radio [35, 36], which is a device that seeks to use parts of the spectrum for communication that are allocated to different services, but are not in constant use (so-called "spectrum holes"). Another obvious idea is to go to higher frequencies, where no other services are allocated and bandwidth is plentiful. Here, most current research focuses on the mmWave band, between 3GHz and 300GHz [37, 38].

### **I.5.3.1 MmWave cellular system**

MmWave is a promising technology for future cellular systems. Since limited spectrum is available. This system is based on a hybrid analog / digital architecture. It can be considered as a massive MIMO system that works in the millimeter wave band for commercial cellular systems. Users communicate with the BS through directional beams. However, this approach still faces many obstacles. For one the common transceiver hardware (esp. the amplifiers) is not yet able to support such high frequencies [39]. Furthermore, the wave propagation characteristics at these frequencies disallow many properties that communications engineers have gotten used to. For example, very short wavelengths are more or less limited to line-of-sight (LOS) paths (much akin to visible light) and are very susceptible to obstruction and weather. There are three major differences between this system and the massive MIMO system. Firstly, the user is equipped with a large number of antennas and thanks to the small dimensions of the antennas in the case of millimetre waves. The second difference is that the cells size in mmwave system is smaller than the cells of the massive MIMO system and the number of users served by each cell and sharing the same resources is reduced. Finally, the massive MIMO system does not use a hybrid beamforming architecture. The current big issue is the integration of the new 5G base stations in the current network (4G, 3G et 2G), (Fig.I.11).

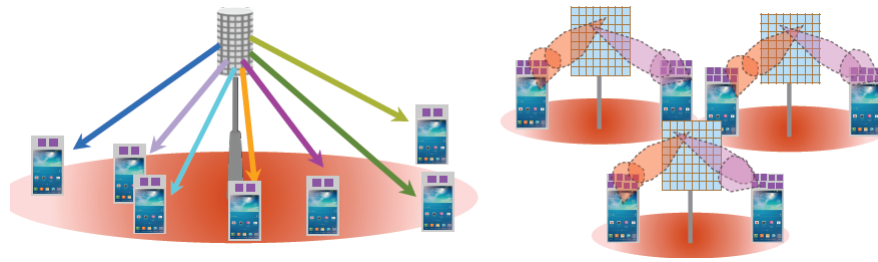


**Figure I.11** — Massive MIMO vs mmWave system

Figures I.12(a) illustrates a hybrid network that combines the mmWave system and the current 4G network. A modem is proposed that allows the user to switch between the two networks for a better experience. Otherwise, the millimeter wave spectrum can also be used only for data communication, whereas control information system can be transmitted using traditional 4G networks [40]. On the other hand, the Figure. I.12(b) shows an operating network only with millimeter waves. The narrow beam concept offers acceptable overlap and also improves the quality of the link between the BS and the user. Thus, it is expected that the management of radio network and air interface of 5G communication are different.

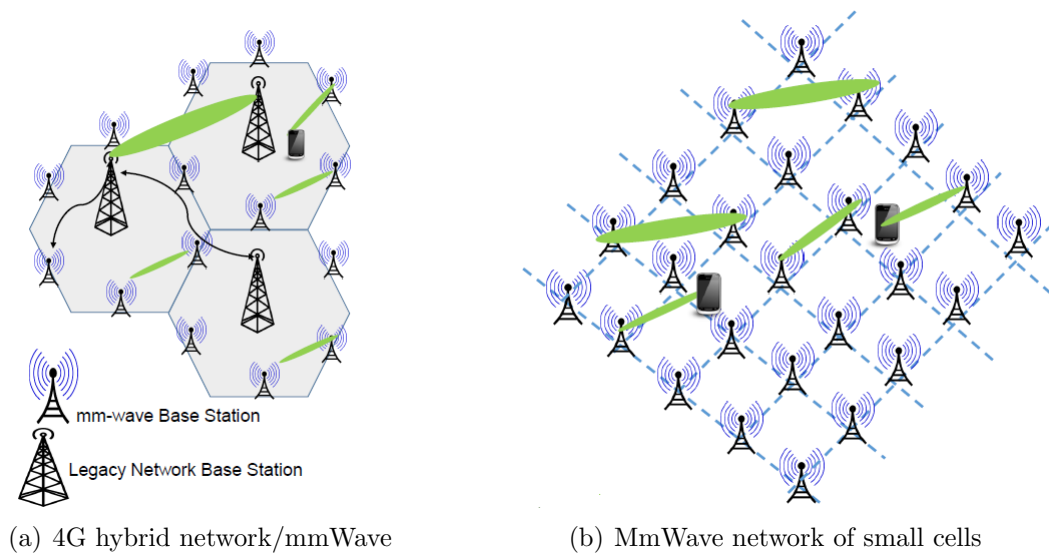


**Figure I.12** — The possible architecture of mmwave systems.

The mmWave system is essentially based on hybrid beamforming techniques to compensate the millimeter wave propagation losses. There is also a proposal to use narrow beams for data and wider beams for control channels [41]. Beamforming is a classic signal processing technique where multiple antenna elements are used to control the signal in the desired direction. Beamforming can be used at both the transmitter and

the receiver to achieve significant gains, thus providing an improvement in signal-to-noise ratio (SNR). Moreover, beamforming reduces interference due to the spatial selectivity of the directional antennas. For millimeter-wave systems, beamforming offers great promise because the small wavelengths allow the use of a large antenna elements number in small antenna arrays, that are capable of creating highly directional beams with significant gains and pointed to various directions in order to exploit the reflections and the diffusion of the waves. According to the architecture of the beamforming system, the weighting coefficients needed to form the beam that can be applied in the digital (Digital beamforming: DBF) or analog (Analog beamforming: ABF) domain.

### 1. Digital beamforming

Digital beamforming is performed as digital precoding, by multiplying the baseband modulated signal of each RF (radio frequency) channel to the transmitter or receiver by a particular coefficient.

Digital beamforming offers flexibility and good performance at the expense of system complexity (undesirable especially for receiver) and a high cost due to the fact that each antenna requires a complete RF chain (low noise amplifier (LNA), local oscillator, analog-to-digital converters, ..), therefore increases enormously the cost and power consumption. For example, a digital beamforming system that has 64 ADCs and works with a bit rate of Gb/s consumes power of about 200 W [42]. Thus, digital beamforming is not practical for the mmWave system.

### 2. Analog beamforming :

The basic idea of analog beamforming is to apply complex coefficients to manipulate the signal of each of the transmitting and receiving antennas using controlled phase shifters and variable gain amplifiers (VGA).

Analog beamforming has the following advantages:

- The system architecture is less complex compared to that of a digital system and allows to generate a larger gain by using a large number of antennas.
- The analog system is less costly and consumption of power compared to the digital case where each antenna is linked to a dedicated RF chain.

The figure (I.13) represents a block diagram of an analog beamforming system Fig.I.13(a) and a digital beamforming system Fig.I.13(b).

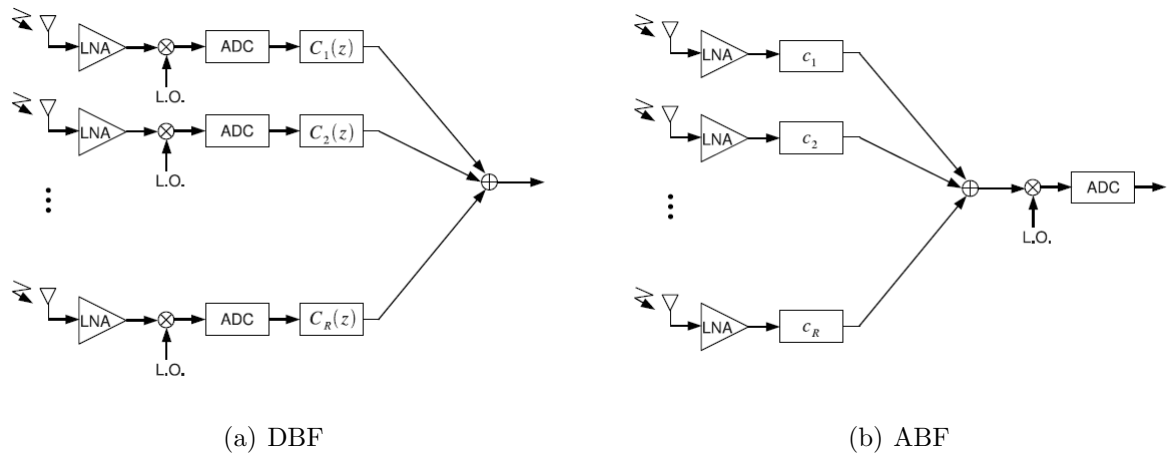


Figure I.13 — Analogue and digital beamforming.

3. **Hybrid beamforming** As we explained previously, analog beamforming is implemented by employing variable gain phase shifters and amplifiers that are low cost. Therefore, the analog solution is economically more attractive than the

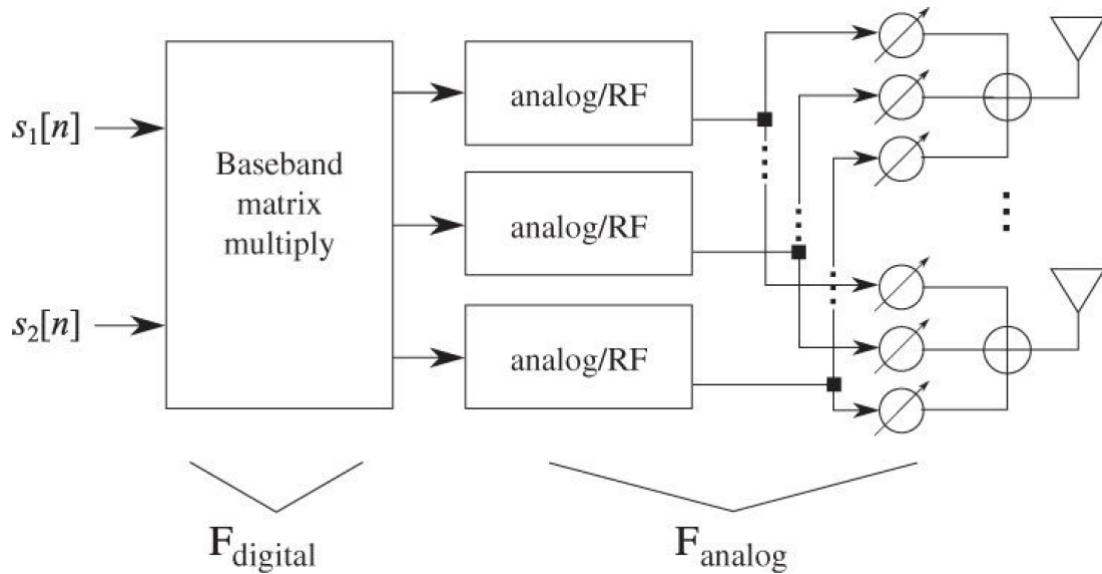


Figure I.14 — Blok diagram of hybrid beamforming applied in mmwave system.

digital solution. On the other hand, it is less flexible because it does not allow to use the various coding algorithms developed to improve the performances of the system. Therefore, it is a tradeoff between flexibility, cost, simplicity and performance that drives the need for a hybrid architecture that combines analog beamforming and digital precoding. The figure (I.14) shows the hybrid architecture of a transmitter-receive mmWave system.

#### **I.5.4 5G: A concentration of new paradigms and innovative technologies**

Meeting the aforementioned requirements necessitate drastic changes in the network paradigm in addition to a large array of disruptive innovations. In this context, 5G networks can call upon a wide range of physical and higher layers new technologies. This enables a leap in wireless networks performance that exceed its predecessors. These innovations will touch on transmission and design of the networks physical layer in addition to introducing evolution in the networking and application layer techniques. As a matter of fact, 5G will employ many key technologies in order to attain new levels of performance and efficiency. The combinations of the latter will expand the importance of mobile communications and enables it play a much central role in a world of changing use cases. Among the potential main innovation in 5G physical layer, one can cite [43]:

- Mmwave mobile communications.
- Massive MIMO communications.
- Non-orthogonal multiple access (NOMA).
- Full-duplex wireless communications.
- Carrier aggregation and multicarrier modulations.
- Larger spectrum.
- Sidelink communication.
- New waveform and heterogeneous OFDM numerology.

In addition to these physical improvement, the innovations in 5G will change how networking is performed. As a matter of fact, 5G concentrates a number of new paradigms which aim at enabling a more agile, automatic and intelligent network in each of its operations [44]. Among the main networking innovations in 5G, one can state [43]:

- Cloud radio access network (CRAN).
- Energy harvesting.
- Green heterogeneous wireless access.
- Self organizing network (SON).

- Fog computing.
- User-centric wireless network (proactive caching, etc).

In this thesis, we mainly focused on three major technologies that will help usher in the age of 5G, namely massive MIMO, mmwave, full duplex. The main goal during the present thesis was to improve the performance of these technologies by introducing algorithm to tackle the pilot contamination (PC) and residual self interference (RSI) problems that face these mentioned systems.

## I.6 Modulation technique for 5G

The 5th generation wireless communication system involves different types of coding and modulation schemes for the better performances and efficient outputs. At present 4G LTE uses QAM with OFDM as modulation and OFDMA as access scheme. The challenge in 5G is high bit rate with mobility. Therefore, spectral efficiency is utmost important. So, given the great success of OFDM in 4G cellular networks, we would think that it will be an intuitive choice for a 5G system [45]. However, an important feature of the use of OFDM below 6 GHz, which is the frequency multiplexing of users, is not necessary for a mmwave system. First, the mmWave system will be deployed in small cells with short frames (example  $100 \mu s$ ). This implies that very few users will transmit in the same time slot (time-slot). In addition, the small OFDM symbol times (eg  $66.67 \mu s$ ) due to the high bandwidth and small propagation delays mean that users can be multiplexed efficiently in time, rather than frequency. Finally, millimeter wave systems use large antenna arrays. Digital beamforming will not be possible because of the unacceptable consumption of power by digital-to-analog converters (DACs) and analog-to-digital converters (ADCs) which are needed behind each of the antennas. This leads to the use of analog beamforming which only requires an ADC/DAC for the entire RF chain. The use of analog beamforming implies that only one RF channel beam can be created at a given time, thus making it necessary to separate the users in time, rather than frequency. Since frequency separation of users is not critical for the mmWave system, it is not necessary to accept some of the disadvantages of OFDM, such as the high PAPR (peak to average power ratio) which negatively affects the system. Potential applications expected from 5G (high-speed video downloads, interactive games, vehicle-to-vehicle communication, machine-to-machine communication, internet of

things, ...) and the adopted system architecture requires certain specifications and conditions on the type of modulation and the waveform to be used. Some specifications that must be satisfied by the chosen modulation system are:

- Capability of handling broadband signals with high data rates.
- The ability of offering low transmission latency, that is, operating with very short transmission time intervals (TTI).
- Fast switching between uplink and downlink for TDD systems that are favored to be employed.

There are several new waveforms (modulation) to consider for 5G. We quote here the most favorable:

- **Generalised frequency division multiplexing (GFDM)**

GFDM is a multicarrier transmission technique that is very similar to OFDM. The main difference is that the carriers are not orthogonal to each other. GFDM allows it possible to better control out-of-band emissions by reducing the PAPR which represents the major disadvantage of an OFDM system. The fundamental concept of the GFDM lies in the subcarriers transmission blocks composed of several time slot. Its flexibility and its block structure makes it possible to meet the low latency specifications of 5G systems [46]. The implementation of GFDM by the FFT/IFFT algorithms presented in the Fig.(I.15) was proposed by the authors of [47].

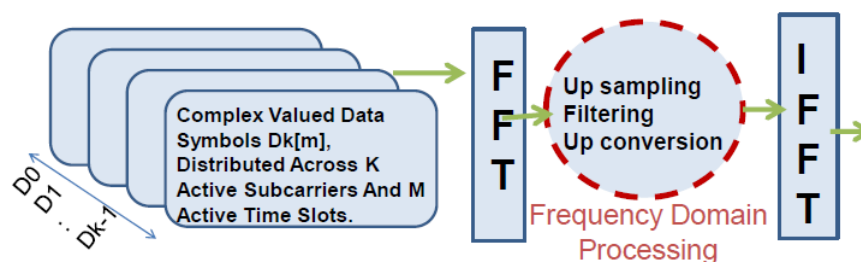


*Figure I.15* — GFDM implementation

- **Filter bank multi carrier (FBMC)**

This technique had a lot of interest as a possible modulation candidate for 5G. It is based on waveform filters for each subcarrier. Better gains are made compared to other existing techniques at the cost of increasing the complexity of the system.



The FBMC does not require orthogonality or complex synchronization which improves system latencies.

GFDM and FBMC are the two most promising modulation techniques for 5G. However, other modulations are considered to be used such as Universal filtered multi carrier (UFMC) and filtered OFDM (F-OFDM). These techniques can bring additional benefits to the new cellular system under certain conditions and circumstances. No waveform brings all the benefits and meets all the requirements. As a result, many predict that the final modulation for 5G may include an adaptive solution that uses an optimal waveform for a given situation.

## **I.7 Research challenges for 5G**

The high bit rates, low latencies, energy saving and other promises made by 5G are associated with their respective challenges. By 2020, the expected date for the deployment of the first 5G networks, there are still a number of research issues and challenges to overcome [48].

### **1. Unavailability of channel models:**

The development of mmWave systems requires a fundamental understanding of the radio channel. Researchers study channel models for different scenarios: indoor, outdoor, LOS, NLOS, . . . Detailed analysis of these studies will allow the design of new methods for the radio interface and multiple access.

### **2. Design of antenna array :**

The small wavelengths in the mmwave band allow the collection of hundreds of antennas in networks of small areas. These networks must be able to direct and combine the energy of the beam. Thus, one of the key topics of research in the field of 5G is the communication by directive beams that completely changes the concept of the cell. There are still research challenges for designing BSs and terminals to achieve this directivity.

### **3. Massive MIMO:**

Another serious challenge is to realize the massive MIMO system that can meet the requirements of 5G services. This system requires a completely different BS structure with a large number of antennas supplied by low power amplifiers. The

adoption of massive MIMO algorithms for the implementation of a future 5G network may represent an important jump in the development of wireless communications.

#### 4. **Network densification :**

The small cell architecture is an essential feature for a future 5G network. Therefore, density of BS is expected to be significant. Coordination and elimination of interference, software radio networks and self-organized cells [14] allow the management of the network. Although these are promising techniques for 5G communications, their deployment for 5G scenarios has not yet been fully explored.

#### 5. **Standardisation**

They already exist several forums and projects devoted to the research and the design of structures valid for the 5G. However, 5G standards formal have not yet been published.

## Chapter II

# RESIDUAL SELF INTERFERENCE MITIGATION FOR FD MASSIVE MIMO

## II.1 Introduction

In recent years, the variety of current and future wireless applications demand high data rates, larger network capacity, better energy efficiency, higher spectral efficiency and more mobility. These exigences are even more important for the wireless communication beyond 4G (B4G) and 5G. A promising technologies such as, a multiple-input multiple-output (MU Massive MIMO), full duplex, non orthogonal division multiple access (NOMA), and orthogonal frequency division multiplexing (OFDM), have been strongly recommended for such purpose for future wireless systems.

This chapter reviews one of the main components on which the thesis are based. Specifically, we first outline the historical development of FD communications and the state-of-the-art techniques on SI cancellation. Then, the description of system model is presented. While, the next section is reserved for the proposed SI channel estimation, transmission and detection schemes. Finally, simulation results and theirs comments are given .

## II.2 Full-duplex communications

The idea of concurrently transmitting and receiving signals of a transceiver over the same frequency band has been noticed for years. For example, it has been first known in continuous wave radar systems at least since the 1940s [49]. Subsequently, FD techniques were realized in the context of a wireless relay system [50] in which a wireless FD repeater, called a FD relay, receives a signal, processes it, and then retransmits it to a destination over the same time-frequency resources, as depicted in Fig. II.1 (a). Such systems have the potential to extend cell coverage and enhance the cell-edge throughput. Note that in most of FD relay topologies only the relay is configured to operate in the FD mode while the remaining nodes such as source and destination do not need to operate in the FD one. Recently, a related but different application of FD relay systems has been gained significant attention in both academia and industry, called FD bi-directional or P2P wireless networks [51, 52, 53] over short ranges as seen in Fig. II.1 (b). In Figure II.1 (b), two nodes with FD operation exchange messages at the same time over the same frequency. More recently, a more general model called FD MU-MIMO systems or FD BS topologies [54, 55] have been investigated (see Fig. II.1 (c)), in which a FD BS is allowed to communicate with multiple users in the DL and UL channels on the same radio resources which is the topic of this chapter.

In a practical environment, it is difficult and tricky to fully cancel the SI due to imperfect

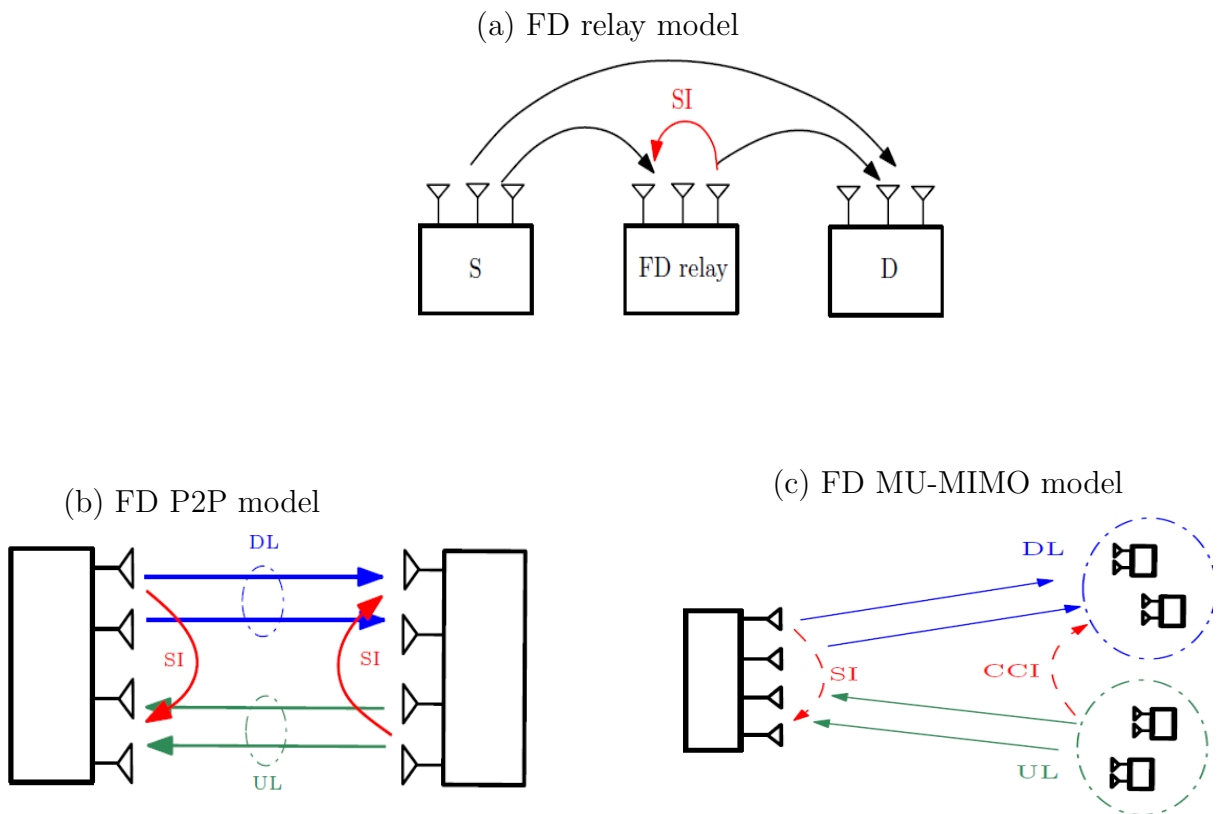


Figure II.1 — FD scenarios

channel estimation [56], and the existence of various imperfections in the transmitting chain [56]. However, an initial estimate of the signal channel is important in the detection of the transmitted signal.

In the field of signal processing the problem of SI has been intensively addressed in FD-systems. Several algorithms that reduce and achieve this goal has been proposed [57]. Furthermore, various works explore the system performance in the presence of residual self interference (RSI) with several benchmark such as achievable sum rate, outage probability, bit error rate, and interference power (IP) [58, 59]. While, these papers do not examine the suppression of the RSI. Some of the works consider perfect channel state information (CSI) [59, 60], while others assume imperfect CSI [58] without seeking how to estimate the channel. The LS channel estimation is also considered in [61] for full-duplex relays and MIMO transceivers, respectively. A maximum likelihood estimator has been proposed in [58] to estimate the SI. In this thesis, we consider the use of a blind channel estimation based on well known algorithm: second order blind identification (SOBI) [62] to suppress the RSI problem in FD system.

### II.3 Multiuser MIMO communications

Basically, the FD MU-MIMO model of interest is a HD MU-MIMO one except that the base station is configured to operate in the FD mode. Hence, this subsection briefly discusses some common transmission schemes for the DL and UL of a conventional MU-MIMO system which is referred to as a HD MU-MIMO system. Specifically, we consider a HD MU-MIMO system including one BS equipped with  $N_t$  antennas,  $K_{dl}$  users in the DL channel and  $K_{up}$  users in the UL channel, as shown in Fig. II.2. The set of users in

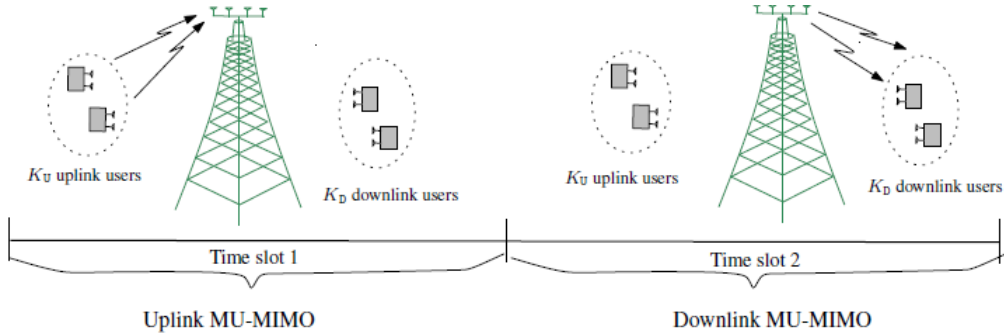


*Figure II.2* — HD MU-MIMO system model.

the DL is denoted by  $K_1 \dots K_{dl}$  and the set of users in the UL is  $K_1 \dots K_{up}$ . In addition, the notations  $M_{dl}$  and  $M_{up}$  refer to the number of antennas at user DL and user UL, respectively.

### II.4 Multiple access technique

A promising technologies such as, a multiple-input multiple-output (MU Massive MIMO), full duplex, non orthogonal division multiple access (NOMA), and orthogonal frequency division multiplexing (OFDM), have been strongly recommended for such purpose for future wireless systems. The so-mentioned technologies have called for to many researchers due to its promising ability of greatly enhancing the spectral efficiency, energy efficiency and robustness of the system [63]. Indeed, the full duplex (FD) technology as been strongly recommended for such purpose for future wireless systems. Which is based on the idea of using the full-duplex communication that allow simultaneous transmission and reception of data in the same frequency band and thus increasing the system spectral efficiency up to two times [1] compared to the half duplex (HD) transmission scheme. Indeed, the promised gains by FD technology is harmed by the self-interference (SI) problem caused by the base station itself. The third technology named NOMA, has recently been recognized

as a key multiple access technique due to its higher spectrum efficiency than traditional orthogonal multiple access (OMA) [2]. The use of so mentioned technique was justified by two benefits. Firstly, its ability to mitigate the multiple access interference (MAI) while ensuring high spectral efficiency. Secondly, user separation is carried out by a proper choice of a different interleaver for each user. There exist two classes of NOMA: power and code domain multiplexing. Where the allocation of users with various power levels depending on their channel conditions, known as power domain. However, when various users are allocated with different codes, and are then incorporated into the same time-frequency resources, it is named code domain. Interleave-division multiple access (IDMA) can be considered as NOMA scheme with code domain multiplexing. The last technology named OFDM, is adopted on physical layer modulation scheme, which has proven to be very efficient for the wireless communication system. Both NOMA and OMA are multiple access techniques which utilize power domain/code domain and time/frequency domain respectively. In the next section, we discuss the various access techniques.

#### II.4.1 Orthogonal multiple access (OMA) techniques

Over the past few decades, wireless communication systems have witnessed a “revolution” in terms of their multiple access techniques. Specifically, for 1G, 2G, 3G, 4G and 5G wireless communication systems, frequency division multiple access (FDMA), time division multiple access (TDMA), code division multiple access (CDMA), and orthogonal frequency division multiple access (OFDMA) have been used as the corresponding key multiple access technologies, respectively. From the perspective of their design principles, these multiple access schemes belong to the category of orthogonal multiple access (OMA), where the wireless resources are orthogonally allocated to multiple users in the time-, frequency-, code-domain or according in fact based on their combinations. We might collectively refer to these domains as “resources”. In this way the users’ information-bearing signals can be readily separated at a low complexity by employing relatively cost-efficient receivers. However, the number of supported users is limited by the number of available orthogonal resources in OMA.

#### II.4.2 Non-Orthogonal multiple access (NOMA) technique

Non-orthogonal multiple access (NOMA) is emerging as a strong candidate for adoption as the multiple access technology to enhance system capacity for 5th generation (5G)

cellular systems. The innovative concept of non-orthogonal multiple access (NOMA) has been proposed in order to support more users than the number of available orthogonal time-, frequency-, or code-domain resources. Where NOMA, unlike the orthogonal multiple access (OMA) methods, exploits the power domain by multiplexing the users (UEs) and intentionally introducing interference by sharing the same resources without spatial separation. The main function of NOMA is to serve multiple user equipments (UEs) using single 5G-NB (Node B or Base Station). It serves multiple users on same time/frequency resources. There are two main techniques employed in NOMA for multiple access.

- Power domain:

Here NOMA achieves multiplexing based on different power levels, including multiple access solutions relying on low-density spreading (LDS) [64, 65], sparse code multiple access (SCMA) [66, 67], multi-user shared access (MUSA) [68], successive interference cancellation amenable multiple access (SAMA) [69], etc. Some other closely-related multiple access schemes, such as spatial division multiple access (SDMA) [70], pattern division multiple access (PDMA) [71] and bit division multiplexing (BD-M) [72].

- Code domain:

Here NOMA achieves multiplexing based on different codes. Code-domain NOMA achieves multiplexing in code domain. Like the basic code division multiple access (CDMA) systems, code-domain NOMA shares the entire available resources (time/frequency). In contrast, code-domain NOMA utilizes user-specific spreading sequences that are either sparse sequences or non-orthogonal cross-correlation sequences of low correlation coefficient. This can be further divided into a few different classes, such as low-density spreading CDMA (LDS-CDMA) [73], low-density spreading-based OFDM (LDS-OFDM) [74, 75], and sparse code multiple access (SCMA) [76]. The use of low-density spreading sequences helps LDS-CDMA to limit the impact of interference on each chip of basic CDMA systems. LDS-OFDM can be thought of as a combination of LDS-CDMA and OFDM, where the information symbols are first spread across low-density spreading sequences and the resultant chips are then transmitted on a set of subcarriers. SCMA is a recent code-domain NOMA technique based on LDS-CDMA. In contrast to LDS-CDMA, the information bits can be directly mapped to different sparse codewords, because both bit mapping and bit spreading are combined.



There exist some other multiple access techniques, which are also closely-related to NOMA, including pattern division multiple access (PDMA) and spatial division multiple access (SDMA) [77, 78]. PDMA can be realized in various domains. Where at the transmitter side, PDMA first maximizes the diversity and minimizes the overlaps among multiple users in order to design non-orthogonal patterns. The multiplexing is then performed either in the code domain, spatial domain, or a combination of them. For SDMA, the working principle is inspired by basic CDMA systems. Instead of using user-specific spreading sequences, SDMA distinguishes different users by using user-specific channel impulse responses (CIRs). This technique is particularly useful for the cases where the number of uplink users is considerably higher than the number of corresponding receiving antennas in BS. The milestones of NOMA techniques are summarized in Fig. II.3

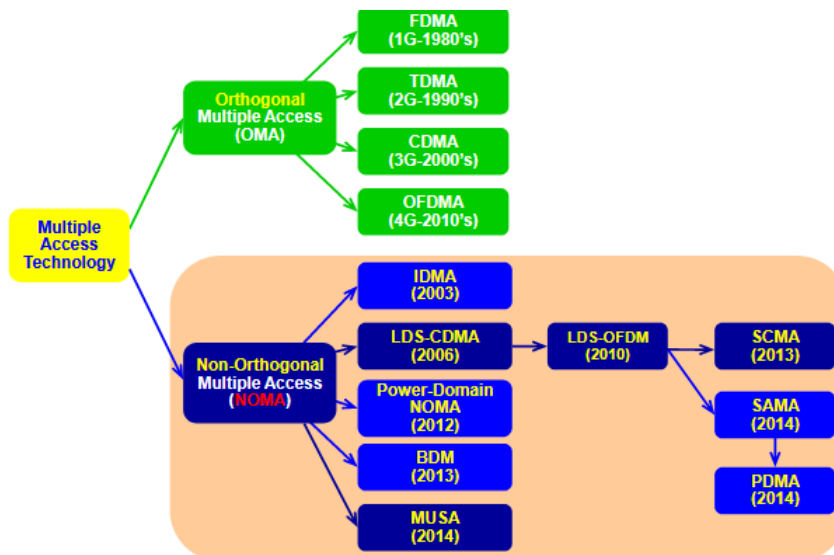


*Figure II.3* — The milestones of multiple access technologies.

### II.4.3 Multiple access IDMA technique

In 2002, Li Ping [79] proposed an innovative multi-access technique called interleaved multiple access or interleaved-division multiple access (IDMA). The separation of users is implemented through interleavers. This technique, candidate of with code division multiple access or code-division multiple access (CDMA), is an alternative. to the problem of interference between users because it does not use spreading sequences: each sequence of data is coded and then interleaved at the chip level. Moreover, interleavers must be different for different users. They are ideally randomly constructed and independent of each other. They disperse the coded sequences so that two adjacent chips are not, or at

least very closed, correlated. The IDMA system structure is given by Fig.II.4.

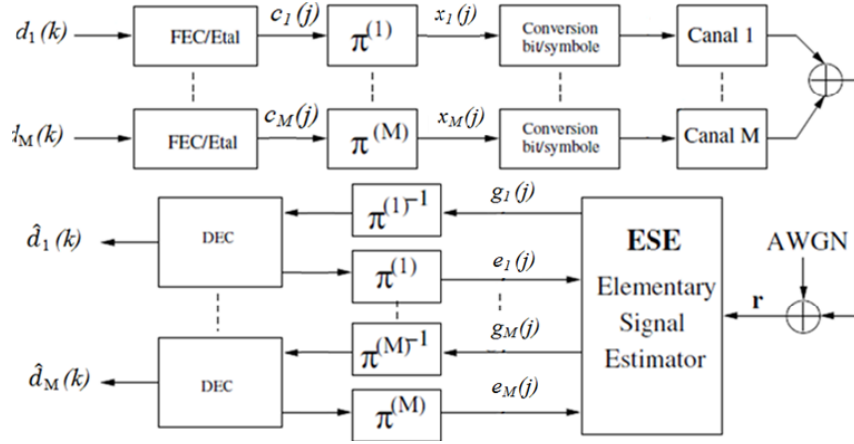


*Figure II.4* — A IDMA-OFDM FD Massive MIMO system model.

### Transmitter

On transmission, the data sequence at the input, noted by  $d_m$ , the  $m^{\text{th}}$  user is first coded with a low rate encoder. This encoder consists of a concatenation of an error correction coder and/or a spreading code of size SP thus generating the chips  $c_m$ . The latter is then permuted in the  $m^{\text{th}}$  user-specific interleaver to produce the sequence that is subsequently modulated QPSK giving birth to a complex sequence of symbols  $x(m) = [x_1(m), \dots, x_m(j), \dots, x_1(m)]$ , where  $J$  is the length of the frame.

The result symbols are then modulated on different carriers via IFFT and the insertion of the CP cyclic prefix which makes it possible to fight the ISI [80] to be transmitted in the channel.

### Receiver

At the receiver, OFDM demodulation is performed before the multiuser detection as shown in Fig.II.5. Here it is assumed that the duration of the cyclic prefix is greater than the maximum delay so that the effect of the ISI is not considered in the model.

## II.5 MIMO-OFDM-IDMA system model

A single cell is considered with adopted FD Massive MIMO-NOMA (IDMA) system architecture for multiple-access channel as illustrated in Fig.II.6. The BS equipped with  $M_{up}$  downlink and  $M_{dl}$  uplink antennas concurrently serving  $K$  user terminals with single

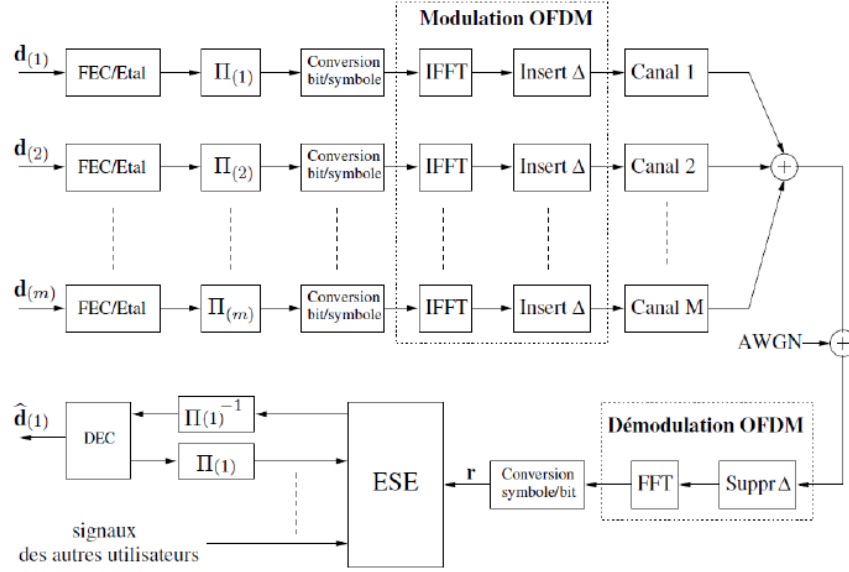


Figure II.5 — OFDM-IDMA system structure of the transmitter/receiver.

antenna each. The users operate with half-duplex (HD) mode. Since the BS transmits and receives simultaneously in the same frequency band, hence, the transmitted and received signals inevitably interferes with each other. This part of the system is equivalent to a  $M_{dl} \times K_{dl}$  system in downlink and a  $M_{up} \times K_{up}$  system in uplink, where  $K_{dl} < M_{dl}$  and  $K_{up} < M_{up}$  [81].

In the BS, the uplink side of the system consist of the FEC operation, pursue by the

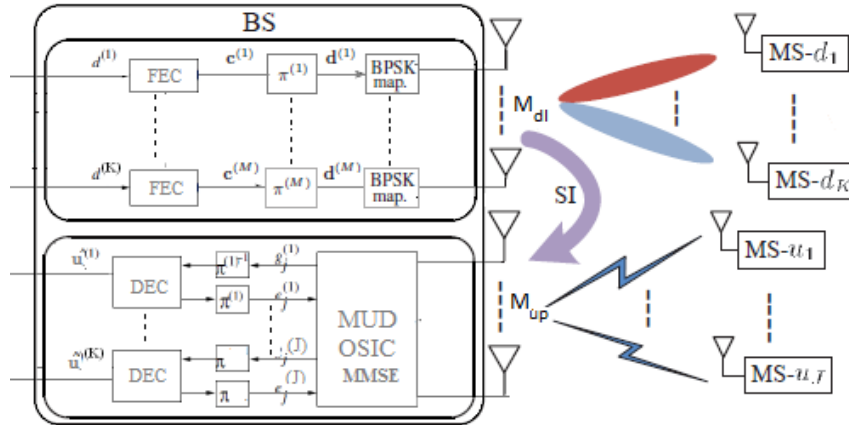


Figure II.6 — A IDMA-OFDM FD Massive MIMO system model.

interleaving and others necessary operations such as OFDM, modulation scheme. Where, the receive side encompasses the blocks performing the adverse operations, in addition to ordered successive interference canceler minimum mean square error (OSIC-MMSE). The

transmitted signal  $\mathbf{u}^{up}$  from  $K$  users to  $M_{up}$  over wireless channel modeled as [82]:

$$\mathbf{y}^{up} = \underbrace{\mathbf{H}^{up}\mathbf{u}^{up}}_{\text{desired signal}} + \underbrace{\mathbf{G}^{SI}\mathbf{d}^{dl}}_{\text{residual SI}} + \underbrace{\mathbf{w}^{up}}_{\text{noise}} \quad (\text{II.1})$$

Where  $\mathbf{u}^{up}$  and  $\mathbf{d}^{dl}$  are the transmitted data vectors for uplink and downlink with dimensions  $K_{up} \times 1$  and  $M_{dl} \times 1$ , respectively. The  $M_{up} \times K_{up}$  matrix  $\mathbf{H}^{up}$  represents the complex Rayleigh Fading channel matrix. The multipath self-interference channels denoted by the matrix  $\mathbf{G}^{SI}$  with dimension of  $M_{up} \times M_{dl}$ . The entries of SI matrix are supposed to be complex Rician random variables with variance  $\beta^2$ . The noise vector  $\mathbf{w}^{up}$  is modeled as the zero mean complex Gaussian with variance  $\sigma^2$ .

At the receiver side, MMSE-OSIC algorithm is performed [83, 84]. Thus, MMSE-OSIC offers an effective multi user interference (MUI) reduction. This type of receiver is performed by nulling and canceling, which is influenced by the order in which the signal are detected and canceled. The original method detects the symbol that offers the maximum SNR and then suppresses its effect on the received signal. By repeating this process we can detect all the layers to recover the original signal. The selection of such a receiver is due to its relative complexity and computation reduction [85].

#### **Sequential interference constellation(SIC):**

When a SIC algorithm is applied, the different layers are not detected in parallel, but one after another [86]. The key idea of SIC detection is layer peeling, that is, the first symbol is decoded first, and then the decoded symbol is cancelled in the next layer peeling. This manipulation is repeated layer by layer until all the symbols are decoded from the received signal. By layer peeling, the interference caused by the already detected symbols is cancelled. The conventional structure of the SIC detection has been given in [87, 88], and multiple channel inversion operations are required, which increases the computational complexity. The SIC detection can be equivalently implemented by a QR decomposition [89, 90], which calculates  $\mathbf{H}=\mathbf{QR}$ , and then computes  $\mathbf{y}' = \mathbf{Q}\mathbf{y}$ . Then, the detected symbol vector  $\tilde{\mathbf{S}}$  is obtained by

$$\tilde{\mathbf{S}} = \mathbf{Q}^H \mathbf{y} = \mathbf{R}\mathbf{S} + \mathbf{Q}^H \mathbf{w} \quad (\text{II.2})$$

and, as  $R$  is upper triangular, the  $i^{\text{th}}$  detected substream is given by

$$\tilde{S} = r_{ii}s_i + \sum_{j=i+1}^{N_b} s_j + \tilde{W} \quad (\text{II.3})$$

Where  $N_b$  is the number of transmit streams.

The computational complexity can be reduced dramatically by the QR decomposition based SIC detection. The detection steps are summarized below :

$$\begin{aligned} \hat{S}_{N_b} &= Q\left(\frac{y'_{N_b}}{r_{N_b, N_b}}\right) \\ \hat{S}_i &= Q\left(\frac{y'_i - \sum_{j=i+1}^{N_b} r_{i,j} \hat{S}_j}{r_{i,i}}\right) \end{aligned} \quad (\text{II.4})$$

where the function  $Q(\bullet)$  quantizes the received signal to the nearest transmitted symbols. Finally, the estimated transmit signal

$$\hat{S}_i = [\hat{S}_1 \ \hat{S}_2 \ \dots \ \hat{S}_{N_b}] \quad (\text{II.5})$$

From the SIC detection steps in (II.4), it is possible that the first decoded stream is the weakest one among all the streams, and thus it is highly possible that the first decoded symbol is wrong. The error will be passed on layer by layer, resulting in a performance loss of SIC detection. This phenomenon is called error propagation. For the reduction of the error propagation effect, we can sort the detection order among all the streams. This is the basic idea of the so called ordered successive interference cancellation (OSIC) detection.

## II.6 Residual self interference (RSI) suppression

As previously discussed, one major task in the RF cancellation stage is to estimate the RSI channel. Thus, in this section we provide two schemes to estimate the RSI channel named: least square (LS) and second order blind identification (SOBI).

### II.6.1 LS estimator

In the first stage SI cancellation, an estimate of the SI channel coefficient is obtained by LS algorithm, where the SI signal is known. Hence, by rearranging equation (II.1), we can

write:

$$\mathbf{y}^{up} = \mathbf{G}^{SI} \mathbf{d}^{dl} + \mathbf{V} \quad (\text{II.6})$$

With  $\mathbf{d}^{dl}$  is the transmitted data vectors for downlink and

$$\mathbf{V} = \mathbf{H}^{up} \mathbf{u}^{up} + \mathbf{w}^{up}$$

Indeed using the LS algorithm, the expression of SI channel is given by:

$$\hat{\mathbf{G}} = ((\mathbf{d}^{dl})^H \mathbf{d}^{dl})^{-1} (\mathbf{d}^{dl}) \mathbf{y}^{up} \quad (\text{II.7})$$

and an estimate of the SI signal can be generated by:

$$\hat{\mathbf{S}}\mathbf{I} = \hat{\mathbf{G}} \mathbf{y}^{up} \quad (\text{II.8})$$

Furthermore, the (II.7) is used for cancel the Self interference signal from the received data. Subtracting (II.8) from (II.1), we get

$$\hat{\mathbf{y}} = \mathbf{y}^{up} - \hat{\mathbf{S}}\mathbf{I} \quad (\text{II.9})$$

The obtained SI-free signal in (II.9) is fed to MMSE-OSIC to perform a multi-user detection.

### II.6.2 SOBI estimator

We use the OFDM-IDMA-FD Massive MIMO system architecture that is described previously but with a little modification. We will inject an estimator block based on SOBI algorithm just before OSIC-MMSE as shown in Fig.II.7. The role of this block is to estimate the SI channel and signals of all users. For this block works properly it is necessary that its signals must meet the following conditions: stationary signals, de-correlated signals and uncorrelated AWGN with user signals.

Concatenating the vectors  $\mathbf{H}^{up}$  with  $\mathbf{G}^{IS}$  and  $\mathbf{u}^{up}$  with  $\mathbf{d}^{dl}$  in sole matrices  $\mathbf{C}$  and  $\mathbf{X}$ , respectively, The equation (II.1) can be written as:

$$\mathbf{y}^{up} = \mathbf{C}\mathbf{X} + \mathbf{w}^{up} \quad (\text{II.10})$$

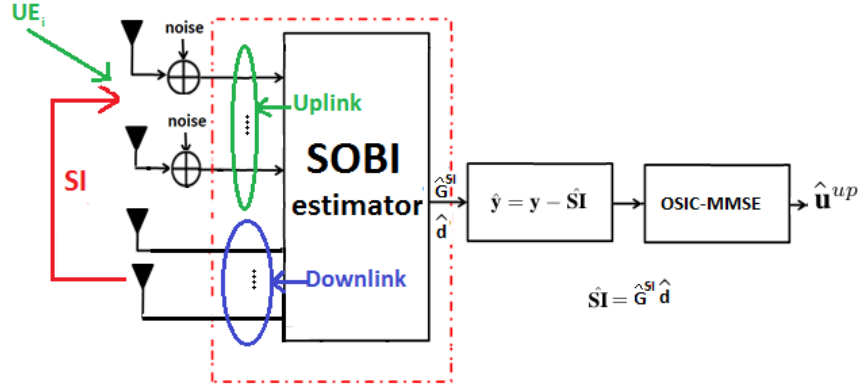


Figure II.7 — Architecture of the separator block

with  $\mathbf{C} = [\mathbf{H}^{up} \quad \mathbf{G}^{IS}]$  and  $\mathbf{X} = [\mathbf{u}^{up} \quad \mathbf{d}^{dl}]^T$ .

From the prospect of blind separation framework, the stochastic vector  $\mathbf{y}^{up}$  defines the observation signals. The elements of  $\mathbf{C}$  construct the mixing matrix. The stochastic matrix  $\mathbf{X}$  represents the transmitted signals. While  $\mathbf{w}^{up}$  denotes additive Gaussian white noise. The purpose of blind separation is estimating the mixing matrix  $\mathbf{C}$  from the observations and recuperate the source signals. In the process of SOBI, we perform two steps: whitening and joint diagonalization operations.

Firstly, the whitening operation is performed to convert a model Equation (II.10) as:

$$\begin{aligned} \hat{\mathbf{y}}^{up} &= \mathbf{Q}\mathbf{y}^{up} \\ &= \hat{\mathbf{C}}\mathbf{X} + \hat{\mathbf{w}}^{up} \end{aligned} \quad (\text{II.11})$$

Secondly, the joint approximate diagonalization (JAD) technique is adopted, which is

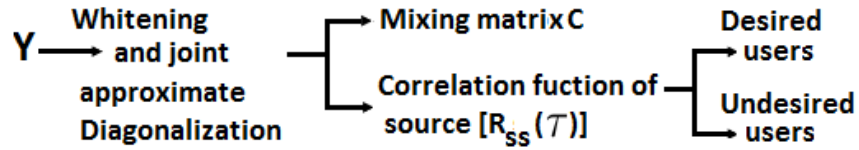


Figure II.8 — Flowchart of second order blind identification (SOBI)

an extension of the Jacobi technique that finds a unitary diagonalizer as a product of the given rotation. An outspread explication can be found in reference [91]. flowchart in Fig.II.8 resume the SOBI algorithm.

After estimating the mixing matrix  $\mathbf{C}$ , we extract the residual self interference (RSI) channel coefficients from this matrix this is done by ordering the element of  $\mathbf{C}$  in ascending manner, with taking in consideration that the power of the self interference signal is greater

than that of the user signal.

Finally, the main steps of the proposed scheme are described bellow:

1. Estimate the mixing matrix  $\mathbf{C}$  and transmission data  $\mathbf{X}$  of equation (II.10) using flowchart presented in Fig.II.8.
2. Calculate the norm of matrix  $\mathbf{C}$  for each user as:  
for  $i=1:M$   
 $\mathbf{c}_1(i) = \|(\mathbf{C}(:, i))\|;$   
end
3. Rearrange the values of the vector  $\mathbf{c}_1$  in ascending order and store the related position  $d$  of each of this vector.
4. Extract the SI channel matrix  $\mathbf{G}^{IS}$  and signal vector  $\mathbf{d}^{up}$  as:

$$\mathbf{G}^{IS} = \mathbf{C}(:, d(M_{dl} + 1 : end)) \quad (\text{II.12})$$

$$\mathbf{d} = \mathbf{X}(d(M_{dl} + 1 : end), :) \quad (\text{II.13})$$

5. Calculate the self interference in (II.9) using equations (II.12) and (II.13)
6. Subtract the SI signal from the received signal  $\mathbf{y}$  using equation (II.9).

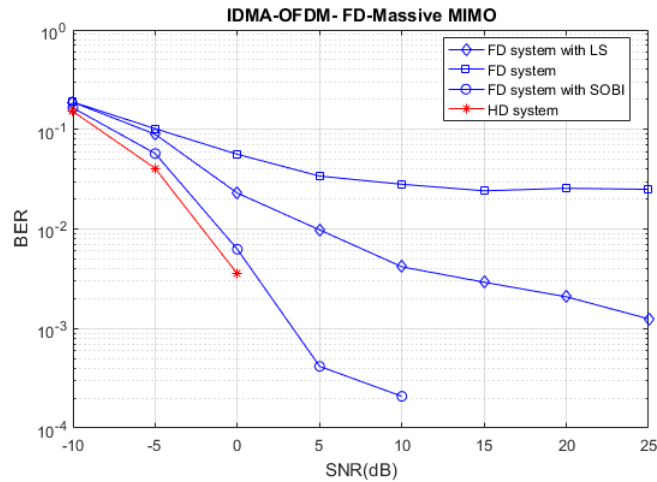
## II.7 Simulation results

In this section, our objective is to elucidate the reliability of a full duplex massive MIMO, by implementing a new scheme. Moreover, the baseband digital system are constructed to model the behaviour of the SI signal and simulation results are carried out on Matlab. As result, we study the performance of the proposed scheme applied to a FD massive MIMO system incorporating IDMA-OFDM-QPSK. The so mentioned scheme is investigated in the wireless selective Rayleigh fading assuming perfect channel state information (CSI) for the uplink scheme. However, the SI channels are generated as complex Rician random variables with variance  $\beta$ . The results are presented along with the system incorporating the OSIC-MMSE as detector. The main parameters of our simulations are listed in Table II.1.



**Table II.1** — Simulation parameters.

Parameters	Attributes
Number of frames	1000
Estimator	SOBI, LS, HD scheme
Number of transmit antenna	20,30,40,50
Number UP user	10
Number DL antenna	5
Spread length	32

**Figure II.9** — The BER comparison performance for different schemes.

In the first set of simulations, we compare the performance proposed scheme based on SOBI algorithm with the LS estimator counterpart when signal interference is set be  $20dB$ . We also compare the proposed method with half-duplex Massive MIMO i.e there is no self interference. Moreover, the received users signals are considered as additional noise and only the residual SI channel is estimated in the presence of 30 users,  $M_{dl} = 50$  and  $M_{up} = 30$ , and the relative results are reported in Fig. II.9. The simulations result confirm that the proposed system with source separation improves in a remarkable way in terms of BER performance compared to a system without source separation. Hence, it is shown that the gain provided by varying SNR in the proposed scheme over the conventional one (LS estimator) offers better bit error rate. This is probably due to the signals dependency (which is a primary requirement for SOBI to run properly) resulting in better performance compared to LS. Interestingly, the presence of the proposed algorithm induces only a slight degradation, as compared to the perfect case (HD), unlike LS estimator. We can also say that the proposed scheme manages to eliminate the saturation of the system, so a success in terms of rejection of the RSI, in this case, OSIC-MMSE can decode the signals from

users in a correct way.

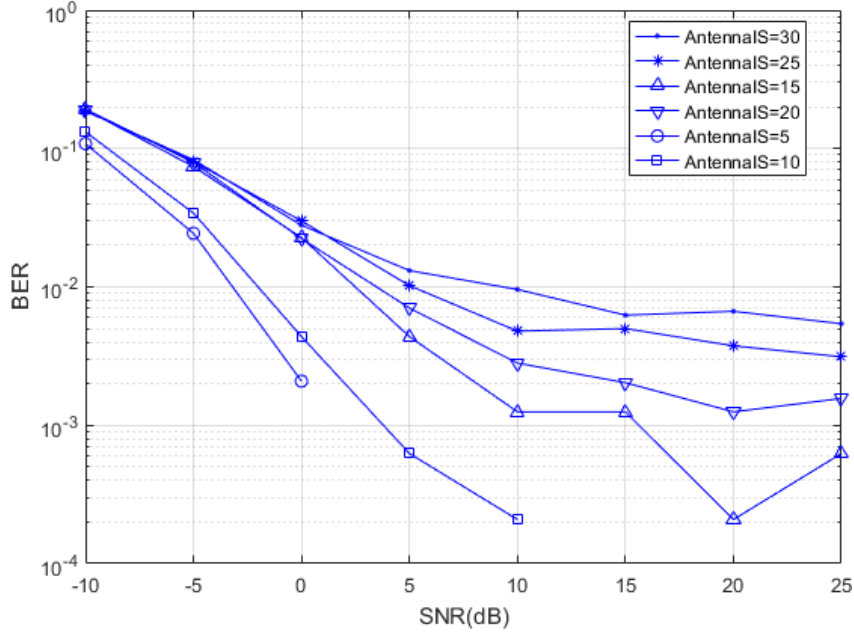


**Figure II.10** — The BER comparison performance for different antenna configuration.

Figure II.10 portray the SNR performance of the proposed scheme under different antenna configuration of the SI channel. So we can say that the effectiveness of SOBI algorithm improves with the decrease of the antenna number of SI signal. From the results illustrated in Fig.II.10, it can be seen that the proposed system is sensitive to the antenna number of the downlink side of the BS. While, increasing the BS antennas configuration, induces a significant performance degradation, especially when the SNR increases. However, when number of uplink antenna is ( $M_{up} = 5$ ) and ( $M_{up} = 10$ ), the BER becomes perfect after  $SNR = 0dB$  and  $SNR = 10dB$ , respectively.

Finally, Figure II.11 investigates the impingement of the power of SI on the BER performance of the whole system. We note that despite the presence of SI with large powers, the association of separation algorithm with IDMA manage to mitigate the effect of such interference. From this figure it is observed that, as expected, the SIR has effect on the BER in particular at high SNR range. In other words, it can be seen that increasing the number of transmit antennas improve the performance of the system. However, it is observed that, when the SNR is lower, the four schemes yield the same performance. On the other hand, increasing the SNR results in a higher performance degradation especially in the case of the  $SIR = 5dB$ . While, increasing the SIR improve the performance of system. This is due to the fact that the SOBI scheme can mitigate the residual SI completely, no

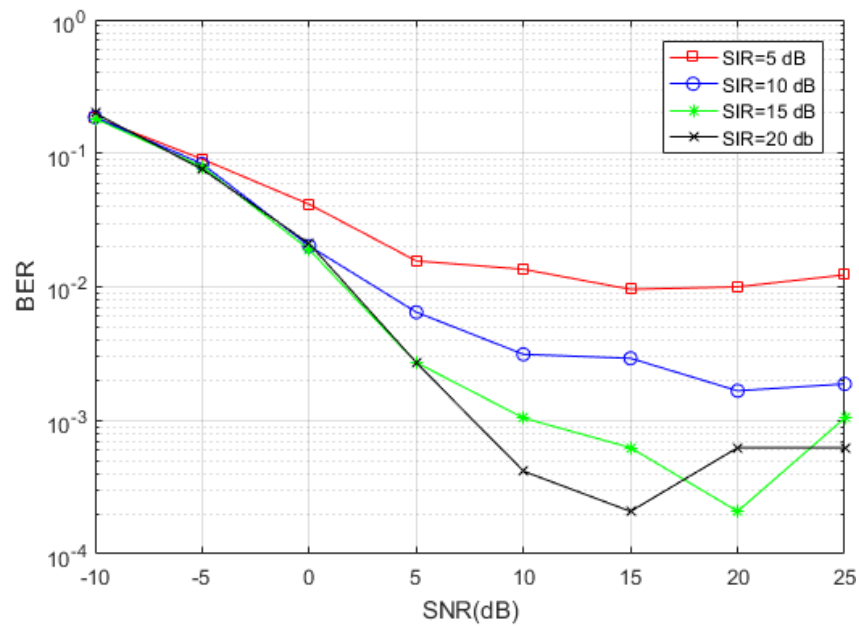


*Figure II.11* — Impact of the SIR on the BER performance of FD-MU-MIMO-IDMA

matter how large the RSI is.

## Chapter III

# CHANNEL PRECODING IN MASSIVE MIMO SYSTEM

### III.1 Introduction

With the exponential increase of the number of users and antennas and the variability of their needs, the variety of current and future wireless applications require high data rates, larger network capacity, better energy efficiency, higher spectral efficiency and more mobility. These requirements are even more important for the wireless communication beyond 4G (B4G) and 5G [20, 92, 93]. One of the promising technologies that has been strongly recommended for such purpose for future wireless systems is the so-called massive MIMO technology which is based on the idea of using large-scale antenna arrays.

This chapter introduce a linear precoding techniques for downlink transmission under multi-cell scenarios to prevent pilot contamination (PC) problem. Then, we present system model and proposed schemes. Finally, simulation results and theirs comments are presented.

### III.2 Precoding in Massive MIMO

Cellular communication are undergoing resurgence of research interest with the development of the fifth generation (5G) cellular system; and the requirements for such systems are not yet totally agreed upon, but essentially industry and research communities want them to be a thousands times better in some dimensions than the old system in order to support the exponentially rising demand for physical layer throughput. To feed these needs, there are three approaches [12, 13]. While the first approach pushes towards getting more spectrum by working in the not exploited millimeter bands [13, 14], still enjoying a huge bandwidth to be offered thus considerable data rates, the second one relies on network densification by integrating small to femto cells thus deploying more infrastructure to get more active users per area [15]. The third approach, on the other hand, involves the incorporation of a considerable number of antennas at the transmit and receive sides with the associated signal processing at the two sides. The third approach takes its origin from point-to-point multiple-input multiple-output (MIMO) systems, which have then evolved into multi-user MIMO to give birth afterwards to the Massive MIMO architectures. These later constitute the third approach and have been proposed as an ultimate solution for 5G wireless systems after research works have appraised and proven their great usefulness [20, 21, 22].

Merging the benefits of adopting very large number of antennas at the base station (BS) and multi-user MIMO (MU-MIMO) technology, high degrees of freedom are offered

which enable a large number of user devices to be simultaneously served at the same set of time-frequency resources. This is quite advantageous provided that the inter-user interference is efficiently reduced.

The two switching modes were studied in the literature in the context of massive MIMO systems namely: frequency division duplex (FDD) and time division duplex (TDD) between the downlink and the uplink. However it seems that TDD mode was favored because of the scarcity of the frequency resources, and the advantages offered by TDD. Indeed, TDD exploits the channel reciprocity which removes the need to channel estimation in the second link and does not involve a higher dimensionality of pilots used for channel estimation in the frame overhead with the increase of the number of antennas [23].

Recently, massive multiple-input multiple-output (MIMO) system has attracted tremendous research interest's in wireless communications. Among various performance aspects and design problems regarding massive MIMO, precoding at the base station (BS) is one of the most important function components to ensure reliable downlink transmission. In an multi-cell scenario, massive MIMO suffers from pilot contamination problems, where orthogonal pilot sequences have to be reused among cells, leading to estimation errors of channel state information at the transmitter.

The notion of precoding appears when performing a digital processing on the transmission coding then distributing the data on each of the antennas, by using a more or less perfect knowledge of the transmission channel. The linear precoding techniques, also sometimes called beamforming.

To harvest the benefit of multi-user (MU) massive MIMO, it is essential to employ a beamforming technique at the BS to suppress the intra-cell inter-user interference. Recall that MU-MIMO is based on using transmit beamforming which is an adaptable technique optimizing the transmission from an array of antennas towards one or multiple users so that to increase the signal power of the wanted user and reduce interference from unwanted users at the reception.

Linear precoding techniques have been extensively developed in the last decades. It is considered as an advantageous way to exploit the full diversity of the channel. For MU-MIMO systems, assuming flat fading channel, the precoding techniques are used to form a beam signal via the target user while reducing the interference to the other users. In general, the linear precoding methods can be classed by two approaches: zero-forcing (ZF) approach and regularized ZF (RZF)/ minimum mean square error (MMSE) [94].

This approach seeks to minimize the MAI among the users and avoid the problem of pilot contamination before happening, therefore, leads to a centralized architecture where the BS collects the channel response of all the users to form the precoder matrix. These precoders matrix are employed to fight against pilot contamination in the processing of the transmitted and received signals by means of linear schemes. For guaranteeing the better performance transmit beamformer, undesired signals need to be suppressed, an oblique projection can be used to achieve the interference signals suppression.

Due to the fact that deploying massive MIMO in multiuser environment critically depends on the efficiency of the transmit beamformer, this work aims at reinforcing its MUI reduction capability by resorting to oblique projection. This implies that the beams resulting from the transmit beamforming should be as narrow as possible, so that the spatial interference mitigation objective is fully met. The idea of this novel massive-MIMO adapted beamformer, which we have chosen to call Oblique Projection based Zero Forcing BeamForming (OPZFBF), was motivated by the inherent advantages of oblique (non-orthogonal approach) projection technique in discriminating signal components lying in different subspaces and estimating the desired signal that is embedded in a structured interference.

Oblique projectors have received relatively little attention in the literature of signal processing. For instance, in reference [95] a first application of oblique projectors to sensor arrays is introduced, while the authors in [96] presented a tutorial study of this topic. More recently, the OP approach has been exploited in various fields such as blind channel identification, image restoration, noise reduction, biomedical signal analysis and harmonic retrieval [97, 98], [99], [100] and in the implementation of a modified version of MUSIC algorithm without a prior knowledge of the values of the signals direction of arrival (DOA) [101].

Its adaptation to beamforming in massive MIMO systems is intuitive and justified as it will be shown through the simulation results.

### III.3 System Model: multi-cell downlink

Figure III.1 depicts the transmission side of a communication downlink at  $l^{th}$  cell, incorporating  $N_t$  transmitting antennas within a base station communicating with  $P$  users devices each having one receiving antenna i.e  $N_r = 1$  for the rest of the chapter.

Furthermore, we consider a cellular system with  $L$  cells .

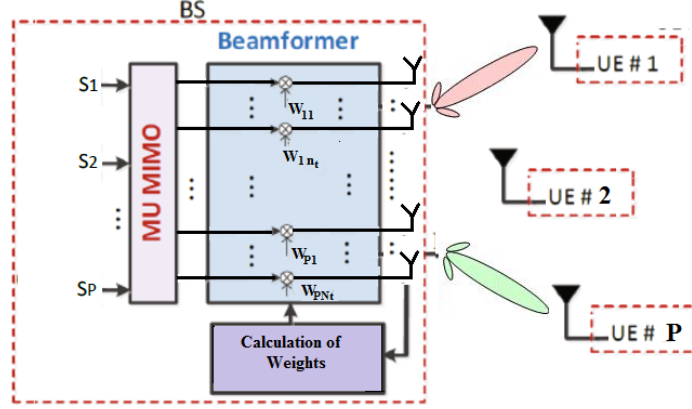


**Figure III.1** — Downlink scheme: base station with  $N_t$  antenna communicating with  $P$  users

As shown in Fig.III.1, the  $P \times 1$  information data vector  $\mathbf{s}$  is weighted by a set of beamforming coefficients to generate the  $N_t \times P$  matrix  $\mathbf{W}$ , as expressed by the following equation:

$$\mathbf{x} = \mathbf{W}\mathbf{s} \quad (\text{III.1})$$

The aims of this work is to derive the beamformer coefficient  $\mathbf{W}$  using Oblique Projection (OP) incorporated with Zero Forcing and apply it as precoder at the base station. Linear precoding presented in (III.1) creates a transmission vector  $\mathbf{x}$  at the base station of the  $l^{th}$  cell. Before going through the derivation of the precoder coefficients, the data model of the received signal by the BS can be written as follows:

$$\mathbf{y}_{l,n_t} = \sum_{i=1}^L \sum_{p=1}^P h_{i,l,n_t}^* \mathbf{x}_{i,p} + \mathbf{n}_{l,n_t} \quad (\text{III.2})$$

Where  $\mathbf{y}_{l,n_t}$  denotes the  $N_t \times 1$  received vector of the  $P$  users in the  $i^{th}$  cell and  $\mathbf{n}_{l,n_t}$  is the  $N_t \times 1$  additive white Gaussian noise vector (AWGN) with zero mean and variance of  $\sigma^2/2$  on each of its real and imaginary elements. The term  $h_{i,l,p}$  denotes the  $N_t \times 1$  channel coefficient element from the BS of the  $p^{th}$  user in the  $i^{th}$  cell.

The equation (III.2) can be rewritten as:

$$\mathbf{y}_{l,n_t} = \underbrace{\sum_{p=1}^P h_{i,l,n_t}^* \mathbf{x}_{l,p}}_{\mathbf{a}_{l,n_t}} + \underbrace{\sum_{j=1, j \neq l}^L \sum_{p=1}^P h_{j,p,n_t}^* \mathbf{x}_{j,p}}_{\mathbf{b}_{j,n_t}} + \mathbf{n}_{l,n_t} \quad (\text{III.3})$$



Letting

$$\mathbf{Y}_l = [\mathbf{y}_{l1} \ \mathbf{y}_{l2} \ \cdots \ \mathbf{y}_{lN_t}]^T,$$

$$\mathbf{N}_l = [\mathbf{n}_{l1} \ \mathbf{n}_{l2} \ \cdots \ \mathbf{n}_{lN_t}]^T,$$

and

$$\mathbf{H}_{jl} = \begin{bmatrix} h_{j,l,1,1} & \cdots & h_{j,l,N_t,1} \\ \vdots & \ddots & \vdots \\ h_{j,l,1,P} & \cdots & h_{j,l,N_t,P} \end{bmatrix} \quad (\text{III.4})$$

The channel coefficients presented in equation (III.4) are resulting from the combined effects of fast fading, geometric attenuation and log-normal shadow fading [102]. We suppose that the channel estimation pertaining to the  $P$  users is known at the base station side through the feedback channel from the receiver to the transmitter, hence the channel state information (CSI) is available at the transmitter. This is made possible since the system is operating in time division duplexing (TDD), therefore rendering the channels reciprocal. Moreover, We assume the base stations share the channel state information of the line and non line of sight links, obtained from the users through feedback channels [103, 104, 105, 106]. The availability of channel state information allows BSs to coordinate beamforming directions.

Referring to equation (III.3) and using the CSI available at BSs, this latter can be rewritten as:

$$\mathbf{Y}_l = \underbrace{\begin{bmatrix} \mathbf{A} & \mathbf{B} \end{bmatrix}}_{\mathbf{H}} \underbrace{\begin{bmatrix} \mathbf{X}_A & 0 \\ 0 & \mathbf{X}_B \end{bmatrix}}_{\mathbf{X}_e} + \mathbf{N}_l \quad (\text{III.5})$$

Where the matrices  $\mathbf{A} = [\mathbf{a}_{l,1} \ \mathbf{a}_{l,2} \ \cdots \ \mathbf{a}_{l,n_t}]$  and  $\mathbf{B} = [\mathbf{b}_{j,1} \ \mathbf{b}_{j,2} \ \cdots \ \mathbf{b}_{j,n_t}]$  contain the elements of  $\mathbf{h}_{l,i,p}$  and  $\mathbf{h}_{j,i,p}$  which correspond to the desired and undesired users from  $l^{th}$  and  $j^{th}$  cells, respectively. The matrices  $\mathbf{X}_A = [\mathbf{x}_{\mathbf{a}_{j,1}} \ \mathbf{x}_{\mathbf{a}_{j,2}} \ \cdots \ \mathbf{x}_{\mathbf{a}_{l,P}}]$  and  $\mathbf{X}_B = [\mathbf{x}_{\mathbf{b}_{j,1}} \ \mathbf{x}_{\mathbf{b}_{j,2}} \ \cdots \ \mathbf{x}_{\mathbf{b}_{j,P}}]$  hold the users signal i.e  $\mathbf{x}_{l,p}$  and  $\mathbf{x}_{j,p}$  corresponding to the  $l^{th}$  and  $j^{th}$  cells, respectively. Furthermore, the vectors  $\mathbf{a}_{l,n_t}$ ,  $\mathbf{b}_{l,n_t}$ ,  $\mathbf{x}_{\mathbf{a}_{l,P}}$  and  $\mathbf{x}_{\mathbf{b}_{j,P}}$  are presented in (III.3). Concatenating the columns of  $\mathbf{A}$  and  $\mathbf{B}$ , into a sole matrix  $\mathbf{H}$ , equation (III.5) becomes:

$$\mathbf{Y}_l = \mathbf{H}\mathbf{X}_e + \mathbf{N} \quad (\text{III.6})$$

The aims of the extraction of the so mentioned matrices are used to derive the beamforming coefficient and main step are explained in the next section.

### III.4 Proposed beamforming scheme

To separate the interference from the desired user by oblique projection, the next key step is to construct the space  $\mathbf{V}$  and its subspace  $\mathbf{A}$  and  $\mathbf{B}$ , respectively. Let us define:

$$\mathbf{V} = \text{span}\{\mathbf{h}_1, \mathbf{h}_2, \dots, \mathbf{h}_P\} \quad (\text{III.7})$$

where  $\text{span}\{.\}$  denotes the column spanned space. Assume that  $\langle \mathbf{A} \rangle$  and  $\langle \mathbf{B} \rangle$  are two subspaces in the space  $\mathbf{V}$ . Then, let us define

$$\langle \mathbf{A} \rangle = \text{span}\{\mathbf{h}_l\} \quad (\text{III.8})$$

$$\begin{aligned} \langle \mathbf{B} \rangle &= \mathbf{V} - \langle \mathbf{A} \rangle \\ &= \text{span}\{\mathbf{h}_i, \quad i = 1, \dots, P; i \neq l\} \end{aligned} \quad (\text{III.9})$$

In the next section, we will describe the mathematical and application to our problem.

#### III.4.1 Mathematics of oblique projection (OP)

In this section, we remind the reader about the principle of projections for both the cases of the usually-adopted orthogonal projection and the oblique projection used in this chapter. As it is commonly known, oblique projections matrices refer to the ones that are not orthogonal. In this framework, the desired signal space is referred to us as the range space, while the interference is termed as the null space. Furthermore, orthogonal projections are represented as  $\mathbf{P}_H$  with a single subscript indicating the range, whereas the oblique projections are represented as  $\mathbf{O}_{AB}$  with a double subscript referring to the range and the null spaces, respectively [96, 107]. It is worthy to remind the reader that an orthogonal projection has a null space that is orthogonal to its range.

Projection matrices that are not orthogonal are referred to as oblique projections. Oblique projections are idempotent but not symmetric [108]. For an orthogonal projection  $\mathbf{P}_H$  whose range is  $\langle A \rangle$  and whose null space is  $\langle G \rangle = \langle A \rangle^\perp$ . However, For an oblique projection  $\mathbf{O}_{AB}$  whose range is  $\langle A \rangle$  and whose null space is  $\langle B \rangle$ .

We can build an orthogonal projector whose range is  $\langle H \rangle^\perp$  by :

$$\mathbf{P}_H = \mathbf{H}(\mathbf{H}^H \mathbf{H})^{-1} \mathbf{H}^H \quad (\text{III.10})$$

The assumption on the column full rank of  $\mathbf{H}$  presented in (III.6), is valid since  $N_r + P < N_t$  is satisfied in massive MIMO context. Thus substituting the formula (III.10) on  $\mathbf{H}$

$$\mathbf{P}_{A \ B} = \begin{pmatrix} \mathbf{A} & \mathbf{B} \end{pmatrix} \begin{pmatrix} \mathbf{A}^H \mathbf{A} & \mathbf{A}^H \mathbf{B} \\ \mathbf{B}^H \mathbf{A} & \mathbf{B}^H \mathbf{B} \end{pmatrix}^{-1} \begin{pmatrix} \mathbf{A}^H \\ \mathbf{B}^H \end{pmatrix} \quad (\text{III.11})$$

### III.4.2 Application of oblique projection to our problem

The proposed solution should be a decomposition of the sum vector into different components of each transmitted signal, to overcome the interference among different undesired users from other cells. In other words, the oblique projection operator  $\mathbf{O}_{AB}$  projects the observation vector  $\mathbf{y}$  into the desired signature space  $\langle \mathbf{A} \rangle$  and nulls the undesired signatures space  $\langle \mathbf{B} \rangle$  as depicted in Fig.III.2, thus:

$$\mathbf{O}_{AB} \mathbf{A} = \mathbf{A} \quad \mathbf{O}_{AB} \mathbf{B} = 0 \quad (\text{III.12})$$

Referring to (III.11), we may decompose this orthogonal projection into two oblique parts

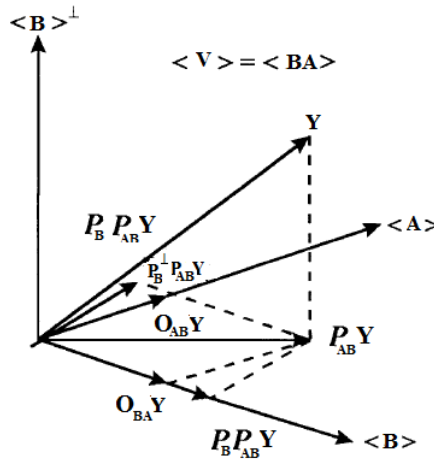


Figure III.2 — Oblique subspace projection geometry

as follows [107, 108]

$$\begin{aligned} \mathbf{P}_{A B} &= \mathbf{O}_{A B} + \mathbf{O}_{B A} \\ \mathbf{O}_{A B} &= \begin{pmatrix} \mathbf{A} & \mathbf{0} \end{pmatrix} \begin{pmatrix} \mathbf{A}^H \mathbf{A} & \mathbf{A}^H \mathbf{B} \\ \mathbf{B}^H \mathbf{A} & \mathbf{B}^H \mathbf{B} \end{pmatrix}^{-1} \begin{pmatrix} \mathbf{A}^H \\ \mathbf{B}^H \end{pmatrix} \end{aligned} \quad (\text{III.13})$$

$$\mathbf{O}_{B A} = \begin{pmatrix} \mathbf{0} & \mathbf{B} \end{pmatrix} \begin{pmatrix} \mathbf{A}^H \mathbf{A} & \mathbf{A}^H \mathbf{B} \\ \mathbf{B}^H \mathbf{A} & \mathbf{B}^H \mathbf{B} \end{pmatrix}^{-1} \begin{pmatrix} \mathbf{A}^H \\ \mathbf{B}^H \end{pmatrix} \quad (\text{III.14})$$

These equations determine the ranges for  $\mathbf{O}_{AB}$  and  $\mathbf{O}_{BA}$  to be  $\langle A \rangle$  and  $\langle B \rangle$ , respectively, and the null spaces to be  $\langle B \rangle$  and  $\langle A \rangle$ , respectively.

We can easily establish that  $\mathbf{O}_{AB}$  and  $\mathbf{O}_{BA}$  are projectors that are idempotent but without the Hermitian propriety [96, 107]. Using the properties of  $2 \times 2$  block matrices, the equation (III.13) can be reformulated as [107]

$$\begin{aligned} \mathbf{O}_{AB} &= \mathbf{A}(\mathbf{A}^H \mathbf{P}_B^\perp \mathbf{A})^{-1} \mathbf{A}^H \\ &\quad - \mathbf{A}(\mathbf{A}^H \mathbf{P}_B^\perp \mathbf{A})^{-1} \mathbf{A}^H \mathbf{B}(\mathbf{B}^H \mathbf{B})^{-1} \mathbf{B}^H \\ &= \mathbf{A}(\mathbf{A}^H \mathbf{P}_B^\perp \mathbf{A})^{-1} \mathbf{A}^H [\mathbf{I} - \mathbf{B}(\mathbf{B}^H \mathbf{B})^{-1} \mathbf{B}^H] \\ &= \mathbf{A}(\mathbf{A}^H \mathbf{P}_B^\perp \mathbf{A})^{-1} \mathbf{A}^H \mathbf{P}_B^\perp \end{aligned} \quad (\text{III.15})$$

Similarly, the other oblique projection  $\mathbf{O}_{BA}$  in (III.14) can be written as

$$\mathbf{O}_{BA} = \mathbf{B}(\mathbf{B}^H \mathbf{P}_A^\perp \mathbf{B})^{-1} \mathbf{B}^H \mathbf{P}_A^\perp \quad (\text{III.16})$$

### III.4.3 Oblique projection zero forcing beamformer

As it is mentioned before, the Zero Forcing-based beamforming coefficient  $\mathbf{W}$  are applied at the transmitter side. Zero-forcing Beamforming (ZF-BF) is a spatial signal processing in multiple antenna wireless devices. The ZF-BF algorithm permits to transmit data to desired users together with nulling out the directions to undesired users. We consider the minimization of transmitted signal [109]:

$$\min_{\mathbf{W}} \mathbf{W}^H \mathbf{R}_S \mathbf{W} \quad (\text{III.17})$$

Where  $\mathbf{R}_S = E \{ \mathbf{S} \mathbf{S}^H \}$  is the array covariance matrix of the transmitted signal.

To avoid the trivial solution  $\mathbf{W} = \mathbf{0}$ , we add some constraints. The equation (III.18) is

used to introduce the constraints about the desired and undesired users. Thus, the first constraint is set to the favored users and the other is fixed so that to cancel the undesired interference.

In other word, we can write

$$\begin{cases} \mathbf{W}^H \mathbf{A} = \mathbf{1}^H \\ \mathbf{W}^H \mathbf{B} = \mathbf{0} \end{cases} \quad (\text{III.18})$$

Equation (III.18) implies that the weight vector  $\mathbf{W}$  lies in the orthogonal complementary subspace of the subspace  $\langle B \rangle$ .

In equation (III.18), the range of  $\mathbf{A}$  define the desired user signal subspace and the range of  $\mathbf{B}$  is the interference subspace. Hence, the orthogonal subspace range of  $(\mathbf{B})^T$  define the interference-free subspace. We note that the orthogonality of the various subspaces representing all the user's signals is not always attainable. Hence,  $\mathbf{A}$  and  $\mathbf{B}$  are not orthogonal.

To deal with this non orthogonality, we should fix the constraint so as to promote the desired signals and null the interference. The equation (III.18) becomes:

$$\begin{cases} \mathbf{W}^H \mathbf{O}_{BA}^\perp \mathbf{A} = \mathbf{f}^H \\ \text{Range}(\mathbf{W}) \subset \text{Null}(\mathbf{B}) \end{cases} \quad (\text{III.19})$$

Where  $\mathbf{f}$  represents the constraint vector. This vector contains ones at the desired users and zeros for the users outside a considered cell.

The optimal closed-form solution of (III.17) under constraints (III.19) is given by the Lagrangian-multiplier method where its equation is given by:

$$\mathbf{W}^H \mathbf{R}_S \mathbf{W} + \lambda (\mathbf{W}^H \mathbf{O}_{BA}^\perp \mathbf{A} - \mathbf{f}^H) \quad (\text{III.20})$$

We differentiate the equation (III.20) with respect to  $\mathbf{W}^H$  then we get the weight coefficient  $\mathbf{W}$  as

$$\mathbf{W} = -\mathbf{R}_S^{-1} \lambda (\mathbf{O}_{BA}^\perp \mathbf{A}) \quad (\text{III.21})$$

By using the constraint of (III.19) and the weight coefficients of equation (III.21). We get the Lagrangian-multiplier vector  $\lambda$  by:

$$\lambda = -\mathbf{R}_s ((\mathbf{O}_{BA}^\perp \mathbf{A})^H)^{-1} \mathbf{f} (\mathbf{O}_{BA}^\perp \mathbf{A})^{-1} \quad (\text{III.22})$$

Finally, the expression of  $\mathbf{W}^H$  is given by:

$$\mathbf{W}^H = \mathbf{f}^H (\mathbf{O}_{BA}^\perp \mathbf{A})^{-1} \quad (\text{III.23})$$

The resulted coefficients in (III.23) are fed into (III.1) forming the transmitted signal. To verify the effectiveness of the proposed oblique projector zero forcing beamformer (OPZFBF), the next section is reserved for more details.

#### III.4.4 Achievable rate

Without loss of generality, we assume that the intra-cell interference is fully suppressed and consider the case of users simultaneously communicating in cell  $l$ . In this section we derive the achievable rate equation with the proposed oblique projector zero forcing beamformer (OPZFBF). For the  $l^{\text{th}}$  desired user signal, the energy is given by

$$E[|\mathbf{h}_l^T \mathbf{w}_l \mathbf{s}_l|^2] = |\mathbf{h}_l^T \mathbf{w}_l|^2 E[|\mathbf{s}_l|^2] \quad (\text{III.24})$$

Also, for the second term in (III.3), the energy is defined in the same manner as

$$E \left[ \left| \sum_{l \neq i, i=1}^P \mathbf{h}_l^T \mathbf{w}_i \mathbf{s}_i + \mathbf{n}_l \right|^2 \right] = \sum_{l \neq i, i=1}^P |\mathbf{h}_l^T \mathbf{w}_i|^2 E[|\mathbf{s}_i|^2] + E[|\mathbf{n}_l|^2] \quad (\text{III.25})$$

From Shannon theorem, the achievable rate of the  $l^{\text{th}}$  user in MU-MIMO context is

$$\begin{aligned} R_l &= E \left[ \log_2 \left( 1 + \frac{|\mathbf{h}_l^T \mathbf{w}_l|^2}{\sum_{l \neq i, i=1}^P |\mathbf{h}_i^T \mathbf{w}_i|^2 + \frac{E[|\mathbf{n}_l|^2]}{E[|\mathbf{s}_l|^2]}} \right) \right] \\ &= E \left[ \log_2 \left( 1 + \frac{|\mathbf{h}_l^T ((\mathbf{O}_{BA}^\perp \mathbf{A})^H)^{-1} \mathbf{f}_l|^2}{\sum_{l \neq i, i=1}^P |\mathbf{h}_i^T ((\mathbf{O}_{BA}^\perp \mathbf{A})^H)^{-1} \mathbf{f}_i|^2 + \frac{E[|\mathbf{n}_l|^2]}{E[|\mathbf{s}_l|^2]}} \right) \right] \end{aligned} \quad (\text{III.26})$$

In the last expression we assumed the energy of all user's signal have same energy, so

$$E[|\mathbf{s}_1|^2] = \dots = E[|\mathbf{s}_l|^2] = \dots = E[|\mathbf{s}_P|^2] \quad (\text{III.27})$$

Using expression presented in (III.23) on the achievable rate equation to eliminate the existing interference term, so we can rewrite (III.26) as:

$$R_l = E \left[ \log_2 \left( 1 + \frac{|\mathbf{h}_l^T ((\mathbf{O}_{BA}^\perp \mathbf{A})^H)^{-1} \mathbf{f}_l|^2}{\frac{E[|\mathbf{n}_l|^2]}{E[|s_l|^2]}} \right) \right] \quad (\text{III.28})$$

### III.5 Simulation results

**Table III.1** — Simulation parameters for massive MIMO system

Parameters	Values
Channel	Geometric channel model
Cell number	3 cell
$D_{max}$	1500
$d_0$	100 m
$\alpha$	0.3
Number of users	20 and 30
Fading type	BlockFading
Channel realization	1.000
Antenna schemes	$50 \times 20$ , $50 \times 30$ , $40 \times 20$ , $60 \times 20$ and $80 \times 20$ schemes
Transmit modes	OP beamforming, transmit MMSE, MRT

In this section, the performance of the proposed ZFOPBF beamformer architecture is investigated by varying a set of parameters and study their impact on the performance. The results are presented along with the system incorporating the conventional beamformers which is taken as a reference. The main parameters which are of interest to our simulations are listed in Table III.1. The average sum rate for different transmit antenna configurations and different number of users as a function of the average SNR is investigated. Again, we consider the presence of  $P$  users and the constraint given in equation (III.18) with the sum rate function:  $f(SINR_1, SINR_2, \dots, SINR_P)$  with  $SINR_p$  referring to the signal-to-interference-plus-noise ratio for each user. The simulation results are averaged over random complex Geometric channel realization  $h_k$ , and the SNR is measured as  $\frac{P_x}{\sigma^2}$  where  $\sigma^2$  and  $P_x$  are the variance of the noise and the power of the signal, respectively.

On the other hand, two algorithms reported in [110] are compared in terms of the achievable sum rate along with the proposed one, namely the transmit MMSE beamforming and maximum ratio transmitter (MRT) beamformer. This performance is studied

when varying the number of users and transmit antenna in the massive MIMO system.

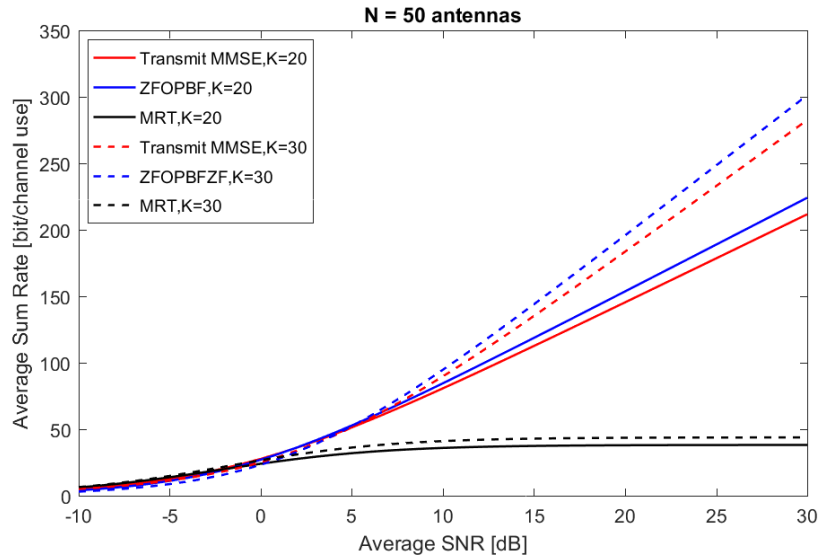


**Figure III.3** — Average sum rate with  $N = 50$  transmit antennas in the presence of  $K = 20$  and  $K = 30$  users as a function of the average SNR

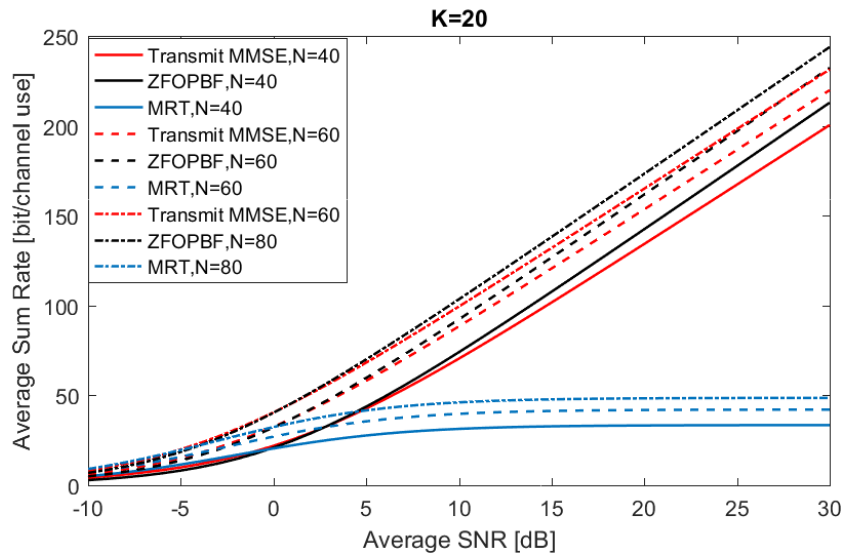


**Figure III.4** — Average sum rates for different transmit antenna configurations and  $K = 20$  users as a function of the average SNR

The simulation results illustrated in Figures III.3 and III.4, show that the proposed ZFOPBF algorithm highlight the performance of our system compared to MRT and MMSE schemes when increasing the number of users and transmit antennas for every value of SNR. In other words, the ZFOPBF technique has outstanding performance



advantages over other conventional beamforming techniques. We can explain this gain by using the oblique projector to separate the interference in the received signal. Furthermore, we combine the oblique projector with zero forcing beamformer to maximize the power of desired users using the cooperation between Base Station (BS) to suppress the inter-cell interference.

## Chapter IV

# PARAMETER CHANNEL ESTIMATION FOR PILOT CONTAMINATION MITIGATION IN MASSIVE MIMO SYSTEM

## IV.1 Introduction

The tremendous development of communication systems is one of the main features of the last decades. These systems have become omni-present and reach virtually every home in large parts of the world. Wireless communication systems have constantly evolved in terms of data rates, network capacity, energy efficiency, spectral efficiency, quality of service and mobility. These requirements are even more important for the wireless communication beyond 4G (B4G) and 5G. For channel estimation, orthogonal pilot symbols are used (a reference signal known by the transmitter and the receiver). In the last few years, pilot contamination (PC) problem in Multicell Massive MIMO systems attracted a great attention from the research community, where PC is defined by re-using the same band of frequencies with different factors among the cells. Hence, the signals from terminals in other cells are combined coherently at the base station.

In this chapter, we are interested in some possible estimation techniques for a future 5G system in the absence and presence of pilot contamination. For this, we consider a massive MIMO system that uses the frequency band around 6 GHz. Afterward, we describe the system model and the estimated algorithms used for the channel parameter estimation in the presence and absence of pilot contamination phenomena. In the rest of the chapter, simulation results and their comments are drawn.

## IV.2 Pilot contamination in Massive MIMO

### IV.2.1 Channel estimation and pilot contamination definition

The estimation of the transmission channel is a key point of digital communications, making it possible to improve greatly the exchanges due to the knowledge of this one. In Massive MIMO, this information is very important because it allows to perform the so-called precoding processing whose role is to form beams focusing energy to or around users of the cell. A poor estimate will therefore cause a significant degradation of the ability of such a system to focus energy.

In the past, it was widely assumed that transmitter and receiver knew the channel perfectly. In fact, some authors still dedicate some of their research to study scenarios where full and error-free channel knowledge is available. However, this leads to unattainable results since in real systems, this information is not given away for free. Therefore, channels must be estimated and the quality of this procedure conditions highly the overall

performance. This is why current investigations focus on this assumption and try to give suitable and feasible solutions [9, 111]. In wireless communication systems, the BS needs to estimate the CSI of each user using pilot sequences, and then use the estimated CSI to detect uplink data and to make precoders for downlink transmissions. To get good estimates of CSI, the number of orthogonal pilot sequences should equal to the number of users. In other words, the number of orthogonal pilot sequences in the system should ideally be  $K \times L$ , where  $K$  is the number of users in each cell,  $L$  is the number of cells in the system. In order to maintain orthogonality of each pilot sequence, the length of the sequence must increase, and the time for transmitting the pilot sequence also increases. However, in a practical wireless system, the coherence interval (the CSI keeps the same in the coherence interval) is limited, and only a fraction of this interval can be devoted to pilot symbols, the rest being reserved for data. So the length of pilot sequence can not be too long, which implies that the maximum number of orthogonal pilot sequences is limited [15]. However, for multi-cell multi-user Massive MIMO systems, since the number of users in the system is very large (all users send pilot sequences to BSs simultaneously), the required number of orthogonal pilot sequences are also large. Therefore, the practical number of available orthogonal pilot sequences are much less than the requirement. Moreover, we want to obtain the maximum sum data-rate of the cell, so we assign orthogonal pilot sequences to users in the same cell. Therefore, the same or partially correlated pilot sequences are reused in different cells.

Since the pilot sequences are transmitted at the same time and frequency, the BS receives the linear combination of all pilot sequences. If these pilot sequences are orthogonal with each other, then the BS can obtain good estimates of the CSI based on these unique pilot sequences. However, if two or several cells share the same pilot sequence or different cells use non-orthogonal pilot sequences, then the BS can not distinguish the pilot sequence of the desired cell. Therefore, the estimate of the desired CSI at the BS will be contaminated by these same or non-orthogonal pilot sequences from adjacent cells. These incorrect estimates of CSI will then have negative effect on downlink beamforming and overall system performance, which termed as pilot contamination [112]. What is worse, this interference caused by pilot contamination will not diminish even when the number of antennas at the BS increases. It has been proven that in Massive MIMO systems, with the help of numerous antennas, other detrimental factors such as noise and fading can be mitigated by increasing the number of antennas at the BS. Thus the main factor which limits Massive MIMO system performance is the pilot contamination.

Figure IV.1 describes the pilot contamination in Massive MIMO systems. In Fig.IV.1 ev-

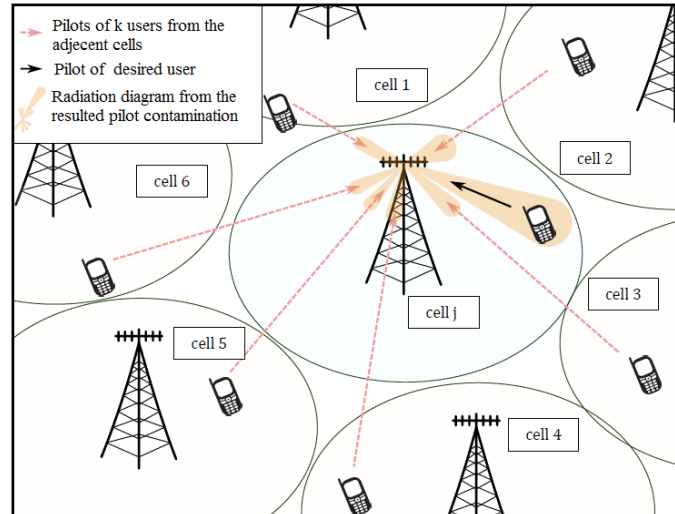


*Figure IV.1* — Illustration of massive MIMO system with pilot contamination problem in multi-cells.

ery BS can receive the combination of all pilot sequences. Take the 1st BS as an example, it receives the combination of all pilot sequences from all users. If there is one user sends P1 pilot sequence in each cell, then the 1st BS can receives the combination of P1 pilot sequence. The channel estimate of user A at the 1st BS is contaminated by those users sharing the same pilot sequence located in adjacent cells.

Pilot contamination can negate the theoretical benefits of increased system capacity, improved energy efficiency and other benefits from having a large number of antennas at the BS. In summary, pilot contamination seriously affects the performance of Massive MIMO systems. Therefore, the problem of pilot contamination must be dealt with.

In what follow, we assume that there is no interference between adjacent cells during the channel estimation, i.e., the BS of the cell receives only the pilot symbols emitted by users inside the cell with a significant power level. We have two possible systems are considered for this study.

To study the channel without pilot contamination in this system, we use the unitary 2D-ESPRIT algorithm proposed in [113]. It's an algorithm that provides joint estimation of arrival and departure angles with automatic coupling from the estimation of the spatial signature proposed in [114]. In this algorithm, the spatial signature is parameterized in terms of AOA and AOD, assuming the use of uniform linear array.

### IV.2.2 Channel estimation without pilot contamination

In this section, we are interested in the 5G candidate system to study the estimation of the channel without pilot contamination in the 6 GHz band. We consider a cellular network where each cell represents a massive MU-MIMO system. BS uses its knowledge of the channel transmission to create separate spatially data streams for each terminal. The spectral efficiency gain obtained by this spatial multiplexing depends on the antenna arrays size used and the accuracy of the channel estimation at the BS level. Therefore, the channel estimation is fundamental for the system.

#### IV.2.2.1 System model

We consider a single cell consisting of a BS provided with an antenna array of  $M$  elements and  $K$  users equipped with an antenna array of  $N$  elements ( $N < K < M$ ). The antenna arrays are assumed to be linear and uniform with an inter-element spacing of  $\lambda/2$ . We consider that the system is operating in TDD, therefore rendering the channels reciprocal. For  $J$  samples, the received signal  $\mathbf{X}[n] \in \mathbb{C}^{J \times N}$  is given by [113]:

$$\mathbf{X}[n] = \mathbf{S}[n]\mathbf{A}[n] + \mathbf{W}[n] \quad (\text{IV.1})$$

With:  $\mathbf{S}[n] \in \mathbb{C}^{J \times M}$  contains the transmitted pilot symbols.

$\mathbf{A}[n] \in \mathbb{C}^{M \times N}$  is the spatial signature matrix.

$\mathbf{W}[\mathbf{n}] \in \mathbb{C}^{J \times N}$  is the zero mean complex Gaussian (ZMCG) matrix with variance  $\sigma^2$ . We also define:

$$\mathbf{A}_\phi = \begin{pmatrix} 1 & \dots & 1 \\ \exp(j\pi \sin \phi_1) & \dots & \exp(j\pi \sin \phi_P) \\ \vdots & & \vdots \\ \exp(j\pi(N-1) \sin \phi_1) & \dots & \exp(j\pi(N-1) \sin \phi_P) \end{pmatrix} \quad (\text{IV.2})$$

$$\mathbf{A}_\theta = \begin{pmatrix} 1 & \dots & 1 \\ \exp(j\pi \sin \theta_1) & \dots & \exp(j\pi \sin \theta_P) \\ \vdots & & \vdots \\ \exp(j\pi(N-1) \sin \theta_1) & \dots & \exp(j\pi(N-1) \sin \theta_P) \end{pmatrix} \quad (\text{IV.3})$$

$$\mathbf{\Delta}_\alpha = \text{diag}([\alpha_1, \dots, \alpha_P]^T) \quad (\text{IV.4})$$

$$\mathcal{A}[n] = \mathbf{A}_\phi \mathbf{\Delta}_\alpha \mathbf{A}_\theta^T \in \mathbb{C}^{M \times N} \quad (\text{IV.5})$$

To extract the AOA and AOD from the different paths from the spatial signature matrix, we reformulate the model of the signal given in the equation (IV.1). We note  $e_{i,j} \in \mathbb{R}^j, i = 1, \dots, j$  as vector of dimension  $j$  with one's for  $i^{\text{eme}}$  elements and zeros otherwise. Thus, the transformation matrix is given by:

$$\mathbf{\Gamma} = \begin{pmatrix} \mathbf{I}_L \otimes e_{1,M}^T \\ \vdots \\ \mathbf{I}_L \otimes e_{M,M}^T \end{pmatrix} \in \mathbb{R}^{ML \times ML} \quad (\text{IV.6})$$

It follows that:

$$\mathbf{S}(\tau) = \mathbf{S}(\tau) \mathbf{\Gamma} \quad (\text{IV.7})$$

$$\mathcal{A}[n] = \mathbf{\Gamma}^T \mathbf{A}[n] \quad (\text{IV.8})$$

This reformulation presented in [113] is developed for the case of a model of the channel consisting of  $L$  diffusers presented between the transmitter and the receiver each of which contributes with  $l$  paths so that the sum  $\sum_{i=1}^L \ell_i = 1$  represents the total number of propagation paths. In our work, we use a geometric model with  $P$  paths between the transmitter and the receiver. This is simply equivalent to considering a single broadcaster at  $P$  paths in the previous reformulation. Therefore, the signal model used for the estimation problem is simplified by:

$$\mathbf{X}[n] = \mathbf{S}(n) \mathcal{A}[n] + \mathbf{W}[n] \quad (\text{IV.9})$$

#### IV.2.2.2 Parameters channel estimation

The shift invariance structure of the decomposition  $\mathbf{A}[n] = \mathbf{A}_\phi \mathbf{\Delta}_\alpha[n] \mathbf{A}_\theta^T$  is used to jointly estimate the AOD and AOA by the 2D-UESPRIT algorithm. The main idea is described as follows. For some  $m < N$ , we define the matrix  $\mathbf{A}^i[n], j = 1, \dots, m$  as the constructed matrix of the  $j^{\text{th}}$  to the  $(N - m + j)^{\text{th}}$  column of the matrix  $\mathbf{A}[n]$ . We construct the Henkel

matrix  $\mathcal{A}_H[n]$  by stacking  $m$  copies of  $\mathbf{A}^j[n]$ , so the Hankel matrix is given by:

$$\mathcal{A}_H[n] = \begin{pmatrix} \mathbf{A}^1[n] \\ \vdots \\ \mathbf{A}^m[n] \end{pmatrix} \in \mathbb{C}^{Mm \times (N-m+1)} \quad (\text{IV.10})$$

We also define the two matrices:

$$\begin{aligned} \dot{\mathbf{A}}_\theta &= \begin{pmatrix} 1 & \dots & 1 \\ \exp(j\pi \sin \theta_1) & \dots & \exp(j\pi \sin \theta_P) \\ \vdots & & \vdots \\ \exp(j\pi(m-1) \sin \theta_1) & \dots & \exp(j\pi(m-1) \sin \theta_P) \end{pmatrix} \\ \ddot{\mathbf{A}}_\theta &= \begin{pmatrix} 1 & \dots & 1 \\ \exp(j\pi \sin \theta_1) & \dots & \exp(j\pi \sin \theta_P) \\ \vdots & & \vdots \\ \exp(j\pi(N-m) \sin \theta_1) & \dots & \exp(j\pi(N-m) \sin \theta_P) \end{pmatrix} \end{aligned} \quad (\text{IV.11})$$

So, the Hankel matrix can be expressed by:

$$\mathcal{A}_H[n] = \mathcal{A}_\phi \Delta_\alpha[n] \ddot{\mathbf{A}}_\theta^T \quad (\text{IV.12})$$

The following selection matrices are defined:

$$\begin{aligned} \mathbf{J}_{1\theta} &= (\mathbf{I}_{m-1}, \mathbf{0}_{m-1}) \\ \mathbf{J}_{x\theta} &= \mathbf{J}_{1\theta} \otimes \mathbf{I}_N \\ \mathbf{J}_{2\theta} &= (\mathbf{0}_{m-1}, \mathbf{I}_{m-1}) \\ \mathbf{J}_{y\theta} &= \mathbf{J}_{2\theta} \otimes \mathbf{I}_N \\ \mathbf{J}_{1\phi} &= (\mathbf{I}_{N-1}, \mathbf{0}_{N-1}) \\ \mathbf{J}_{x\phi} &= \mathbf{I}_m \otimes \mathbf{J}_{1\theta} \\ \mathbf{J}_{2\phi} &= (\mathbf{0}_{N-1}, \mathbf{I}_{N-1}) \\ \mathbf{J}_{y\phi} &= \mathbf{I}_m \otimes \mathbf{J}_{2\theta} \end{aligned} \quad (\text{IV.13})$$



Where  $\mathbf{0}_K \in \mathbb{R}^K$  denotes a vector filled with zeros of dimension K. We apply these selection matrices to the equation (IV.10) :

$$\begin{cases} \mathbf{X}_\phi[n] &= \mathbf{J}_{x\phi}\mathcal{A}_H[n] \\ \mathbf{Y}_\phi[n] &= \mathbf{J}_{y\phi}\mathcal{A}_H[n] \end{cases} \quad (\text{IV.14})$$

The decomposition of these matrices gives us:

$$\begin{cases} \mathbf{X}_\theta[n] &= \mathbf{J}_{x\theta}\mathcal{A}_H[n] \\ \mathbf{Y}_\theta[n] &= \mathbf{J}_{y\theta}\mathcal{A}_H[n] \end{cases} \quad (\text{IV.15})$$

With  $\mathcal{A}_{x\phi} = \mathbf{J}_{x\phi}\mathcal{A}_\phi$  and  $\mathcal{A}_{x\theta} = \mathbf{J}_{x\theta}\mathcal{A}_\theta$ .  $\mathbf{U}$  and  $\mathbf{V}$  denote the two diagonal matrices  $\mathbf{U} = (\exp(j\pi \sin \theta_1), \dots, \exp(j\pi \sin \theta_P))$  and  $\mathbf{V} = (\exp(j\pi \sin \phi_1), \dots, \exp(j\pi \sin \phi_P))$ , respectively.

The 2D-ESPRIT algorithm is then applied to estimate the elements of matrices  $\mathbf{U}$  and  $\mathbf{V}$  from which AOD and AOA can be calculated directly. From the equation (IV.15), we write:

$$\begin{aligned} \mathbf{Y}_\phi - \lambda\mathbf{X}_\phi &= \mathcal{A}_{x\phi}(\mathbf{V} - \lambda\mathbf{I}_P)\Delta_\alpha[n]\ddot{\mathbf{A}}_\theta^T \\ \mathbf{Y}_\theta - \lambda\mathbf{X}_\theta &= \mathcal{A}_{x\theta}(\mathbf{U} - \lambda\mathbf{I}_P)\Delta_\alpha[n]\ddot{\mathbf{A}}_\theta^T \end{aligned} \quad (\text{IV.16})$$

This eigenvalue decomposition problem can be solved by looking for the non-zero eigenvalues of the two matrices  $\mathbf{X}_\theta^\dagger\mathbf{Y}_\theta$  and  $\mathbf{X}_\phi^\dagger\mathbf{Y}_\phi$ . Since these two matrices have the same eigenvectors because of the factor  $\ddot{\mathbf{A}}_\theta^T$ , the correct matching is obtained by the following joint diagonalization:

$$\begin{aligned} \mathbf{X}_\theta^\dagger\mathbf{Y}_\theta &= \mathbf{T}^{-1}\mathbf{U}_i\mathbf{T} \\ \mathbf{X}_\phi^\dagger\mathbf{Y}_\phi &= \mathbf{T}^{-1}\mathbf{V}_i\mathbf{T} \end{aligned} \quad (\text{IV.17})$$

To improve the performance of the algorithm, techniques for extending observed data such as spatial smoothing and forward backward averaging (FBA) [115] are applied to the matrix  $\mathcal{A}_H[n]$ . This is followed by a processing that transforms the complex matrix into a real-valued matrix. In the following steps, the complete procedure for the joint estimation of AOA and ODA by these techniques is detailed.

#### A- Step 1: Spatial smoothing and FBA

The spatial smoothing [116] was originally proposed to solve the problem of estimating AOA in the presence of coherent signals. Spatial smoothing makes it possible to decorrelate the sources at the reception. This method is based on subdivision of the main reception network reception to sub-networks and averaging matrices of sub-network. In addition to classical assumptions about noises (uncorrelated with transmitted signals, uncorrelated between them with equal power on all sensors), this method assumes that the receiving antenna is linear and with equidistant sensors. It is obvious that the spatial smoothing method increases the time and computing resources. However, this disadvantage is depend on the performances of the results that one wishes to obtain [117].

The ESPRIT algorithm employs shifted and identical sub-networks. The FBA uses the prior information on sub-network symmetry to increase the number of available data vectors and to decorrelate highly correlated signals. The most important advantage of the combination of the FBA and the ESPRIT algorithm is the reduction of computational complexity. For the integers  $2 \leq m_1 \leq N$  and  $1 \leq m_2 \leq M - 1$ , we define the matrix:

$$\mathcal{A}^{(r,l)}[n] = \begin{pmatrix} \mathcal{A}_{r,l}[n] & \dots & \mathcal{A}_{r,N-m_1+l}[n] \\ \vdots & & \vdots \\ \mathcal{A}_{M-m_2+r,l}[n] & \dots & \mathcal{A}_{M-m_2+r,N-m_1+l}[n] \end{pmatrix}, 1 \leq r \leq m_2, 1 \leq l \leq m_1, \quad (\text{IV.18})$$

And we redefined the hankel matrix as:

$$\mathcal{A}_H[n] = \begin{pmatrix} \mathcal{A}^{(1,1)}[n] & \dots & \mathcal{A}^{(m_2,1)}[n] \\ \vdots & & \vdots \\ \mathcal{A}^{(1,m_1)}[n] & \dots & \mathcal{A}^{(m_2,m_1)}[n] \end{pmatrix} \in \mathbb{C}^{m_1(M-m_2+1) \times m_2(N-m_1+1)} \quad (\text{IV.19})$$

Where the matrix  $\mathbf{\Pi}_N$  is defined as the identity matrix  $\mathbf{I}_N$  with an inverted order of lines. The extension of the new Hankel matrix by introducing the Digital Beamforming (BFA) operation is obtained by:

$$\begin{aligned} \mathcal{A}_{c,H}[n] &= (\mathcal{A}_H[n], \mathbf{\Pi}_{m_1(M-m_2+1)} \mathcal{A}_H^*[n]) \in \mathbb{C}^{m_1(M-m_2+1) \times 2m_2(N-m_1+1)} \\ &= (\mathcal{A}_\phi \Delta_\gamma[n] \ddot{\mathbf{A}}_\theta^T, \mathbf{\Pi}_{m_1(M-m_2+1)} \mathcal{A}_\phi^* \Delta_\gamma^*[n] (\ddot{\mathbf{A}}_\theta^T)^*) \end{aligned} \quad (\text{IV.20})$$

Where  $\ddot{\mathbf{A}}_\theta^T = (\ddot{\mathbf{A}}_\theta^T, \mathbf{V} \ddot{\mathbf{A}}_\theta^T, \dots, \mathbf{V}^{m_2-1} \ddot{\mathbf{A}}_\theta^T) \in \mathbb{C}^{P \times m_2(N-m_1+1)}$

We also show that

$$\begin{aligned}
\Pi_{m_1(M-m_2+1)} \mathcal{A}_\phi^* &= (\Pi_{m_1}(\dot{\mathbf{A}}_\theta)^*) \diamond (\Pi_{m_1(M-m_2+1)} \mathbf{A}_\phi^*) \\
&= (\dot{\mathbf{A}}_\theta \mathbf{U}^{-(m_1-1)}) \diamond (\mathbf{A}_\phi \mathbf{V}^{-(M-m_2)}) \\
&= (\dot{\mathbf{A}}_\theta \diamond \mathbf{A}_\phi) \mathbf{U}^{-(m_1-1)} \mathbf{V}^{-(M-m_2)} \\
&= (\mathcal{A}_\phi) \mathbf{U}^{-(m_1-1)} \mathbf{V}^{-(M-m_2)} \tag{IV.21}
\end{aligned}$$

$\ddot{\mathbf{A}}_\theta$  and  $\dot{\mathbf{A}}_\theta$  are defined in (IV.11) by replacing  $m$  with  $m_1$ . Substituting the equation (IV.21) in the equation (IV.20), we find:

$$\begin{aligned}
\mathcal{A}_{c,H}[n] &= \mathcal{A}_1 \mathcal{A}_2 \\
\mathcal{A}_1 &= \mathcal{A}_\phi \boldsymbol{\theta}^{-(m_1-1)/2} \boldsymbol{\phi}^{-(M-m_2)/2} \\
&= (\dot{\mathbf{A}}_\theta \boldsymbol{\theta}^{-(m_1-1)/2}) \diamond (\mathbf{A}_\phi \boldsymbol{\phi}^{-(M-m_2)/2}) \\
&\triangleq \bar{\mathbf{A}}_\theta \diamond \bar{\mathbf{A}}_\phi \\
\mathcal{A}_2 &= (\boldsymbol{\theta}^{(m_1-1)/2} \boldsymbol{\phi}^{(M-m_2)/2} \Delta_\gamma[n] \ddot{\mathbf{A}}_\theta^T, \\
&\quad \boldsymbol{\theta}^{-(m_1-1)/2} \boldsymbol{\phi}^{-(M-m_2)/2} \Delta_\gamma^*[n] (\ddot{\mathbf{A}}_\theta^T)^*) \tag{IV.22}
\end{aligned}$$

### B- Step 2: Real processing (non-complex) and reduction of rank

In order to use the 2D-UESPRIT algorithm for joint diagonalization in order to estimate AOA and AOD, real processing (non-complex) is used to transform the matrix  $\mathcal{A}_{c,H}[n]$  to a real-valued matrix using two transform matrices  $\mathbf{T}_L$  defined in [113] as:

$$\begin{aligned}
\mathbf{T}_L &= \mathbf{Q}_{m_1} \otimes \mathbf{Q}_{M+m_2+1} \\
\mathbf{T}_R &= \begin{pmatrix} \mathbf{I}_{m_2(N-m_1+1)} & j\mathbf{I}_{m_2(N-m_1+1)} \\ \mathbf{I}_{m_2(N-m_1+1)} & -j\mathbf{I}_{m_2(N-m_1+1)} \end{pmatrix} \tag{IV.23}
\end{aligned}$$

The two unitary matrices  $\mathbf{Q}_m$  are defined as:

$$\mathbf{Q}_N = \begin{cases} \frac{1}{\sqrt{2}} \begin{pmatrix} \mathbf{I}_K & j\mathbf{I}_K \\ \mathbf{\Pi}_K & -j\mathbf{\Pi}_K \end{pmatrix}, & N = 2K \\ \frac{1}{\sqrt{2}} \begin{pmatrix} \mathbf{I}_K & 0 & j\mathbf{I}_K \\ \mathbf{0}_K^T & \sqrt{2} & \mathbf{0}_k^T \\ \mathbf{\Pi}_K & 0 & -j\mathbf{\Pi}_K \end{pmatrix}, & N = 2K + 1 \end{cases} \tag{IV.24}$$

Due to the conjugated centro-symmetry property of matrices  $\bar{\mathbf{A}}_\theta$ , we will have the two real matrices:

$$\begin{aligned}\mathbf{D}_\theta &= Q_{m_1}^H \bar{\mathbf{A}}_\theta \\ \mathbf{D}_\phi &= Q_{M-m_2+1}^H \bar{\mathbf{A}}_\theta\end{aligned}\quad (\text{IV.25})$$

Therefore,  $\mathcal{A}_1$  and  $\mathcal{A}_2$  become real-valued matrices  $\mathcal{A}_{1,R}$  and  $\mathcal{A}_{2,R}$  by the multiplication on the left and on the right by the transform matrices  $\mathbf{T}_L$  and  $\mathbf{T}_R$  respectively:  $\mathcal{A}_{1,R}$  and  $\mathcal{A}_{2,R}$  by the multiplication on the left and on the right by the transform matrices  $\mathbf{T}_L$  and  $\mathbf{T}_R$  respectively:

$$\begin{aligned}\mathcal{A}_{1,R} &= \mathbf{T}_L \mathcal{A}_1 \\ &= \mathbf{D}_\theta \diamond \mathbf{D}_\phi\end{aligned}\quad (\text{IV.26})$$

$$\begin{aligned}\mathcal{A}_{2,R} &= \mathcal{A}_2 \mathbf{T}_R \\ &= 2(\text{Re}(\boldsymbol{\theta}^{(m_1-1)/2} \phi^{(M-m_2)/2} \Delta_\gamma[n] \ddot{\mathcal{A}}_\theta^T), \\ &\quad -\text{Im}(\boldsymbol{\theta}^{(m_1-1)/2} \phi^{(M-m_2)/2} \Delta_\gamma[n] \ddot{\mathcal{A}}_\theta^T))\end{aligned}\quad (\text{IV.27})$$

Thus the complex Hankel matrix  $\mathcal{A}_{e,H}[n]$  can be transformed into the matrix  $\mathcal{A}_{e,R}[n]$ :

$$\begin{aligned}\mathcal{A}_{e,R}[n] &= \mathbf{T}_L \mathcal{A}_{e,H}[n] \mathbf{T}_R \\ &= \mathcal{A}_{1,R} \mathcal{A}_{2,R}\end{aligned}\quad (\text{IV.28})$$

In the next step, we use the  $P$  dimension space generated by  $\mathcal{A}_{1,R}$  to extract the desired information on AOA and AOD. In practice,  $\mathcal{A}_{e,R}[n]$  is at full rank because of the presence of noise. Therefore, we apply the SVD decomposition to  $\mathcal{A}_{e,R}[n]$  and we use the space generated by the  $P$  dominant columns as an approximation of the space generated by  $\mathcal{A}_{1,R}[n]$ , i.e  $\mathcal{A}_{1,R} = U_R \mathbf{T}$  and  $\mathbf{T} \in \mathbb{R}^{P \times P}$ .

### C- step 3: Application of the 2D-UESPRIT algorithm

Due to shift invariance structure characteristic presented in  $\bar{\mathbf{A}}_\theta$  and  $\bar{\mathbf{A}}_\phi$ , the following expressions can be obtained:

$$\begin{aligned}\mathbf{J}_{x\theta} \mathbf{T}_L^H \mathbf{T}_L \mathcal{A}_1 \mathbf{U} &= \mathbf{J}_{y\theta} \mathbf{T}_L^H \mathbf{T}_L \mathcal{A}_1 \\ \mathbf{J}_{x\phi} \mathbf{T}_L^H \mathbf{T}_L \mathcal{A}_1 \mathbf{V} &= \mathbf{J}_{y\phi} \mathbf{T}_L^H \mathbf{T}_L \mathcal{A}_1\end{aligned}\quad (\text{IV.29})$$

Where  $\mathbf{J}_{x\theta}\mathbf{J}_{y\theta}\mathbf{J}_{x\phi}$  and  $\mathbf{J}_{y\phi}$  are calculated as shown in equation (IV.29) by replacing  $m$  and  $M$  with  $m_1$  and  $N_T - m_2 + 1$  respectively. From equation (IV.26), we have:

$$\begin{aligned}\mathbf{J}_{x\theta}\mathbf{T}_L^H\mathcal{A}_{1,R}\mathbf{U} &= \mathbf{J}_{y\theta}\mathbf{T}_L^H\mathcal{A}_{1,R} \\ \mathbf{J}_{x\phi}\mathbf{T}_L^H\mathcal{A}_{1,R}\mathbf{V} &= \mathbf{J}_{y\phi}\mathbf{T}_L^H\mathcal{A}_{1,R}\end{aligned}\quad (\text{IV.30})$$

By multiplying the two terms of the equation (IV.30) by  $\mathbf{Q}_{m_1-1}^H \otimes \mathbf{Q}_{M-m_2+1}^H$ , we obtain:

$$(\mathbf{Q}_{m_1-1}^H\mathbf{J}_{1\theta}\mathbf{Q}_{m_1} \otimes \mathbf{I}_{M-m_2+1})\mathcal{A}_{1,R}\boldsymbol{\theta} = (\mathbf{Q}_{m_1-1}^H\mathbf{J}_{2\theta}\mathbf{Q}_{m_1} \otimes \mathbf{I}_{M-m_2+1})\mathcal{A}_{1,R} \quad (\text{IV.31})$$

$$(\mathbf{I}_{m_1} \otimes \mathbf{Q}_{M-m_2}^H\mathbf{J}_{1\phi}\mathbf{Q}_{M-m_2+1})\mathcal{A}_{1,R}\boldsymbol{\phi} = (\mathbf{I}_{m_1} \otimes \mathbf{Q}_{M-m_2}^H\mathbf{J}_{2\phi}\mathbf{Q}_{M-m_2+1})\mathcal{A}_{1,R} \quad (\text{IV.32})$$

We define:

$$\begin{aligned}\mathbf{B}_\theta &= (\mathbf{Q}_{m_1-1}^H\mathbf{J}_{1\theta}\mathbf{Q}_{m_1} \otimes \mathbf{I}_{M-m_2+1}) \\ &= \mathbf{B}_{\theta,R} + j\mathbf{B}_{\theta,I} \\ \mathbf{B}_\phi &= (\mathbf{I}_{m_1} \otimes \mathbf{Q}_{M-m_2}^H\mathbf{J}_{1\phi}\mathbf{Q}_{M-m_2+1}) \\ &= \mathbf{B}_{\phi,R} + j\mathbf{B}_{\phi,I} \\ \hat{\boldsymbol{\theta}} &= \text{diag}(\hat{\theta}_1, \dots, \hat{\theta}_P) \\ \hat{\boldsymbol{\phi}} &= \text{diag}(\hat{\phi}_1, \dots, \hat{\phi}_P)\end{aligned}\quad (\text{IV.33})$$

Substituting the equation (IV.33) in the equations (IV.31) and (IV.32), we find the following two expressions:

$$\begin{aligned}\mathbf{B}_{\theta,R}\mathcal{A}_{1,R}\hat{\boldsymbol{\theta}} &= \mathbf{B}_{\theta,I}\mathcal{A}_{1,R} \\ \mathbf{B}_{\phi,R}\mathcal{A}_{1,R}\hat{\boldsymbol{\phi}} &= \mathbf{B}_{\phi,I}\mathcal{A}_{1,R}\end{aligned}\quad (\text{IV.34})$$

It follows that:

$$\begin{aligned}\mathbf{T}\hat{\boldsymbol{\theta}}\mathbf{T}^{-1} &= (\mathbf{B}_{\theta,R}\mathbf{U}_R)^\dagger\mathbf{B}_{\theta,I}\mathbf{U}_R \\ \mathbf{T}\hat{\boldsymbol{\phi}}\mathbf{T}^{-1} &= (\mathbf{B}_{\phi,R}\mathbf{U}_R)^\dagger\mathbf{B}_{\phi,I}\mathbf{U}_R\end{aligned}\quad (\text{IV.35})$$

Note that the two terms to the right of matrices from equation (IV.35) have the same eigenvectors. It is deduced that the AOA and AOD can be estimated jointly

by a complex eigenvalues decomposition:

$$\begin{aligned}\mathbf{\Lambda} &= EIG((\mathbf{B}_{\theta,R}\mathbf{U}_R)^\dagger\mathbf{B}_{\theta,I}\mathbf{U}_R + j(\mathbf{B}_{\phi,R}\mathbf{U}_R)^\dagger\mathbf{B}_{\phi,I}\mathbf{U}_R) \\ \hat{\boldsymbol{\theta}} &= Re(\mathbf{\Lambda}) \\ \hat{\boldsymbol{\phi}} &= Im(\mathbf{\Lambda})\end{aligned}\tag{IV.36}$$

We see well in the equation (IV.36) that  $\hat{\boldsymbol{\theta}}$  and  $\hat{\boldsymbol{\phi}}$  corresponding to the same eigenvectors, i.e the same eigenvalues of the matrix  $T$ , are associated with the same propagation paths which ensures the automatic matching of AOA and AOD. After obtaining the estimated values of the AOD / AOA, the gains of the corresponding propagation paths are estimated. According to the data model, we write:

$$\mathbf{X} = \mathbf{S}\hat{\mathbf{A}} + \mathbf{W}\tag{IV.37}$$

By using the pilot symbols orthogonality , we obtain:

$$\begin{aligned}\frac{1}{M}(\mathbf{S}^H\mathbf{X}) &= \hat{\mathbf{A}} + \frac{1}{M}\mathbf{S}^H\mathbf{W} \\ &= \hat{\mathbf{A}}_\phi\hat{\boldsymbol{\Delta}}_\alpha\hat{\mathbf{A}}_\theta^T + \frac{1}{M}\mathbf{S}^H\mathbf{W}\end{aligned}\tag{IV.38}$$

Applying the vec operator, we find:

$$vec\left(\frac{1}{M}(\mathbf{S}^H\mathbf{X})\right) = (\hat{\mathbf{A}}_\phi \otimes \hat{\mathbf{A}}_\theta)vec(\hat{\boldsymbol{\Delta}}_\alpha) + vec\left(\frac{1}{M}\mathbf{S}^H\mathbf{W}\right)\tag{IV.39}$$

Thus, the gains are given by:

$$vec(\hat{\boldsymbol{\Delta}}_\alpha) = (\hat{\mathbf{A}}_\phi \otimes \hat{\mathbf{A}}_\theta)^\dagger [vec\left(\frac{1}{M}(\mathbf{S}^H\mathbf{X})\right) - vec\left(\frac{1}{M}\mathbf{S}^H\mathbf{W}\right)]\tag{IV.40}$$

### IV.2.2.3 Cramer-rao bound derivation

The problem of interest here is to estimate the angular AoDs ( $\theta$ ) and AoAs ( $\phi$ ), as well as the corresponding channel path gains  $\alpha$  from the received signal  $\mathbf{y}$ . The Cramer-rao bound (CRB) of the AOD/AOA and gains is widely studied in the literature [113, 118, 119]. In the following, we derive the performance bound in terms of the CRBs for any unbiased

estimator of these unknown parameters. First we group all unknown parameters as:

$$\mathbf{\Phi} = [ \boldsymbol{\alpha}^T \ \boldsymbol{\theta}^T \ \boldsymbol{\phi}^T ] \quad (\text{IV.41})$$

Where  $\boldsymbol{\alpha} = [ \alpha_1 \dots \alpha_P ]$ ,  $\boldsymbol{\theta} = [ \theta_1 \dots \theta_P ]$ ,  $\boldsymbol{\phi} = [ \phi_1 \dots \phi_P ]$ . The CRB is equal to the inverse of the Fisher Information Matrix (FIM) defined by:

$$\mathbf{CRB} = (\mathbf{FIR})^{-1}$$

Therefore CRB can be rewritten as:

$$\mathbf{CRB} = \text{Re} \begin{bmatrix} \mathbf{f}_{\theta\theta} & \mathbf{f}_{\theta\phi} & \mathbf{f}_{\theta\alpha} \\ \mathbf{f}_{\phi\theta} & a_{\phi\phi} & \mathbf{f}_{\phi\alpha} \\ \mathbf{f}_{\theta\alpha} & \mathbf{f}_{\alpha\phi} & \mathbf{f}_{\alpha\alpha} \end{bmatrix}^{-1} \quad (\text{IV.42})$$

Where  $\mathbf{f}_{ij}$  is the second differentiation function. With  $\mathbf{f}_{\theta\phi} = \mathbf{f}_{\phi\theta}$ ,  $\mathbf{f}_{\phi\alpha} = \mathbf{f}_{\alpha\phi}$ ,  $\mathbf{f}_{\theta\theta} = \mathbf{f}_{\theta\theta}$ . After simplification done in [120, 121, 122], this bound becomes:

$$\text{CRB}(\alpha, \theta, \phi) = \frac{\sigma^2}{2} \text{Re}(\boldsymbol{\Lambda}_\alpha^H \mathbf{D}^H \mathbf{P}_\mathbf{A}^\perp \boldsymbol{\Lambda}_\alpha^H \mathbf{D})^{-1} \quad (\text{IV.43})$$

With:

$$\begin{aligned} \boldsymbol{\Lambda}_\alpha &= \mathbf{I}_3 \otimes \boldsymbol{\Delta}_\alpha, \\ \mathbf{P}_\mathbf{A}^\perp &= \mathbf{I}_{MN} - \mathbf{A}_{\alpha,\theta,\phi} (\mathbf{A}_{\alpha,\theta,\phi}^H \mathbf{A}_{\alpha,\theta,\phi})^{-1} \mathbf{A}_{\alpha,\theta,\phi}, \\ \mathbf{D} &= (\mathbf{A}'_\alpha \diamond \mathbf{A}_\theta \diamond \mathbf{A}_\phi, \mathbf{A}_\alpha \diamond \mathbf{A}'_\theta \diamond \mathbf{A}_\phi, \mathbf{A}_\alpha \diamond \mathbf{A}_\theta \diamond \mathbf{A}'_\phi), \\ \mathbf{A}'_\alpha &= \left( \frac{da_{\alpha,1}}{d\alpha}(\alpha), \dots, \frac{da_{\alpha,P}}{d\alpha}(\alpha) \right), \\ \mathbf{A}'_\theta &= \left( \frac{da_{\theta,1}}{d\theta}(\theta), \dots, \frac{da_{\theta,P}}{d\theta}(\theta) \right), \\ \mathbf{A}'_\phi &= \left( \frac{da_{\phi,1}}{d\phi}(\phi), \dots, \frac{da_{\phi,P}}{d\phi}(\phi) \right) \\ &\cdot \end{aligned} \quad (\text{IV.44})$$

Where  $\mathbf{A}_{\alpha,\theta,\phi}$  is defined as  $\mathbf{A}_{\alpha,\theta,\phi} = \mathbf{A}_\alpha \diamond \mathbf{A}_\theta \diamond \mathbf{A}_\phi$  with  $\diamond$  is the Khatri-Rao product.

After estimating the transmission channel, the BS precodes jointly the data of all users. The BS must have a good estimate of the channel to create spatially multiplexed data streams for each terminal. The coding data is done by a precoder ZF. The ZF encoder

is used to evaluate the performance of the entire system after the estimation phase. The coding matrix of the ZF precoder is given by:

$$\mathbf{F} = (\hat{\mathbf{H}}^H \hat{\mathbf{H}})^{-1} \hat{\mathbf{H}}^H \quad (\text{IV.45})$$

The ZF precoder is used in the IEEE 802.11n (MIMO) standard. It is useful for our system because it reduces intersymbol interference (ISI) and which is helpful when the ISI is significant with respect to noise (frequency-selective mobile radio channel and presence of several users). Studies on massive MU-MIMO systems [123] have shown that this equalizer offers good performance for high SNR values. For the low SNR, its performance improves by increasing the number of antennas used in the BS which is valid for our system.

### IV.2.3 Channel estimation with pilot contamination

In the last few years, pilot contamination (PC) problem in multicell Massive MIMO systems attracted a great attention from the research community. There are several studies on eliminating inter-cell interference in multi-cell systems in which it is assumed that the CSI at the BS is known. However, in practical implementation, estimation of channel state information is required. Several pioneering papers describe the main historical milestones of PC issue in Massive MIMO and its impacts on system performance under different scenarios in the literature [112, 124, 125, 126]. In this chapter, we propose a scheme based on Beamspace Unitary ESPRIT (BU-ESPRI) algorithm [127, 128] for the parameter channel estimation to combat the pilot contamination in Massive MIMO system. The so-mentioned algorithm is used for the estimation of angle of departure (AOD)/angle of arrival (AOA) and then calculate the gains of the different paths. Hence, this will allow us to reconstruct the desired and interfered channel. This last step is possible thanks to the comparison of the path gains magnitude.

#### IV.2.3.1 System model

We consider a system with two joint cell consisting of a base station (BS) equipped with an antenna array with  $M$  elements concurrently serving to  $K$  user terminals with  $N$  an antenna array ( $N < K < M$ ). The antenna arrays are assumed to be linear and uniform with an inter-element spacing of  $\lambda/2$ . We assume that the system is operating in TDD, therefore rendering the channels reciprocal.



The received signal  $\mathbf{R} \in \mathbb{C}^{M \times P}$  for  $P$  paths, is given by:

$$\mathbf{R} = \mathbf{H}\mathbf{S} + \mathbf{W} \quad (\text{IV.46})$$

Where  $\mathbf{S} \in \mathbb{C}^{N \times P}$  contains the transmission pilots symbols.  $\mathbf{H} \in \mathbb{C}^{M \times N}$  represents the complex Rayleigh Fading geometric channel matrix.  $\mathbf{W} \in \mathbb{C}^{M \times P}$  is the zero mean complex Gaussian (ZMCG) matrix with variance  $\sigma^2$ .

### IV.2.3.2 The geometric channel model

We suppose the presence of  $P$  path from the users to BS, each have the same transmission pilot. So, each  $i^{\text{th}}$  path characterized by its angles of transmission  $\theta_i$  and reception  $\phi_i$ . The geometric channel model  $\mathbf{H}$  is given by:

$$\mathbf{H} = \mathbf{A}_r(\theta) \mathbf{diag}(\alpha) \mathbf{A}_t^T(\phi) \quad (\text{IV.47})$$

With:  $\mathbf{A}_r(\theta) = [\mathbf{a}_r(\theta_1), \dots, \mathbf{a}_r(\theta_P)]$  and  $\mathbf{A}_t(\phi) = [\mathbf{a}_t(\phi_1), \dots, \mathbf{a}_t(\phi_P)]$  represent the reception and transmission antenna array with dimensions  $(M \times P)$  and  $(N \times P)$ , respectively. Moreover, each vector of the so-mentioned matrices denoted by  $\mathbf{a}_r(\theta_i) = [1, \exp(j\pi \sin(\theta_i)), \dots, \exp(j\theta(M-1) \sin(\theta_i))]^T$  and  $\mathbf{a}_t(\phi_i) = [1, \exp(j\pi \sin(\phi_i)), \dots, \exp(j\pi(N-1) \sin(\phi_i))]^T$ , each with dimension  $(M \times 1)$ . The diagonal matrix  $\mathbf{diag}(\alpha)$  contain the vector  $\alpha = [\alpha_1, \dots, \alpha_P]$  with  $\alpha_1, \dots, \alpha_P$  denotes the path loss gain.

In our case, we consider the presence of pilot contamination (PC) where each transmitted symbol contain the same pilots. Thus, the  $j^{\text{th}}$  transmitted symbol, is denoted as  $\mathbf{s}_j = [s_j(1), \dots, s_j(P)]^T, j = 0, \dots, M-1$ . For the  $P$  paths defined by the angles  $\theta_i$  and  $\phi_i, i = 1, \dots, P$ , the equation (IV.46) of received signal can be re-written as:

$$\left\{ \begin{array}{l} r_1 = h_{11}s_1 + h_{12}s_1 + \dots + h_{1P}s_1 \\ \quad + h_{1(P+1)}s_2 + h_{1(P+2)}s_2 + \dots + h_{1(2P)}s_2 + w_1 \\ r_2 = h_{21}s_1 + h_{22}s_1 + \dots + h_{2P}s_1 \\ \quad + h_{2(P+1)}s_2 + h_{2(P+2)}s_2 + \dots + h_{2(2P)}s_2 + w_2 \\ \quad \vdots \\ r_N = h_{M1}s_1 + h_{M2}s_1 + \dots + h_{MP}s_1 \\ \quad + h_{M(P+1)}s_2 + h_{M(P+2)}s_2 + \dots + h_{M(2P)}s_2 + w_M \end{array} \right.$$

Which can be written as:

$$\mathbf{r} = \mathbf{H}\hat{\mathbf{S}} + \mathbf{W} \quad (\text{IV.48})$$

Where the  $(2P \times 1)$  transmitted pilot vector defined by  $\hat{\mathbf{S}} = [\underbrace{\hat{s}_1 \dots \hat{s}_1}_{P \text{ times}} \underbrace{\hat{s}_2 \dots \hat{s}_2}_{P \text{ times}}]^T$ , Which represents the multi-copie of transmitted pilot coming from different paths.

In this chapter, we are interested with a scenario in which the two users are transmitting the same pilot symbol such as  $s_1 = s_2 = s$ , that correspond to worth case of PC. Hence, we obtain a vector  $\mathbf{S} = [\underbrace{s \dots s}_{P \text{ times}} \underbrace{s \dots s}_{P \text{ times}}]^T$  with dimension  $(2P \times 1)$ . The received signal is written as:

$$\mathbf{r} = \mathbf{A}_r(\theta) \text{diag}(\boldsymbol{\alpha}) \mathbf{A}_r(\phi)^H \mathbf{S} + \mathbf{W} \quad (\text{IV.49})$$

At the receiver side, the output of the adaptive filter is:

$$\begin{aligned} \mathbf{y} &= \frac{1}{P} \sum_{n=1}^P \mathbf{r} \mathbf{S}^H \\ &= \frac{1}{P} \sum_{n=1}^P \mathbf{H} \mathbf{S} \mathbf{S}^H + \mathbf{w} \mathbf{S}^H \end{aligned} \quad (\text{IV.50})$$

The orthogonality of symbols implies that:

$$\mathbf{I} = \frac{1}{P} \sum_{n=1}^P \mathbf{S} \mathbf{S}^H \quad (\text{IV.51})$$

Where  $\mathbf{I}$  is the identity matrix. After simplifying (IV.50) and applying the vectorization operation, we obtain:

$$\begin{aligned} \mathbf{z} &= \text{vec}(\mathbf{y}) \\ &= \text{vec}(\mathbf{H}) + \text{vec}\left(\frac{1}{J} \sum_{n=1}^P \mathbf{w} \mathbf{S}^H\right) \\ &= \text{vec}(\mathbf{A}_r(\theta) \text{diag}(\boldsymbol{\alpha}) \mathbf{A}_t^T(\phi)) + \text{vec}\left(\frac{1}{J} \sum_{n=1}^P \mathbf{w} \mathbf{S}^H\right) \\ &= (\mathbf{A}_r(\theta) \otimes \mathbf{A}_t(\phi)) \text{vec}(\text{diag}(\boldsymbol{\alpha})) + \text{vec}\left(\frac{1}{J} \sum_{n=1}^P \mathbf{w} \mathbf{S}^H\right) \end{aligned} \quad (\text{IV.52})$$

Finally, we write the signal model as:

$$\begin{aligned}\mathbf{x} &= \mathbf{z} \\ \mathbf{x} &= \mathcal{A}\mathbf{g} + \mathbf{v}\end{aligned}\tag{IV.53}$$

With:  $\mathcal{A} = [\mathbf{a}_t(\theta_1) \otimes \mathbf{b}_r(\phi_1), \dots, \mathbf{a}_r(\theta_P) \otimes \mathbf{b}_t(\phi_P)]$  is matrix with dimension  $MN \times 4 * P^2$ , and the vector  $\mathbf{g} = [\alpha_1, \dots, \alpha_p]^T$  of dimension  $2P \times 1$  contains the gains of multi-path. The vector  $\mathbf{v}$  denotes for the complex Gaussian distribution with mean and variance of zero and  $\sigma^2$  respectively,  $\mathbf{v} \sim (0, \sigma^2 \mathbf{I}_{MN})$ .

Introducing the Khatri-Rao product, we can rewrite equation (IV.53) as:

$$\mathbf{x} = (\mathbf{A}_r(\theta) \circ \mathbf{A}_t(\phi))\mathbf{g} + \mathbf{v}.\tag{IV.54}$$

For  $P$  path, the equation (IV.53) can be expressed in matrix form as :

$$\mathbf{X} = \mathcal{A}\mathbf{G} + \mathbf{V}\tag{IV.55}$$

### IV.3 Proposed beamspace unitary (BU-ESPRIT) parameter channel estimation

In this section, we start by applying the BU-ESPRIT algorithm to estimate the AOA/AOD. Then, these values are used to evaluate the path gains. These gains correspond to paths of the nearest distance between the MS and SB, which necessarily constitute the desired paths. After extracting the channel parameters between the user and BS, it is introduced to a precoder for data transmission.

#### 1. Joint estimation of AOD/AOA:

The conjugate centro-symmetric DFT matrix is used as the transformed beamspace matrices to conceive the structure of the invariance rotational of the beamspace transformation [129].

Let  $\mathbf{W}_r^H$  and  $\mathbf{W}_t^H$  be the transformation beamspace matrices of reception and transmission, respectively. Their  $m^{th}$  line is given by :

$$\begin{aligned}W_{(t,r),m}^H &= e^{j((N-1)/2)m(2\pi/N)}[1, e^{-jm(2\pi/N)}, \dots \\ & \dots e^{-j(N-1)m(2\pi/N)}], m = 0, \dots, N - 1\end{aligned}\tag{IV.56}$$

Each line represents the DFT beam steered at a spatial frequency  $\mu = m(2\pi/N)$  and  $\nu = m(2\pi/M)$  for  $\mathbf{W}_r^H$  and  $\mathbf{W}_t^H$ , respectively. The beamspace formats of the transmitter and receiver are defined by  $\mathbf{B}_r = \mathbf{W}_r^H \mathbf{A}_r$  and  $\mathbf{B}_t = \mathbf{W}_t^H \mathbf{A}_t$ , respectively. Consequently, the final beamspace formats are given by:

$$\begin{aligned} \mathbf{B} &= \mathbf{W}^H \mathbf{A} \\ &= \mathbf{B}_r \otimes \mathbf{B}_t \\ &= \mathbf{W}_r^H \mathbf{A}_r \otimes \mathbf{W}_t^H \mathbf{A}_t \end{aligned} \quad (\text{IV.57})$$

Using the following Kronecker product property  $(\mathbf{A} \otimes \mathbf{B})(\mathbf{C} \otimes \mathbf{D}) = \mathbf{AC} \otimes \mathbf{BD}$ , we obtain the final transformed beamspace matrix:

$$\mathbf{W}^H = \mathbf{W}_r^H \otimes \mathbf{W}_t^H \quad (\text{IV.58})$$

The matrix  $\mathbf{W}$  of dimension  $K_t K_r \times MN$  with  $K_t$  and  $K_r$  define the beams number for transmission and reception, respectively. The received signal is re-defined as:

$$\begin{aligned} \mathbf{Y} &= \mathbf{W}^H \mathbf{A} \mathbf{G} + \bar{\mathbf{V}} \\ &= \mathbf{B} \mathbf{G} + \bar{\mathbf{V}} \end{aligned} \quad (\text{IV.59})$$

Where  $\bar{\mathbf{V}} = \mathbf{W}^H \mathbf{V}$  represents the beamspace format of the noise. The  $p^{\text{th}}$  element of  $\mathbf{B}_r$  with  $\mathbf{b}_r(\mu_p) = [b_{r,0}(\mu_p), \dots, b_{r,N-1}(\mu_p)]^T$  and the  $p^{\text{th}}$  element of  $b_r(\mu_p)$  is:

$$\begin{aligned} b_{r,m}(\mu_p) &= w_{r,m}^H a(\theta_p) \\ &= \frac{\sin[(N/2)(\mu_p - m(2\pi/N))]}{\sin[(1/2)(\mu_p - m(2\pi/N))]} \end{aligned} \quad (\text{IV.60})$$

The two adjacent components of the  $\mathbf{b}_r(\mu_p)$  are linked by [130]

$$\sin\left[\frac{1}{2}\left(\mu_p - m\frac{2\pi}{N}\right)\right]b_{r,m}(\mu_p) + \sin\left[\frac{1}{2}\left(\mu_p - (m+1)\frac{2\pi}{N}\right)\right]b_{r,m+1}(\mu_p) = 0 \quad (\text{IV.61})$$

Seeing that the beams of indices  $m = 0$  and  $m = N - 1$  are directed to spacial

frequencies  $\mu_{p,0} = 0$  and

$$\begin{aligned}\mu_{p,N-1} - 2\pi &= (N-1)\left(\frac{2\pi}{N}\right) - 2\pi \\ &= -\frac{2\pi}{N}\end{aligned}\quad (\text{IV.62})$$

Or both beams are adjacent physically, we observe:

$$\begin{aligned}b_N(\mu_p) &= \frac{\sin[(N/2)(\mu_p - N(2\pi/N))]}{\sin[(1/2)(\mu_p - N(2\pi/N))]} \\ &= \frac{\sin((N/2)\mu_p - N\pi)}{\sin((1/2)\mu_p - \pi)} \\ &= \frac{(-1)^N \sin((N/2)\mu_p)}{-\sin((1/2)\mu_p)} \\ &= (-1)^N \cdot b_0(\mu_p)\end{aligned}\quad (\text{IV.63})$$

The first and last element of  $\mathbf{b}_r(\mu_p)$  are linked with equation:

$$\begin{aligned}\tan\left(\frac{\mu_p}{2}\right)\left\{\cos\left(m\frac{\pi}{N}\right)b_{r,m}(\mu_p) + \cos\left((m+1)\frac{\pi}{N}\right)b_{r,m+1}(\mu_p)\right\} \\ = \sin\left(m\frac{\pi}{N}\right)b_{r,m}(\mu_p) + \sin\left((m+1)\frac{\pi}{N}\right)b_{r,m+1}(\mu_p)\end{aligned}\quad (\text{IV.64})$$

We suppose  $m = N - 1$ :

$$\begin{aligned}\tan\left(\frac{\mu_p}{2}\right)\left\{\cos\left((N-1)\frac{\pi}{N}\right)b_{r,N-1}(\mu_p) + \cos(\pi)(-1)^{N-1}b_{r,0}(\mu_p)\right\} \\ = \sin\left((N-1)\frac{\pi}{N}\right)b_{r,N-1}(\mu_p) + \sin(\pi)(-1)^{N-1}b_{r,0}(\mu_p)\end{aligned}\quad (\text{IV.65})$$

Thereby, all N equations ( $0 \leq m \leq N - 1$ ) lead to an invariance relation for  $\mathbf{b}_r(\mu_p)$  as follow:

$$\tan\left(\frac{\mu_p}{2}\right)\mathbf{\Gamma}_1\mathbf{b}_r(\mu_p) = \mathbf{\Gamma}_2\mathbf{b}_r(\mu_p)\quad (\text{IV.66})$$

With  $\mathbf{\Gamma}_1$  and  $\mathbf{\Gamma}_2$  are two selection matrices defined as:

$$\mathbf{\Gamma}_1 = \begin{bmatrix} 1 & \cos\left(\frac{\pi}{N}\right) & 0 & 0 & \dots & 0 & 0 \\ 0 & \cos\left(\frac{2\pi}{N}\right) & \cos\left(\frac{2\pi}{N}\right) & 0 & \dots & 0 & 0 \\ 0 & 0 & \cos\left(\frac{2\pi}{N}\right) & \cos\left(\frac{3\pi}{N}\right) & \dots & 0 & 0 \\ \vdots & \vdots & \vdots & \vdots & \dots & \vdots & \vdots \\ 0 & 0 & 0 & 0 & \dots & \cos\left(\frac{(N-2)\pi}{N}\right) & \cos\left(\frac{(N-1)\pi}{N}\right) \\ (-1)^N & 0 & 0 & 0 & \dots & 0 & \cos\left(\frac{(N-1)\pi}{N}\right) \end{bmatrix}\quad (\text{IV.67})$$

$$\mathbf{\Gamma}_2 = \begin{bmatrix} 0 & \sin(\frac{\pi}{N}) & 0 & 0 & \dots & 0 & 0 \\ 0 & \sin(\frac{\pi}{N}) & \sin(\frac{2\pi}{N}) & 0 & \dots & 0 & 0 \\ 0 & 0 & \sin(\frac{2\pi}{N}) & \sin(\frac{3\pi}{N}) & \dots & 0 & 0 \\ \vdots & \vdots & \vdots & \vdots & \ddots & \vdots & \vdots \\ 0 & 0 & 0 & 0 & \dots & \sin(\frac{(N-2)\pi}{N}) & \sin(\frac{(N-1)\pi}{N}) \\ 0 & 0 & 0 & 0 & \dots & 0 & \sin(\frac{(N-1)\pi}{N}) \end{bmatrix} \quad (\text{IV.68})$$

For  $P$  paths, the (IV.66) becomes the beamspace matrix equation at the reception:

$$\mathbf{\Gamma}_1 \mathbf{B}_r \mathbf{\Omega}_\mu = \mathbf{\Gamma}_2 \mathbf{B}_r \quad (\text{IV.69})$$

Where the matrix  $\mathbf{\Omega}_\mu = \text{diag}\{\tan(\mu_1/2), \dots, \tan(\mu_p/2)\}$  with real values and whose diagonal element contain the DOA's information.

Similarly, we find the equation of beamspace matrix in emission side as:

$$\mathbf{\Gamma}_3 \mathbf{B}_t \mathbf{\Omega}_\nu = \mathbf{\Gamma}_4 \mathbf{B}_t \quad (\text{IV.70})$$

With  $\mathbf{\Gamma}_3$  and  $\mathbf{\Gamma}_4$  are defined in a similar manner to  $\mathbf{\Gamma}_1$  and  $\mathbf{\Gamma}_2$  replacing  $N$  by  $M$ , the matrix  $\mathbf{\Omega}_\nu = \text{diag}\{\tan(\nu_1/2), \dots, \tan(\nu_p/2)\}$ ,  $\nu_p = \pi \sin(\theta_p)$  contains real values and whose diagonal elements hold the AOA's information. Using the previous property of the Kronecker product, we find that:

$$\begin{aligned} \mathbf{\Gamma}_{\mu_1} \mathbf{B} \mathbf{\Omega}_\mu &= \mathbf{\Gamma}_{\mu_2} \mathbf{B} \\ \mathbf{\Gamma}_{\nu_1} \mathbf{B} \mathbf{\Omega}_\nu &= \mathbf{\Gamma}_{\nu_2} \mathbf{B} \end{aligned} \quad (\text{IV.71})$$

With  $\mathbf{\Gamma}_{\mu_1} = \mathbf{\Gamma}_1 \otimes \mathbf{I}_M$  and  $\mathbf{\Gamma}_{\mu_2} = \mathbf{\Gamma}_2 \otimes \mathbf{I}_M$  represent the selection beamspace matrices in reception,  $\mathbf{\Gamma}_{\nu_1} = \mathbf{I}_N \otimes \mathbf{\Gamma}_3$  and  $\mathbf{\Gamma}_{\nu_2} = \mathbf{I}_N \otimes \mathbf{\Gamma}_4$  are the selection beamspace matrices in transmission.

According to the received signal defined in equation (IV.46). The subspace signal matrix with dimension  $(MN \times P)$  can be constructed from the largest  $P$  singular vectors of the real-valued matrix  $[\mathbf{Re}(\mathbf{Y}), \mathbf{Im}(\mathbf{Y})]$ . The signal subspace  $\mathbf{E}_s$  can be generated by the matrix  $\mathbf{B}$ :

$$\mathbf{E}_s = \mathbf{B} \mathbf{T} \quad (\text{IV.72})$$

Where the matrix  $\mathbf{T}$  with dimension  $(P \times P)$  contains real values. From equations

(IV.71) and (IV.72), we find:

$$\begin{aligned}\Gamma_{\mu_1} \mathbf{E}_s \Psi_\mu &= \Gamma_{\mu_2} \mathbf{E}_s \\ \Gamma_{\nu_1} \mathbf{E}_s \Psi_\nu &= \Gamma_{\nu_2} \mathbf{E}_s\end{aligned}\quad (\text{IV.73})$$

With:

$$\begin{aligned}\Psi_\mu &= \mathbf{T}^{-1} \Omega_\mu \mathbf{T} \\ \Psi_\nu &= \mathbf{T}^{-1} \Omega_\nu \mathbf{T}\end{aligned}\quad (\text{IV.74})$$

The automatically matching of frequency  $\mu$  et  $\nu$  is obtained using:

$$\Psi_\mu + j\Psi_\nu = \mathbf{T}^{-1} \{ \Omega_\mu + j\Omega_\nu \} \mathbf{T} \quad (\text{IV.75})$$

So, the real and imaginary values of the eigenvalues  $\{ \Omega_\mu + j\Omega_\nu \}$  form the estimation of  $\{ \mu, \nu_p \}, p = 1, \dots, P$ , and thus the DOD and DOA of the paths are given by:

$$\begin{aligned}\hat{\theta}_p &= \arcsin \left\{ \frac{2 \arctan[\Omega_\nu]_p}{\pi} \right\}, p = 1, \dots, P \\ \hat{\phi}_p &= \arcsin \left\{ \frac{2 \arctan[\Omega_\mu]_p}{\pi} \right\}, p = 1, \dots, P\end{aligned}\quad (\text{IV.76})$$

## 2. Estimation of path gains:

The BU-ESPRIT algorithm is developed for radar application, thus it is not concerned on estimating the path gains. In our case, the evaluation of this parameter is essential to solve pilot contamination problem. After estimating the AOA and AOD, we can calculate the path gains by solving the following equation:

$$\mathbf{X} = \hat{\mathcal{A}} \hat{\mathbf{g}} + \mathbf{v} \quad (\text{IV.77})$$

Where  $\hat{\mathcal{A}}$  is constructed as the matrix  $\mathcal{A}$  using the estimated angles. The estimated paths gains are given by:

$$\hat{\mathbf{g}} = \hat{\mathcal{A}}^\dagger \mathbf{X} \quad (\text{IV.78})$$

The estimation of AOD, AOA, path gains can be summarized in the following steps:

- (a) Transform the matrix of the received data  $\mathbf{X}$  to  $\mathbf{Y} = \mathbf{W}^H \mathbf{X}$ .
- (b) Calculate the singular values decomposition of matrix  $[\mathbf{Re}(\mathbf{Y}), \mathbf{Im}(\mathbf{Y})]$ . The  $P$  left dominant singular vectors form the matrix  $\mathbf{E}_s$ .
- (c) Calculate the matrices  $\Psi_\mu$  and  $\Psi_\nu$  by solving the systems of equations  $\Gamma_{\mu_1} \mathbf{E}_s \Psi_\mu = \Gamma_{\mu_2} \mathbf{E}_s$  and  $\Gamma_{\nu_1} \mathbf{E}_s \Psi_\nu = \Gamma_{\nu_2} \mathbf{E}_s$ , respectively, using the least square algorithm.
- (d) Calculate the eigenvalues and eigenvectors decomposition of the matrix  $\Psi_\mu + j\Psi_\nu$ .
- (e) The automatically matched DOA and AOA are given by the solutions of equations

$$\hat{\theta}_p = \arcsin \left\{ 2 \arctan[\Omega_\nu]_p / \pi \right\} \quad (\text{IV.79})$$

$$\hat{\phi}_p = \arcsin \left\{ 2 \arctan[\Omega_\mu]_p / \pi \right\} \quad (\text{IV.80})$$

- (f) Calculate the paths gain given by equation  $\hat{\mathbf{g}} = \hat{\mathcal{A}}^\dagger \mathbf{X}$

At this stage, we estimated the AOD/AOA and the gains of all the propagation paths received by the BS that contain the wanted and the interference channel. In the next step, we will compare the gains of the different paths and choose those with the highest values. Indeed, these gains correspond to the nearest propagation distances between the MS and the BS which necessarily form the desired paths. So, using the equation of (IV.78) we obtain:

$$\hat{\mathbf{g}}_{\text{desired}} = \mathbf{max}_{i=1:P}(\hat{\mathbf{g}}) \quad (\text{IV.81})$$

Where  $\hat{\mathbf{g}}_{\text{desired}}$  is the vector containing the  $P$  first largest values of  $\mathbf{g}$  that correspond to the gains user from  $p$  path.

This reasoning is based on the path loss model which specifies that the propagation losses increase with the distance traveled by the wave, and the fact that the MS inside the cell is closer than that of the neighboring cell. It is possible that the paths of the neighboring cell have higher gains than those of the desired cell due to the propagation conditions. This will produce errors in the phase estimation. If



the number of paths in the cell is not known a priori, it must be estimated [131] especially in the case where the values of the estimated gains are very close.

#### IV.4 Simulation results

We consider a system consisting of two adjacent cells A and B. Each cell adopts massive MIMO system. Furthermore, we assume simultaneously use of the same pilot symbol for each user in each cell. We denote the separating distance from the user of the cell B to the user of the cell A by  $d$ . Indeed, we study the effect of this interference on the phase channel estimation of user in cell A. Further, we evaluate the quality of service offered in each cell in term of BER in the presence of pilot contamination. To the reminder, the urban environment in each cell is characterized by a small rays densification therefore, creating pilot contamination phenomenon which can degrade the channel estimation. So, the channels between the BS of the cell A and the user within the cell and the cell B are characterized using geometric model with different path loss values for each distance  $d$ . The AOA and AOD angles are uniformly distributed between 0 and  $2\pi$ . BU-ESPRIT algorithm is used to estimate the so-mentioned geometric channel model. Hence, the resulted parameter is constructed to the linear precoder at the base station level for data transmission in cell A.

The first simulation examines the accuracy of the channel estimation incorporating the BU-ESPRIT algorithm by calculating the MSE of the AOA, AOD and path loss of the useful channel in the presence of pilot contamination. It is assumed that the user of cell A is 50 m away from his BS while the user of the other cell is 150 m from the BS of cell A, that contains a number of antennas of  $M = 40$ . The MSE for the three parameters is given by the equations:

$$\begin{aligned}
 EQM(\theta) &= \frac{1}{L} \sum_{\ell=1}^L \sqrt{\frac{1}{R} \sum_{r=1}^R (\hat{\theta}_{\ell,r} - \theta_{\ell})^2} \\
 EQM(\phi) &= \frac{1}{L} \sum_{\ell=1}^L \sqrt{\frac{1}{R} \sum_{r=1}^R (\hat{\phi}_{\ell,r} - \phi_{\ell})^2} \\
 EQM(\alpha) &= \frac{1}{L} \sum_{\ell=1}^L \sqrt{\frac{1}{R} \sum_{r=1}^R (\hat{\alpha}_{\ell,r} - \alpha_{\ell})^2}
 \end{aligned} \tag{IV.82}$$

With  $\theta_\ell$ ,  $\phi_\ell$ ,  $\alpha_\ell$  and  $\hat{\theta}_{\ell,r}$ ,  $\hat{\phi}_{\ell,r}$ ,  $\hat{\alpha}_{\ell,r}$  define the AOD, AOA and path gains and their estimation respectively. The monte carlo iteration are fixed to  $R = 200$  and the path number is  $P = 3$ .

Figures (IV.2, IV.3) represent the MSE of AOD, AOA (IV.2) and the path loss (IV.3) in

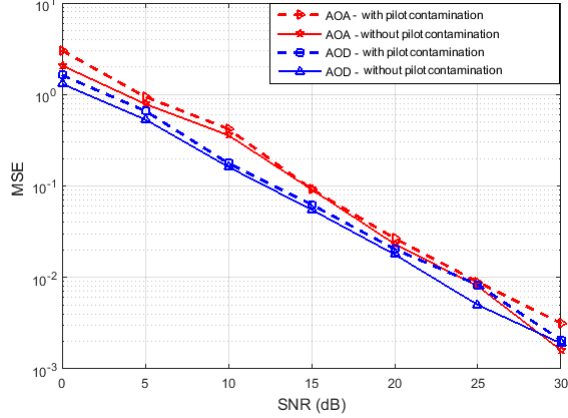


*Figure IV.2* — MSE of estimated angles

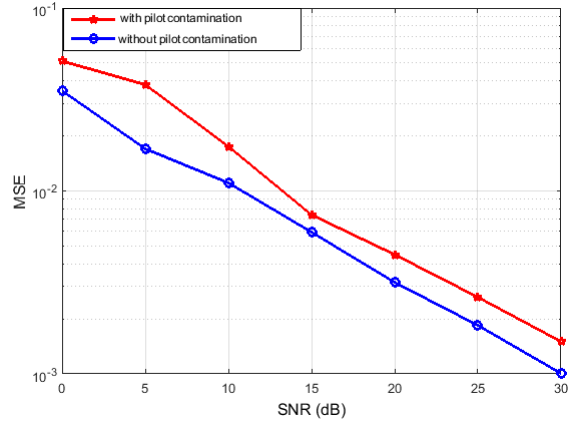


*Figure IV.3* — MSE of estimated path losses

the presence and absence of pilot contamination. It is noted that the MSE obtained with inter-cell interference is slightly greater compared to that is resulted from the two cells without interference. It can be explained by the ability of the BU-ESPRIT estimation algorithm to reject the effect of the interference between the identical pilot symbols without causing a great additional error on the estimation. It is also noted that the behaviour of the estimation algorithm is similar in the two cases for different value of SNR.

The figure (IV.3) confirms the results obtained in the previous simulation. It shows that the MSE of the system with pilot contamination is slightly higher than that obtained for a single cell. Moreover, these results are obtained without additional processing at the receiver side. Indeed, The only processing is carried out at the BS in form of ZF precoding.

Hence, It can be confirmed that the interference between the pilots of the two cells have not greatly affected the channel estimation by incorporating the BU-ESPRIT algorithm therefore, the data transmission toward the contaminated user.

Figures (IV.4, IV.5) illustrate the MSE of AOA, AOD and path gain estimation. In par-

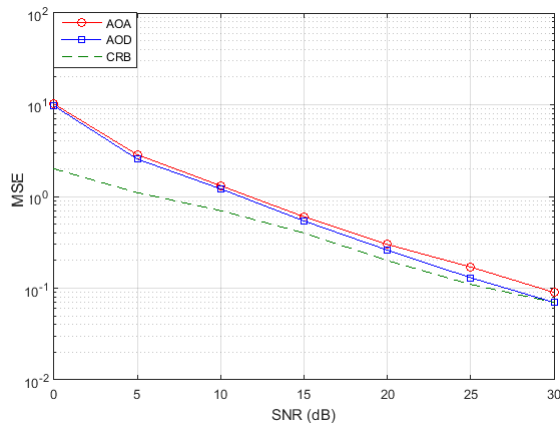


**Figure IV.4** — MSE of estimated angles for BU-ESPRIT

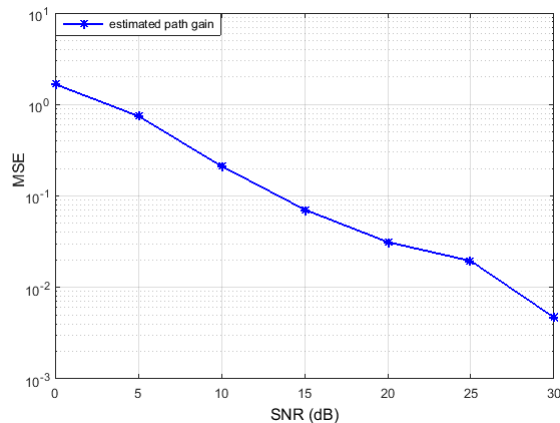


**Figure IV.5** — MSE of estimated path losses for BU-ESPRIT

ticular, the algorithm is close to the CRB for the large values of the SNR. To improve the performance of the algorithm for the low values of the SNR, the number of observations of the spatial signature matrix can be increased. Since the pilot symbols are periodically retransmitted into the system, the accuracy of the DOD and DOA estimation and therefore that of the path gains can be improved by averaging the estimated AOA and AOD obtained in the channel coherence time.

In Figure (IV.6) we examine the effect of the distance between the BS of the cell A and the contaminated user of the cell B. It is assumed first that this user is between the two cells at  $d = 150m$ . Then, the user is inside cell B at  $d = 170m$ . Finally, the user is positioned

at  $d = 120m$ . This last distance implies that the user of cell B is now inside cell A. This case is possible because of the overlapping of cells in certain networks. The BER entire system performance is evaluated for the three different distances. Figure (IV.6) shows that

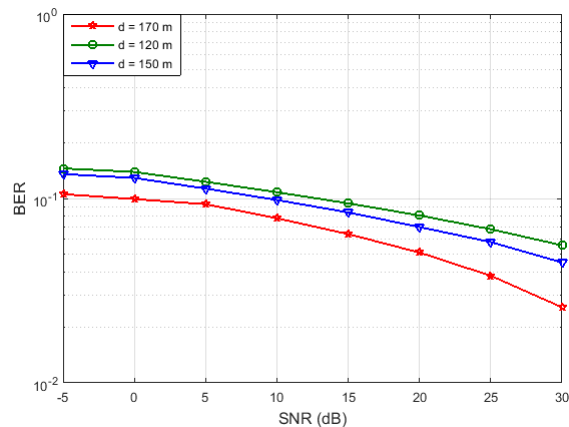


*Figure IV.6* — BER performance under different BS-MS distance

the BER depends on the separation distance of the contaminated user. Thus, as the user moves closer to the BS, the received power of contaminated pilot become important, and since the algorithm is based on the choice of the highest path gains, the user may be found sufficiently close to the BS. However, according to the propagation conditions in the two cells, the path gains become greater compared to the user's paths within the cell, which produce channel estimation error. The results of the simulation show similar performances for the different distances, which can be explained by the ability of the proposed method to combat the pilot contamination problem.

**Chapter V**

**PILOT CONTAMINATION MITIGATION  
FOR MMWAVE MASSIVE MIMO**

## V.1 Introduction

The fifth generation completes wireless communication with almost no limitation. Its goals include improving spectral efficiency and services, lowering cost and making uses of new spectrum. To meet these needs, many approaches are active research areas. Among these techniques, we cite millimeter wave, small cell densification, and massive MIMO paradigm [132]. While the first approach pushes towards getting more spectrum by working in the non-exploited millimeter bands, the second one relies on network densification by integrating small to femtocells thus deploying more infrastructure to get more active users per area. The third approach involves the incorporation of a considerable number of antennas at the transmit and receive sides with the associated signal processing. Designing channel estimation (CE) based on pilot sequence with exploiting the sparsity of the channel is an important issue for mmWave Massive MIMO. Prior work has focused on hybrid beamforming design for multiuser channels and does not tackle the inter-cell interference problem [133]. However, Inter-cell interference in mmWave systems may be less severe due to signal blockage by urban objects. Furthermore, as next-generation networks are expected to have ultra-dense small cells, the dramatic shortening of inter-cell distances will reduce the blockage density in channels, resulting in sparse or even line-of-sight (LoS) interference channels. Hence, this problem becomes more critical in the presence of pilot contamination (PC).

In this chapter, we are interested in some possible estimation techniques for a future 5G system in the absence and in the presence of the pilot contamination phenomenon. For this, we consider famous candidate systems for a fifth-generation cellular network. named the hybrid analogue/digital system operating in the millimeter wave band. At the end, we present the simulations results and their comments.

## V.2 Channel estimation in mmwave

Millimeter wave communication is a promising technology for future cellular networks [134]-[135]. Beamforming with wide antenna arrays is unavoidable to ensure a sufficient level of power in reception. Fortunately, large antenna arrays can be packed in small areas in the case of millimeter waves [136], [137]. High power consumption in a fully digital system makes the unique use of digital baseband precoding impossible [134]. In addition, coding matrix design is usually based on full knowledge of the channel, which is difficult to achieve in the millimeter band because of the large number of antennas used and the

low SNR values before beamforming. Therefore, new channel estimation and coding algorithms need to be developed to fit the mmWave systems.

Analog beamforming solutions have been proposed in [138] and [139]. The main idea is to control the phase of the transmitted signal by each antenna through a network of analog phase shifters. Several solutions, known as "beam training algorithms", have been proposed for the iterative construction of analog beamforming coefficients in the system without channel knowledge at the transmitter. In [138] and [140], adaptive beamforming algorithms and multi-resolution dictionaries have been developed and used jointly by the transmitter and the receiver to build their beamforming vectors. In [139], several beams with unique signatures have been used to reduce the time required for the phase learning. Despite the reduction of complexity in [138] and [141], these methods have always the disadvantage of converging on a single communication beam. Thus, these algorithms are not able to achieve gains in multiplexing by sending several simultaneous data streams. In addition, the performance of analog methods such as [138] and [140], are not optimal in comparison with digital coding solutions because of the constant amplitude constraint on the analog phase shifters and the low resolution of the phase control signal. To allow transmission on several data streams, [141]-[142] propose to share coding operations between the analog and digital domain. In [141], the problem of joint design of an analog and digital precoder has been considered for systems with spatial diversity. In [143], hybrid analog/digital algorithms have been developed to minimize the mean squared error of the received signal in the presence of interference when using phase shifters with quantized phases. The works [141] and [143] are not dedicated for mmWave systems and do not take into account the characteristics of the mmWave channel. In [142], the structure of the mmWave channel and the algorithmic concept of "basis pursuit" are favoured in the design of low-complexity hybrid precoders in order to approach the capacity obtained when the receiver has a perfect knowledge of the channel state. In [144], the construction problem of the hybrid precoder has been considered in the case of systems where the channel is partially known to the transmitter. Even if the hybrid precoding algorithms developed in [142] and [144] manage to overcome the hardware limitations of the analog part and support the transmission of several data streams, the realization of these gains requires some channel knowledge at the transmitter before the construction of the precoding matrices. This encourages the development of multi-path mmWave channel estimation algorithms that allow hybrid precoding to approach the performance of fully digital precoding algorithms.

In [145], algorithms of low computational complexity for the estimation of the mmWave channel and the hybrid precoding in a system equipped with broad antenna arrays in transmission and reception are proposed. These algorithms take into consideration practical assumptions about the mmWave system equipment. This includes the constant modulus and quantized values of the analog phase shifters and the limited number of RF chains. It is shown that channel estimation in massive MIMO multi-cell system hampered by the pilot contamination effect, constitutes a major bottleneck for overall performance [3]. This problem is a famous challenging issue that channel estimation suffer from. PC is defined by re-using the same band of frequencies with different factors among the cells. Moreover, the same orthogonal pilot sequences are re-used possibly and multiplied by an orthogonal transformation among the cells. Hence, the base station coherently combines signals from terminals in other cells. Recently, pilot contamination issue has attracted a great attention from the research community [4, 146]. Indeed, Marzetta in [4] pointed out the presence of this phenomenon which was not encountered in the single-cell scenario. There are several strategies proposed in the literature to overcome the pilot contamination issue. The main historical milestones of PC problem based on some pioneering papers are described in [4, 9, 146, 147]. In [4], authors analyze the PC problem with setting one user per cell and matched-filter (MF) precoding. Furthermore, they develop a new multi-cell MMSE-based precoding method that mitigates this problem. The authors in [148] have proposed a channel estimation strategy which can mitigate PC without the knowledge of any side-information. There are several studies on suppressing inter-cell interference in multi-cell Massive MIMO mmWave systems. For instance, authors in [149] proved that the inter-cell interference level diminishes inversely with the array size, the square root of pilot sequence length and the spatial separation between paths, suggesting different ways of tackling pilot contamination. The paper [150] presents a direction of arrival (DOA) estimation using an estimation of the signal parameter via rotational invariance technique. Furthermore, authors in [151] study the impact of pilot contamination in mmWave and UHF-based Massive MIMO systems, considering a regular hexagonal geometry with a random deployment of users.

Wireless Massive MIMO mmWave communication systems offer many opportunities for 5G such as achieving significant higher spectral efficiency than conventional single-antenna systems [152, 153, 154]. But this performance gain comes at the cost of signal processing complexity increase at the receiver in order to counter-act the multi-user interference (MUI) in the presence of pilot contamination, that is emanated from the simultaneous



data streams receptions from different users.

Many of the proposed techniques, cited above, to deal with PC issue introduce a high complexity load or suppose a cooperation between BS. In this chapter, we address the problem of PC that beamforming can suffer due to the sidelobe signals [4]. The main contribution lies in the innovative systematic design of the analog beamformer precoder based on antenna subset transmission (AST) in mmWave massive MIMO cellular system. The AST has been proposed in [155] that is based on randomizing the sidelobe' patterns. Herein, the main idea of incorporating the AST is to cancel out the interfering signals by randomization in contaminated direction and keeping intact the transmission via the main lobe. Afterward, the standard channel estimation algorithms can then be applied. Also, the proposed approach exploits all transmit antennas. As result, the design respect mmWave hardware constraints.

### V.3 Data model and pilot contamination problem for single path

Consider a mmWave MIMO system composed of  $M_t$  and  $M_r$  transmit and receive antennas, respectively. We consider that both the transmitter and receiver are equipped with a limited number of radio frequency (RF) chains. To estimate the channel matrix, the transmitter sends a pilot signal  $\mathbf{s}$ , with unit energy, ( $\|\mathbf{s}\|_2 = 1$ ) to the receiver. We consider the hybrid beamforming architecture, which combines  $M_r \times N_{RF}$  analog beamformer, denoted by  $\mathbf{F}$ ,  $N_{RF}$  RF chains, and  $N_{RF} \times M_t$  digital beamformer, denoted by  $\mathbf{W}$ , with  $\|\mathbf{F}\|_2 = \|\mathbf{W}\|_2 = 1$ , respectively. The conventional estimator suffers from a lack of orthogonality between the desired and interfering pilots, an effect known as pilot contamination. In particular, when the same pilot sequence is reused in all  $L$  cells, i.e,  $\mathbf{s}_1 = \dots = \mathbf{s}_L = \mathbf{s}$ . Without loss of generality, we consider a system with two cells and each with one user as

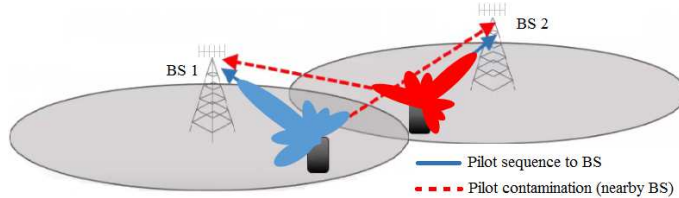


*Figure V.1* — Pilot contamination problem illustration.

the other users have orthogonal pilot sequences within the same considered cell. As shown in Fig. V.1, each user streams toward his BS via the main lobe, and signals from side-lobes reach the nearby BS. In order to transmit a signal, the BS applies two consecutive precod-

ing operations  $\mathbf{F} = \mathbf{F}_{BB}\mathbf{F}_{RF}$ , where  $\mathbf{F}_{BB}$  is the  $N_{RF} \times N_s$  digital precoding performed in the base band and  $\mathbf{F}_{RF}$  with a dimension of  $M \times N_{RF}$  denotes the analog precoder. The elements of  $\mathbf{F}_{RF}$  are considered as constant modules which are implemented using analog phase shifters. At the receiver side, the combiner  $\mathbf{W} = \mathbf{W}_{RF}\mathbf{W}_{BB}$ , composed of an RF combiner  $\mathbf{W}_{RF}$  and a digital one  $\mathbf{W}_{BB}$ , is used to extract the transmitted data from the received signal. After different signal processing operations, the received signal at  $l^{th}$  BS is:

$$\mathbf{y} = \mathbf{w}^H(\sqrt{P_j}\mathbf{h}_{lj}(\theta, \alpha, \phi)\mathbf{f}_j\mathbf{s}_j + \sqrt{P_i}\mathbf{h}_{li}(\theta, \alpha, \phi)\mathbf{f}_i\mathbf{s}_i + \mathbf{n}) \quad (\text{V.1})$$

Where  $(.)^H$  stands for the Hermitian. The indices  $j$  and  $i$  refer to the desired and interfering user of the  $l^{th}$  BS, respectively.  $P_j$  and  $P_i$  are the transmitted power of the desired and interfering user, respectively. The complex additive white Gaussian noise (AWGN) component is denoted by  $\mathbf{n}$  with  $\mathbf{n} \sim \mathcal{N}(0, \sigma_n^2)$ . We adopt a geometric channel model along with a uniform linear array for simplicity of mathematical derivation but the proposed technique can be extended to any other antenna array configuration. The geometric channel model  $\mathbf{h}(\theta, \alpha, \phi)$  is given by:

$$\mathbf{h} = \sqrt{\frac{M_t M_r}{L}} \sum_{j=1}^L \alpha_j \mathbf{a}_{Rx}(\theta_{lj}) \mathbf{a}_{Tx}^*(\phi_{lj}) \quad (\text{V.2})$$

Where  $(.)^*$  stands for the conjugate operator.  $\mathbf{a}_{Rx}$  and  $\mathbf{a}_{Tx}$  denote the reception and transmission antenna array manifold, respectively. Since the array is located along the x-y plane, the receiver's location is specified by the azimuth angle of arrival/departure. Therefore,  $\theta_{lj}$  and  $\phi_{lj}$  are the angles of arrival (AOA) and departure (AoD) between the user and the  $l^{th}$  BS respectively. The path loss gain is denoted by  $\alpha_j$ . The received signal in (V.1) can be rewritten as:

$$\mathbf{y} = \mathbf{w}^H(\sqrt{P_j}\alpha_j\mathbf{h}_{lj}(\theta, \phi)\mathbf{f}_l\mathbf{s}_l + \sqrt{P_i}\alpha_i\mathbf{h}_{li}(\theta, \phi)\mathbf{f}_i\mathbf{s}_i + \mathbf{n}) \quad (\text{V.3})$$

For simplicity, the receiver and transmitter beams are assumed to be aligned for maximum reception i.e  $\mathbf{w} = \mathbf{a}_r(\phi)$ . This assumption is related to beam alignment problem, the reader may see [156] and [157] for more details about this issue. Replacing  $\mathbf{w}$  in (V.3), we get:

$$\begin{aligned} \mathbf{y} &= \sqrt{P_j}\alpha_j\mathbf{a}_r^*(\phi)\mathbf{h}_{lj}(\theta, \phi)\mathbf{f}_l\mathbf{s}_l + \sqrt{P_i}\alpha_i\mathbf{a}_r^*(\phi)\mathbf{h}_{li}(\theta, \phi)\mathbf{f}_i\mathbf{s}_i + \mathbf{v} \\ &= \left(\sqrt{P_j}\alpha_j\mathbf{h}_{lj}(\theta)\mathbf{f}_l + \sqrt{P_i}\alpha_i\mathbf{h}_{li}(\theta)\mathbf{f}_i\right)\mathbf{s} + \mathbf{v} \end{aligned} \quad (\text{V.4})$$

Where the modified noise component is denoted by  $\mathbf{v} = \mathbf{w}^H(\phi)\mathbf{n}$ .

### V.3.1 Proposed solution strategy

If we use directly the equation (V.4) to estimate the channel coefficients, the second term in the equation will make the estimation doubtful. Especially if we assume a perfect synchronization between the desired user and the interfering one which is the worst case in PC scenario.

In this section, we give details about the proposed solution. we incorporate AST to tackle the PC problem in mmWave Massive MIMO cellular system. Indeed a new precoder design  $\mathbf{F}$  is proposed based on AST. Instead of employing all antennas for beamforming, a set of random antennas are used for coherent beamforming, whereas the remaining antennas are set to combine destructively. The indices of these antennas are randomized in every symbol transmission. This randomizes the beam pattern sidelobes and as a result, produces noise-like signals at non-desired directions. Indeed, the BS would observe a fixed gain reduction (due to destructive combining) and a noise-like interference coming from the contaminating user. As mentioned, we adopt a uniform linear array (ULA) with isotopic antennas along the x-axis and the array centered at the mid of the array. Even so, the proposed technique can be adapted to any arbitrary antenna structures. Let  $I_{M_{sub}}(k)$  be the random subset of  $M_{sub}$  out of  $M_t$  antennas used to transmit the  $k^{th}$  symbol,  $I_{L_t}(k)$  be a subset that contains the indices of the remaining antennas. The precoder design is a function of symbol index  $k$ , so with every symbol, a new precoder is used with a different beam pattern. Indeed, we are changing the phase  $\theta$  randomly in the interval  $(0, 2\pi)$ . Hence,  $\theta$  is uniformly distributed. To obtain the randomization, we use a Walsh sequence generator. Walsh Codes are a set of orthonormal codes. Therefore, the generated Walsh sequences  $C$  contains an equal number of 1's and -1's but they are randomly distributed from one shot to another. Walsh is closed in a standard interval  $(0, 1)$  and every function takes the values  $+1, -1$  except the final number, which is zero [158]. The resulted antenna phase shifts are:

$$\Psi_n(k) = \begin{cases} \Upsilon_n(k) & n \in I_{M_{sub}}(k) \\ \Upsilon_n(k) * C, & n \in I_{L_t}(k) \end{cases} \quad (\text{V.5})$$

Where  $(*)$  stands for element-wise multiplication and  $\Upsilon_n(k) = (\frac{M_t-1}{2} - n)2\pi\frac{d}{\lambda}\cos(\theta_{lj})$  is a phase shift valid for the adopted antenna array configuration (ULA). . Therefore, the

transmitter precoder defined by:

$$\mathbf{f}(k) = \frac{1}{\sqrt{M_t}} e^{j\Psi(k)} \quad (\text{V.6})$$

An example of random selection of uniform linear array ULA is illustrated in Fig.V.2. For every pilot symbol, a set of antennas are settled to combine coherently (black color) whereas the other remaining antennas (black and red antennas) are set to combine destructively. After choosing randomly the  $M_{sub}$  antennas for the main beam pattern (black antennas), one of the random Walsh sequences is set to the black and red antennas. For example, for  $C = [1 -1 -1 -1 1 1 -1 1]$  will give us the configuration in figure V.2 where 1's are set for antennas in red and -1s for black antennas. This configuration is altered at every new pilot symbol. For example, the first "black antenna" can become a red or a black one and so is for other antennas.

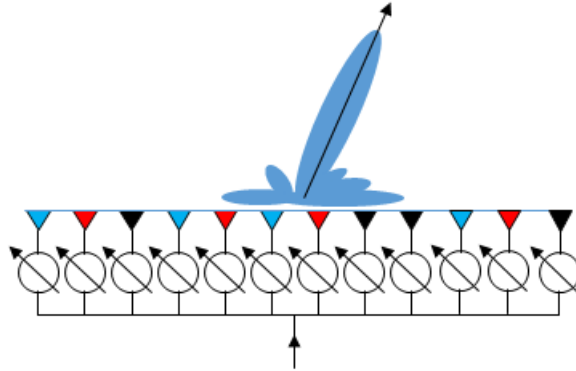


**Figure V.2** — Antenna selection pattern for a uniform linear array: black antennas coherently co-phased to combine at BS, black and red antennas co-phased to destructively combine at BS.

Another example concerning the obtained antenna beam pattern is depicted in Fig. V.3. In this figure, we plot the beam-pattern versus the transmitted angle using 32 and 16 transmit antennas. In Fig. V.3, the randomness of antenna selection only appears in the region of side lobes, and there is no randomness in the region of the main lobe. Also, it is shown that the beam-pattern of the proposed technique varies at all angular locations except at the transmitted angular location ( $\theta = 30^\circ$  in this example). While the conventional array transmission techniques result in a constant radiation pattern at contaminated user i.e large sidelobes on average and a unique beam pattern along all the emitted symbols.

To show the contribution of the used approach, the data models obtained for the two

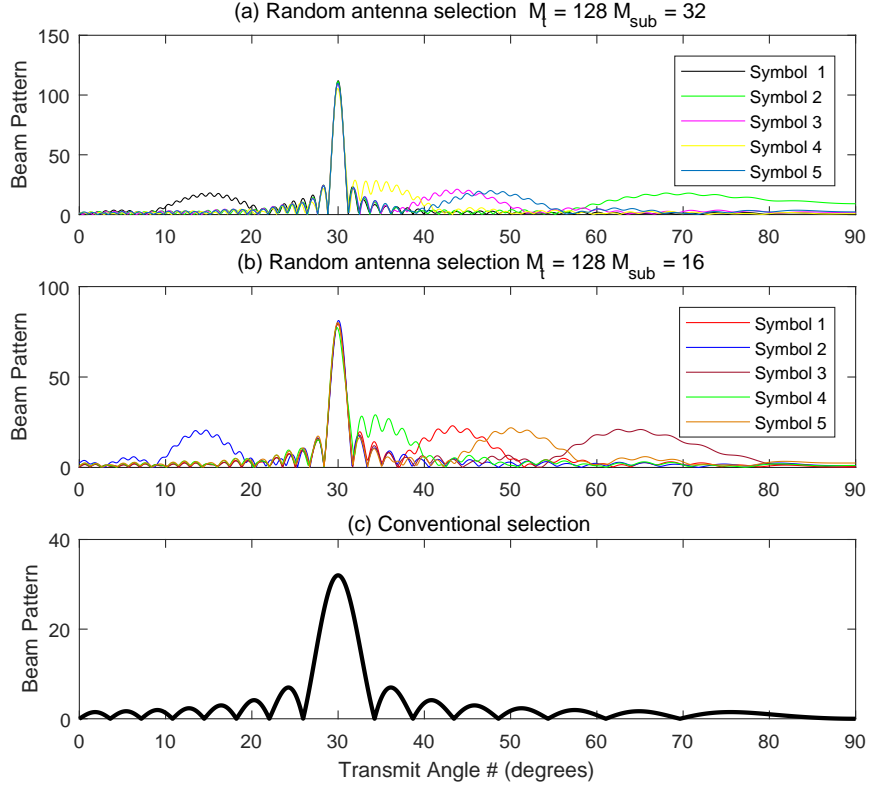


**Figure V.3** — Successive antenna beam patterns using randomization (a and b) and conventional radiation (c) .

cases: conventional and AST transmissions are to be considered.

### V.3.1.1 Conventional array transmission

In conventional array transmission, the transmitter precoder defined in (V.6) is placed in the equation (V.4), we get:

$$\begin{aligned}
 \mathbf{y} &= \sqrt{\frac{P_j M_r}{M_t}} \alpha_j \sum_{n=0}^{M_t-1} e^{j(n-\frac{M_t-1}{2})\frac{2\pi d}{\lambda}(\cos\theta_{l_j}-\cos\theta_{l_i})} \mathbf{s} + \sqrt{\frac{P_i M_r}{M_t}} \alpha_i \sum_{n=0}^{M_t-1} e^{j(n-\frac{M_t-1}{2})\frac{2\pi d}{\lambda}(\cos\theta_{l_j}-\cos\theta_{l_i})} \mathbf{s} + \mathbf{v} \\
 &= \sqrt{P_j M_r M_t} \alpha_j \mathbf{s} + \sqrt{\frac{P_i M_r}{M_t}} \alpha_i \left( e^{-j\frac{M_t-1}{2}\frac{2\pi d}{\lambda}(\cos\theta_{l_j}-\cos\theta_{l_i})} \sum_{n=0}^{M_t-1} e^{jn\frac{2\pi d}{\lambda}(\cos\theta_{l_j}-\cos\theta_{l_i})} \right) \mathbf{s} + \mathbf{v} \quad (\text{V.7})
 \end{aligned}$$

Where the angles  $\theta_{l_j}$  and  $\theta_{l_i}$  are the AOAs of mainlobe and sidelobes of users signals  $j$  and  $i$ , respectively. The angle  $\theta_{l_i}$  belongs to the contaminating user. Whereas  $\theta_{l_j}$  behooves to the desired user.

The summation in the second term of (V.7) is an exponential sum of the form  $\sum_{k=0}^{N-1} r^k =$

$\frac{1-r^N}{1-r}$ . Hence, we get:

$$\begin{aligned} \mathbf{y} &= \sqrt{P_j M_r M_t} \alpha_j \mathbf{s} + \sqrt{\frac{P_i M_r}{M_t}} \alpha_i \left[ e^{-j(\frac{M_t-1}{2})2\pi\frac{d}{\lambda}(\cos\theta_{lj}-\cos\theta_{li})} \left( \frac{1 - e^{jM_t 2\pi\frac{d}{\lambda}(\cos\theta_{lj}-\cos\theta_{li})}}{1 - e^{j2\pi\frac{d}{\lambda}(\cos\theta_{lj}-\cos\theta_{li})}} \right) \right] \\ &= \sqrt{P_j M_r M_t} \alpha_j \mathbf{s} + \sqrt{\frac{P_i M_r}{M_t}} \alpha_i \left( \frac{\sin M_t \frac{\pi d}{\lambda} (\cos\theta_{lj} - \cos\theta_{li})}{\sin \frac{\pi d}{\lambda} (\cos\theta_{lj} - \cos\theta_{li})} \right) \mathbf{s} + \mathbf{v} \end{aligned} \quad (\text{V.8})$$

### V.3.1.2 Antenna subset transmission (AST)

In Antenna subset transmission, the entries of the transmitting beamformer vector  $\mathbf{f}(k)$  are placed in (V.5). Hence, the received signal in (V.4) becomes:

$$\begin{aligned} \mathbf{y} &= \sqrt{\frac{P_j M_r}{M_t}} \alpha_j \left[ \sum_{m \in I_{M_{sub}}(k)} e^{-j(\frac{M_t-1}{2}-m)\frac{2\pi d}{\lambda} \cos\theta_{lj}} e^{j(\frac{M_t-1}{2}-m)\frac{2\pi d}{\lambda} \cos\theta_{lj}} \right. \\ &+ \sum_{n \in I_{L_t}(k)} e^{-j(\frac{M_t-1}{2}-n)\frac{2\pi d}{\lambda} \cos\theta_{lj}} e^{j(\frac{M_t-1}{2}-n)\frac{2\pi d}{\lambda} \cos\theta_{lj}} - \sum_{n \in I_{L_t}(k)} e^{-j(\frac{M_t-1}{2}-n)\frac{2\pi d}{\lambda} \cos\theta_{lj}} e^{j(\frac{M_t-1}{2}-n)\frac{2\pi d}{\lambda} \cos\theta_{lj}} \left. \right] \mathbf{s} \\ &+ \sqrt{\frac{P_i M_r}{M_t}} \alpha_i \left[ \sum_{m \in I_{M_{sub}}(k)} e^{-j(\frac{M_t-1}{2}-m)\frac{2\pi d}{\lambda} \cos\theta_{lj}} e^{j(\frac{M_t-1}{2}-m)\frac{2\pi d}{\lambda} \cos\theta_{li}} \right. \\ &+ \sum_{n \in I_{L_t}(k)} e^{-j(\frac{M_t-1}{2}-n)\frac{2\pi d}{\lambda} \cos\theta_{lj}} e^{j(\frac{M_t-1}{2}-n)\frac{2\pi d}{\lambda} \cos\theta_{li}} \\ &- \sum_{n \in I_{L_t}(k)} e^{-j(\frac{M_t-1}{2}-n)\frac{2\pi d}{\lambda} \cos\theta_{lj}} e^{j(\frac{M_t-1}{2}-n)\frac{2\pi d}{\lambda} \cos\theta_{li}} \left. \right] \mathbf{s} + \mathbf{v} \\ &= \sqrt{\frac{P_j M_r}{M_t}} \alpha_j \left[ \sum_{m \in I_{M_{sub}}(k)} e^{-j(\frac{M_t-1}{2}-m)\frac{2\pi d}{\lambda} (\cos\theta_{lj}-\cos\theta_{lj})} + \sum_{m \in I_{L_t}(k)} e^{-j(\frac{M_t-1}{2}-m)\frac{2\pi d}{\lambda} (\cos\theta_{lj}-\cos\theta_{lj})} \right. \\ &- \sum_{n \in I_{L_t}(k)} e^{-j(\frac{M_t-1}{2}-n)\frac{2\pi d}{\lambda} (\cos\theta_{lj}-\cos\theta_{lj})} \left. \right] \mathbf{s} + \sqrt{\frac{P_i M_r}{M_t}} \alpha_i \left[ \sum_{m \in I_{M_{sub}}(k)} e^{-j(\frac{M_t-1}{2}-m)\frac{2\pi d}{\lambda} (\cos\theta_{lj}-\cos\theta_{li})} \right. \\ &+ \sum_{n \in I_{L_t}(k)} e^{-j(\frac{M_t-1}{2}-n)\frac{2\pi d}{\lambda} (\cos\theta_{lj}-\cos\theta_{li})} - \sum_{n \in I_{L_t}(k)} e^{-j(\frac{M_t-1}{2}-n)\frac{2\pi d}{\lambda} (\cos\theta_{lj}-\cos\theta_{li})} \left. \right] \mathbf{s} + \mathbf{v} \\ &= \left( \sqrt{\frac{P_j M_r}{M_t}} \alpha_j M_{sub} + \sqrt{P_i M_r} \alpha_i \beta \right) \mathbf{s} + \mathbf{v} \end{aligned} \quad (\text{V.9})$$

The term  $\beta$  in (V.9) is:

$$\begin{aligned} \beta &= \sqrt{\frac{1}{M_t}} \left( \sum_{m \in I_{M_{sub}}(k)} e^{-j(\frac{M_t-1}{2}-m)\frac{2\pi d}{\lambda}(\cos\theta_{l_j}-\cos\theta_{l_i})} + \sum_{n \in I_{L_t}(k)} e^{-j(\frac{M_t-1}{2}-n)\frac{2\pi d}{\lambda}(\cos\theta_{l_j}-\cos\theta_{l_i})} \right. \\ &\quad \left. - \sum_{n \in I_{L_t}(k)} e^{-j(\frac{M_t-1}{2}-n)\frac{2\pi d}{\lambda}(\cos\theta_{l_j}-\cos\theta_{l_i})} \right) \end{aligned} \quad (\text{V.10})$$

Since the entries of  $I_{M_{sub}}(k)$  and  $I_{L_t}(k)$  are randomly selected for each data symbol, (V.10) can be simplified to

$$\beta = \sqrt{\frac{1}{M_t}} \sum_{m=0}^{M_t-1} B_m e^{-j(\frac{M_t-1}{2}-m)\frac{2\pi d}{\lambda}(\cos\theta_{l_j}-\cos\theta_{l_i})} \quad (\text{V.11})$$

In AST, the selected number of antenna  $M_{sub}$  are chosen independently at random from  $M_t$  for each symbol, therefore, by definition, we adopt an independent Bernoulli random variable. Indeed, the well know distribution is characterized by its parameters  $p$  and  $q$ . By denoting  $B_m$  as the Bernoulli random variable so, when  $B_m = 1$  the probability is  $p = \frac{(M_{sub} + \frac{M_t - M_{sub}}{2})}{M_t} = \frac{M_t + M_{sub}}{2M_t}$  whereas, for  $B_m = -1$  the probability is  $q = \frac{M_t - M_{sub}}{2M_t}$  [155]. We note that if  $\theta_{l_i} = \theta_{l_j}$ ,  $\beta$  will be a constant, the random behavior is obtained when  $\theta_{l_i} \neq \theta_{l_j}$ , thus the destructive combination is obtained in the last case. As  $\beta$  is a random variable, we need to evaluate its statistical characteristics. For a large number of antennas  $M_t$ ,  $\beta$  is a summation of distributions. Referring to central limits theorem,  $\beta$  is a Gaussian random variable that is completely characterized by its mean and variance.

### 1. Mean of $\beta$ :

$$E(\beta) = \sqrt{\frac{1}{M_t}} \sum_{m=0}^{M_t-1} E(B_m) e^{-j(\frac{M_t-1}{2}-m)\frac{2\pi d}{\lambda}(\cos\theta_{l_j}-\cos\theta_{l_i})} \quad (\text{V.12})$$

Where  $E$  is the mathematical expectation, with

$$\begin{aligned} E(B_m) &= p \times (1) + q \times (-1) \\ &= \frac{M_t + M_{sub}}{2M_t} - \frac{M_t - M_{sub}}{2M_t} = \frac{M_{sub}}{M_t} \end{aligned} \quad (\text{V.13})$$

Equation (V.12) can be rewritten as :

$$E(\beta) = \frac{M_{sub}}{M_t} \sqrt{\frac{1}{M_t}} \sum_{m=0}^{M_t-1} e^{-j(\frac{M_t-1}{2}-m)\frac{2\pi d}{\lambda}(\cos\theta_{lj}-\cos\theta_{li})} \quad (V.14)$$

Using the same steps in (V.7) and (V.8), we obtain:

$$E(\beta) = \frac{M_{sub}}{M_t} \sqrt{\frac{1}{M_t}} \left( \frac{\sin M_t \frac{\pi d}{\lambda} (\cos\theta_{lj} - \cos\theta_{li})}{\sin \frac{\pi d}{\lambda} (\cos\theta_{lj} - \cos\theta_{li})} \right) \quad (V.15)$$

## 2. Variance of $\beta$ :

$$\text{Var}(\beta) = \frac{1}{M_t} \sum_{m=0}^{M_t-1} \text{Var}(B_m) e^{-j2(\frac{M_t-1}{2}-m)\frac{2\pi d}{\lambda}(\cos\theta_{lj}-\cos\theta_{li})} \quad (V.16)$$

Where:

$$\text{Var}(B_m) = E(B_m^2) - (E(B_m))^2 \quad (V.17)$$

We Calculate the first term of (V.17) as:

$$E(B_m^2) = (1)^2 + q(-1)^2 = \frac{M_t + M_{sub}}{2M_t}(1) + \frac{M_t - M_{sub}}{2M_t}(1) = 1 \quad (V.18)$$

Hence, we obtain the variance:

$$\text{Var}(B_m) = 1 - \frac{M_{sub}^2}{M_t^2} \quad (V.19)$$

Finally, the variance in (V.16) can be expressed as:

$$\begin{aligned} \text{Var}(\beta) &= \frac{M_t^2 - M_{sub}^2}{M_t^3} \sum_{m=0}^{M_t-1} m = 0^{M_t-1} e^{-j2(\frac{M_t-1}{2}-m)\frac{2\pi d}{\lambda}(\cos\theta_{lj}-\cos\theta_{li})} \\ &= \frac{M_t^2 - M_{sub}^2}{M_t^3} \left( \frac{\sin M_t \frac{2\pi d}{\lambda} (\cos\theta_{lj} - \cos\theta_{li})}{\sin \frac{2\pi d}{\lambda} (\cos\theta_{lj} - \cos\theta_{li})} \right) \end{aligned} \quad (V.20)$$



### V.3.2 Signal to interference ratio derivation

In this section, we derive the signal-to-interference ratio (SIR) for both two cases: antenna subset and conventional array transmissions [9]. The SIR formula is given as:

$$\mathbf{SIR} = \frac{\|\sqrt{P_j}\alpha_j\mathbf{a}_r^*(\phi)\mathbf{h}_{lj}\mathbf{f}_l\|^2}{\|\sqrt{P_i}\alpha_i\mathbf{a}_r^*(\phi)\mathbf{h}_{li}\mathbf{f}_i\|^2} \quad (\text{V.21})$$

1. Conventional array transmission: Using equations (V.8) and (V.21), the obtained SIR is:

$$\begin{aligned} \mathbf{SIR}_{\text{CAT}} &= \frac{\left(\sqrt{P_j M_r M_t} \alpha_j\right)^2}{\left(\sqrt{\frac{P_i M_r}{M_t}} \alpha_i \frac{\sin\left(M_t \frac{\pi d}{\lambda} (\cos\theta_{lj} - \cos\theta_{li})\right)}{\sin\left(\frac{\pi d}{\lambda} (\cos\theta_{lj} - \cos\theta_{li})\right)}\right)^2} \\ &= \frac{P_j M_t^2 \alpha_j^2}{P_i \alpha_i^2 \left(\frac{\sin\left(M_t \frac{\pi d}{\lambda} (\cos\theta_{lj} - \cos\theta_{li})\right)}{\sin\left(\frac{\pi d}{\lambda} (\cos\theta_{lj} - \cos\theta_{li})\right)}\right)^2} \end{aligned} \quad (\text{V.22})$$

2. Antenna Subset Transmission (AST) selection: By using (V.9), the SIR presented in (V.21) becomes:

$$\begin{aligned} \mathbf{SIR}_{\text{AST}} &= \frac{\frac{P_j M_r \alpha_j^2 M_{sub}^2}{M_t}}{P_i M_r \alpha_i^2 \text{Var}(\beta)} \\ &= \frac{P_j \alpha_j^2 M_{sub}^2 M_t^2}{P_i \alpha_i^2 \left[ (M_t^2 - M_{sub}^2) \left( \frac{\sin M_t \frac{2\pi d}{\lambda} (\cos\theta_{lj} - \cos\theta_{li})}{\sin \frac{2\pi d}{\lambda} (\cos\theta_{lj} - \cos\theta_{li})} \right) \right]} \end{aligned} \quad (\text{V.23})$$

Now, using some trigonometric identities, we express the following ratio :

$$\begin{aligned} Fa &= \frac{\mathbf{SIR}_{\text{AST}}}{\mathbf{SIR}_{\text{CAT}}} \\ &= \frac{M_{sub}^2}{(M_t^2 - M_{sub}^2)} \times \left( \frac{\tan\left(M_t \frac{\pi d}{\lambda} (\cos\theta_{lj} - \cos\theta_{li})\right)}{\tan\left(\frac{\pi d}{\lambda} (\cos\theta_{lj} - \cos\theta_{li})\right)} \right) \end{aligned} \quad (\text{V.24})$$

In the above equation, we have assumed that the path losses  $\alpha_i$  and  $\alpha_j$  are equal and the signal power  $P_i = P_j = 1$ .

To determine the suitable number  $M_{sub}$  to have a factor greater than unity, we have represented the factor  $Fa$ , defined in V.24, versus  $M_{sub}$  in Fig. V.4. According to the obtained curves, it follows that it is desirable to use  $M_{sub}$  as close as possible to  $M_t$  to have a factor  $Fa$  greater than unity. If  $M_{sub}$  is correctly settled, this will lead to  $\mathbf{SIR}_{AST} > \mathbf{SIR}_{CAT}$ .

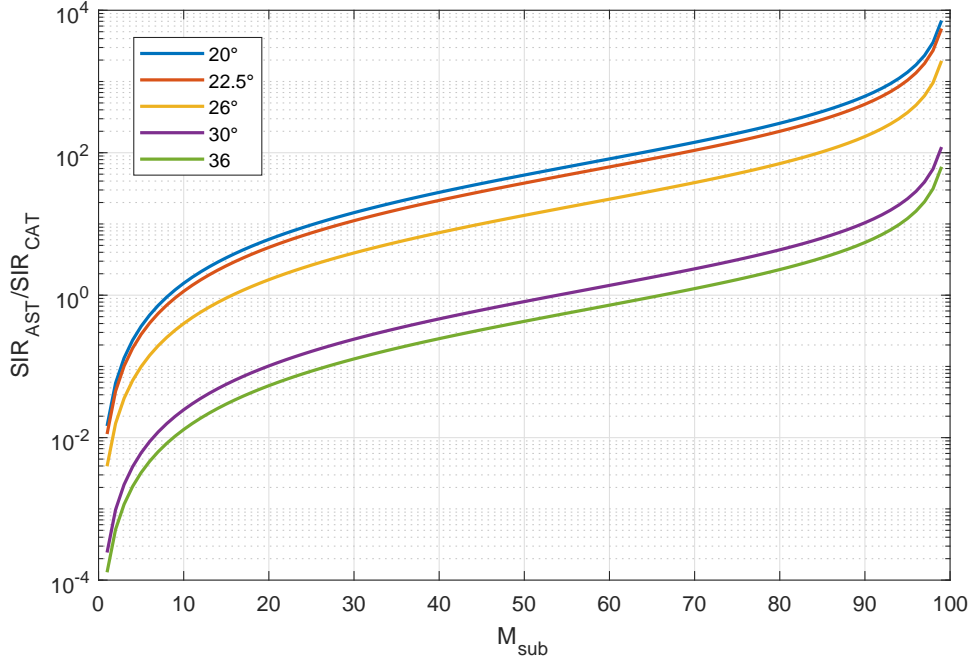


**Figure V.4** — Ratio  $Fa$  versus  $M_{sub}$ ,  $M_t = 100$  and  $\theta_i = 22^\circ$ .

Thereby, the key feature in the AST based PC mitigation is the choice of the number of antennas  $M_t$  and  $M_{sub}$ . In figure V.5, we sketch the  $SIR$  evolution versus the number of used antennas  $M_t$  in user side where  $M_{sub}$  is taken as a factor of  $M_t$ . The obtained results reveal that increasing  $M_t$  gives better performance while increasing the ratio  $\frac{M_t}{M_{sub}}$  degrades the performance for all cases. This is due to the fact that increasing the ratio, makes the main lobe much wider as fewer antennas are used for streaming the symbols thus the BS receive less power from the desired direction. Hence, the best interval for the ratio is  $[1.2, 2]$ . Also, this figure reveals that using less than the half of antennas for the mainlobe is not suitable as the performance degrades dramatically. Generally, using more antennas is beneficial and the only limit is the practical realization of such array, in some UE it is not possible to use a large number of antennas.

The designed precoder can be used at UE or BS level. The only requirement is the presence of an antenna array (this condition may be not satisfied in some microwave systems at UE level). Thus, it is not specific to the mmWave system but can be used in microwave

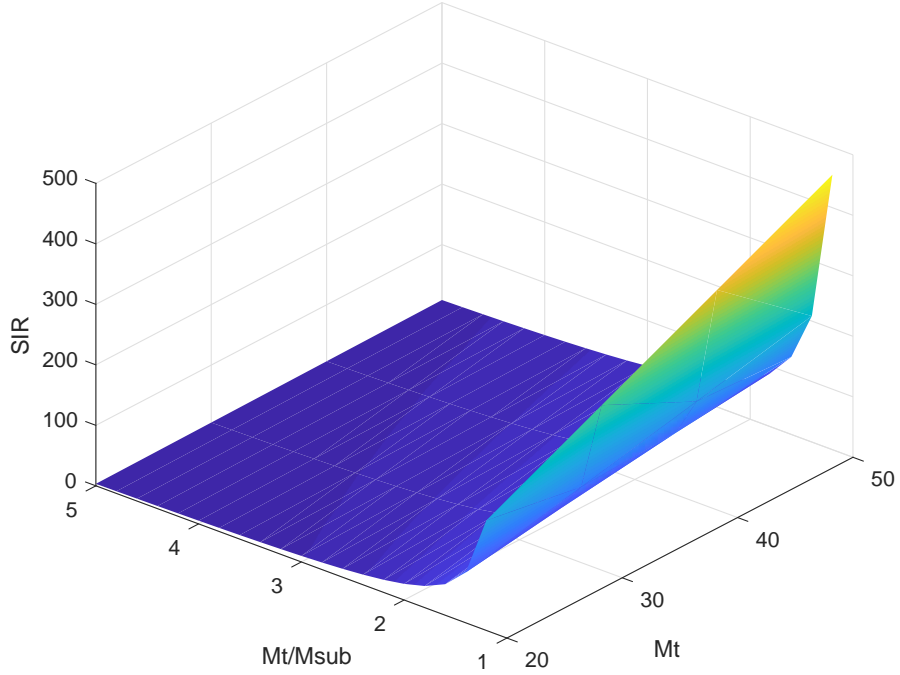


**Figure V.5** — Signal to interference ratio (SIR) versus  $M_t$  and  $M_{sub}$ .  $\theta_i = 70^\circ$  and  $\theta_j = 160^\circ$

system at least in the BS. After designing the AST-based precoder, a channel estimation algorithm can be used in presence of PC. Afterward, hybrid precoders/combiners,  $(\mathbf{F}_{RF}, \mathbf{F}_{BB}, \mathbf{W}_{RF}, \mathbf{W}_{BB})$  are settled at both the BS and UE to maximize the data rate of transmission over the Massive MIMO mmWave systems (V.1). Hence, to confirm the effectiveness of the proposed approach, spectral efficiency (SE) is calculated at the user level. The equation of SE is defined as [159]:

$$\text{Rate} = \log_2 \left( |\mathbf{I}_{N_s} + \frac{\alpha}{N_s} \mathbf{R}_n^{-1} \mathbf{W}_{BB}^* \mathbf{W}_{RF}^* \mathbf{H} \mathbf{F}_{RF} \mathbf{F}_{BB} \times \mathbf{F}_{BB}^* \mathbf{F}_{RF}^* \mathbf{H} \mathbf{W}_{RF} \mathbf{W}_{BB}| \right) \quad (\text{V.25})$$

Where  $\mathbf{R}_n^{-1} = \sigma_n^2 \mathbf{W}_{BB}^* \mathbf{W}_{RF}^* \mathbf{F}_{RF} \mathbf{F}_{BB}$  denotes for the noise covariance matrix and  $\sigma_n^2$  is the noise variance at UE level. The expression of the matrices  $\mathbf{W}_{BB}^*$ ,  $\mathbf{W}_{RF}^*$ ,  $\mathbf{F}_{RF}$ ,  $\mathbf{F}_{BB}$  depend on the used precoding techniques (purely digital, purely analog or hybrid precoding) [133]-[149]-[160]-[161].

### V.3.3 Simulation results

In this section, we consider two simulation configurations, we begin with two cells system each with one user sending the same pilot signals to BS of cell 1. The second configuration considers three cells configuration. Simulations are carried out for the proposed AST scheme along with the conventional transmission counterpart in the presence of PC. The

simulation parameters are fixed and generated as the ones used in [133] and we used the same channel estimation technique. Herein, the BS has  $M_r = 64$  antennas, the AST technique is applied in the MS side, so  $M_r$  has not an impact on the AST performance. Certainly, increasing  $M_r$  will increase performance but this is due to MIMO gain rather than to AST technique. 10 RF chains are used with a transmitted power of 37 dBm. The mobile station (MS) uses 64, 128, and 256 antennas and 6 RF chains. Both the BS and the MS are equipped with uniform linear array (ULA) with an inter-element spacing of  $\lambda/2$ . The number of transmitted data streams is  $N_s = 3$ . Hybrid precoder concept divides the precoding operations into two cascaded stages, namely, the low-dimensional baseband precoding and the high dimensional phase-only processing at the RF domain. We use the geometric channel model with an average power gain of  $P_R = 1$  and a single path. The AoAs/AoDs are assumed to be uniformly distributed between 0 and  $2\pi$ . The system is assumed to operate at 28 GHz carrier frequency and has a band width of 100 MHz with path loss exponent  $n_{pl} = 3$ . Moreover, to examine the behavior of the SE, four scenarios are simulated. The first scenario is based on the perfect CSI knowledge along with unconstrained precoding and is used as a benchmark to other scenarios. Here, unconstrained precoding means that only digital beamforming (no analog precoding is in order) is used. The second and the third scenario are constrained cases where we use an hybrid precoding but with and without pilot contamination. We expect that the proposed technique lies between these last two scenarios. In all the three scenarios, conventional transmission is used, only our proposal uses AST-based precoder with  $M_{sub} = 32$ .

It appears from the results reported in Fig V.6 that the application of the proposed AST in the presence of PC allows achieving better SE, as compared to conventional one. Whereas, the results indicate that comparable gains can be achieved using the proposed scheme with a perfect CSI. We can remark that at SNR of  $-5dB$ , the random selection has SE gain of  $5bps/Hz$  compared to conventional selection. Also, we can see that the achieved SE in the presence of PC of the proposed scheme is very close to the case without PC. This results are confirmed in the figures V.7 and V.8 where  $M_t$  is set to 128 and 256 respectively. The SE performance keeps increasing. Noting also that a slight difference occurs when we increase  $M_t$  and keeping  $M_{sub}$  fixed (comparing AST-based technique to the PC-free system), in fact, it confirms the results in V.5 where it is suitable to keep a factor around 2 for better performance.

In the second part, we consider the configuration case of three cells (two neighboring cells each with one contaminating UE), a slight decrease of SE (dashed green line curves in

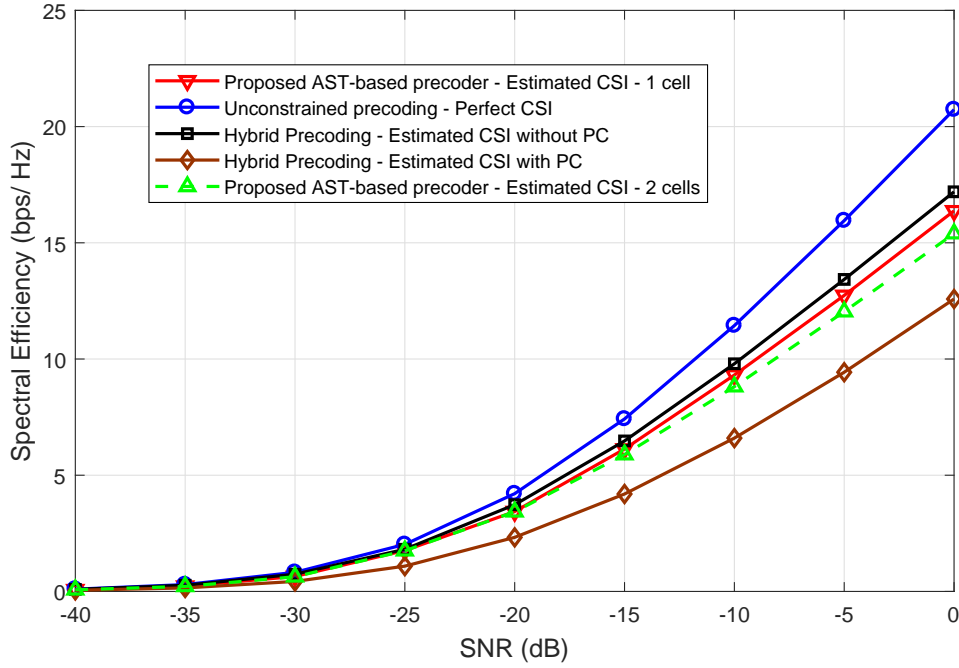


Figure V.6 — Spectral efficiency (SE) comparison with  $M_t = 64$ .

figures V.6, V.7 and V.8) is observed but our proposal still achieve good performance. Hence, we can deduce that the random antenna selection has better performance than the fixed antenna selection even in the presence of PC. This can be explained by the gain factor of  $(M_{sub}^2)$  that appear in (V.23), and reduction of the amount of contaminating user interference when comparing the two equations (V.22) and (V.23). Hence, The SIR improvements achieved by the proposed configuration provides a significant gain in SE.

To assess the performance of the proposed technique in term of used antennas for randomization, the spectral efficiency of the proposed antenna selection is compared for a different number  $M_t$  and  $M_{sub}$ , while keeping the same ratio, i.e  $R = \frac{M_t}{M_{sub}} = 4$  for each curve. We assume the same simulation parameters with Fig. V.6 except for the number of antennas  $M_t$ . From Fig. V.9, it is observed that the spectral efficiency brought from  $M_{sub} = 32$  is significant over  $M_{sub} = 16$ ,  $M_{sub} = 8$  and  $M_{sub} = 4$ . Thereby, increasing the number of random and total antenna, while fixing the ratio between them results in improvement of the performance. This can be explained by the fact that increasing  $M_{sub}$  makes the sidelobes signals more noise-like and also keeping the ratio constant makes the main lobe more directive, hence more effective in directing the desired signal power to the desired BS. As a result, the number of selected random antenna arising from the proposed scheme in mmWave Massive MIMO has a drastic effect on the performance. Figure V.10

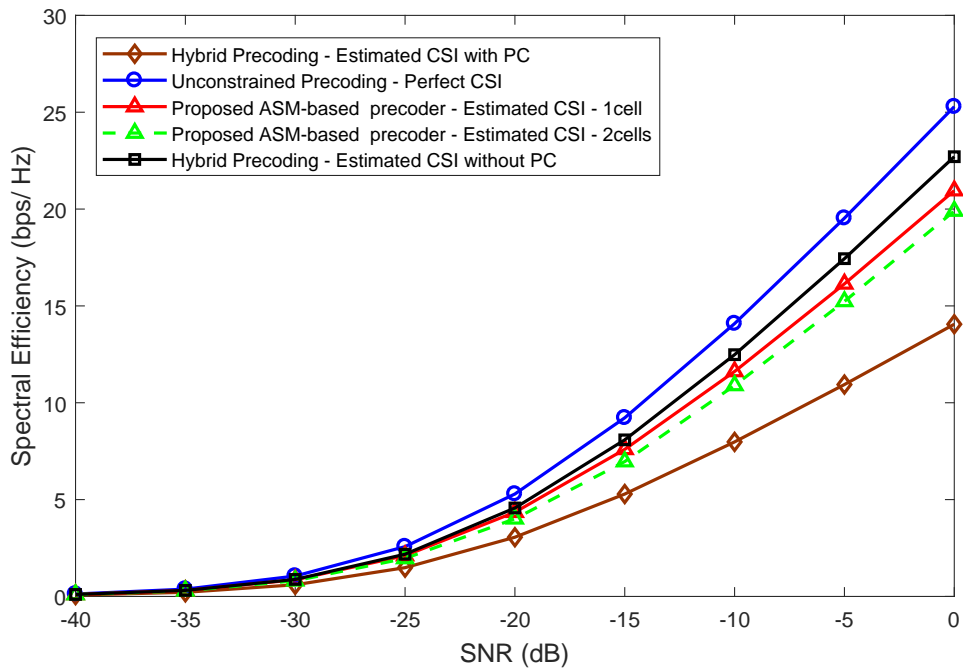


Figure V.7 — Spectral efficiency (SE) comparison with  $M_t = 128$ .

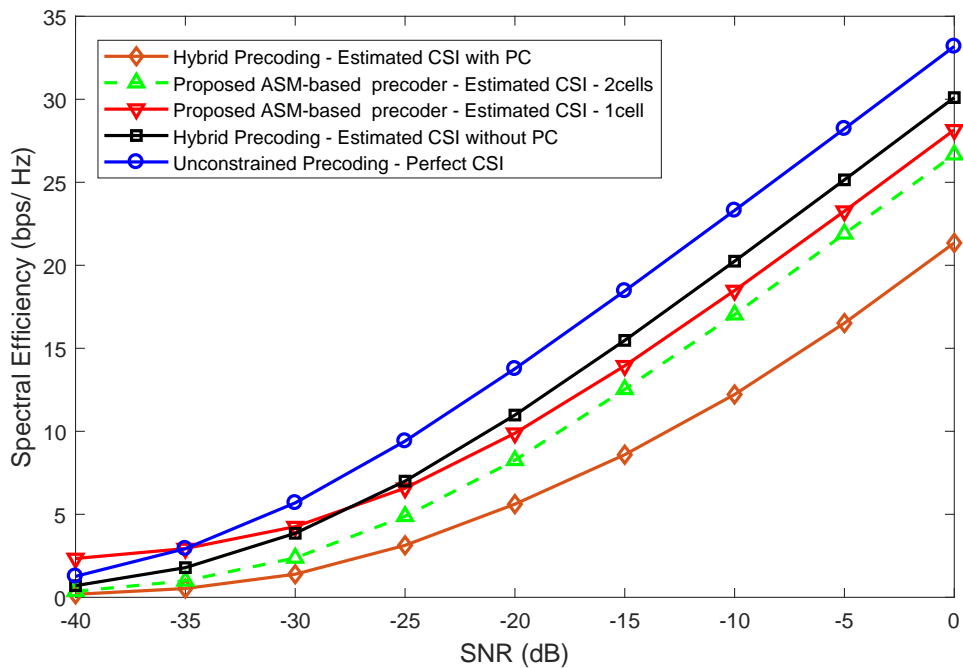


Figure V.8 — Spectral efficiency (SE) comparison with  $M_t = 256$ .

depicts the SE performance while keeping  $M_t$  fixed and varying  $M_{sub}$ , the same remark can be made, increasing  $M_{sub}$  increase the performance, it is better to have  $M_{sub}$  close to  $M_t$  to maximize the performance.

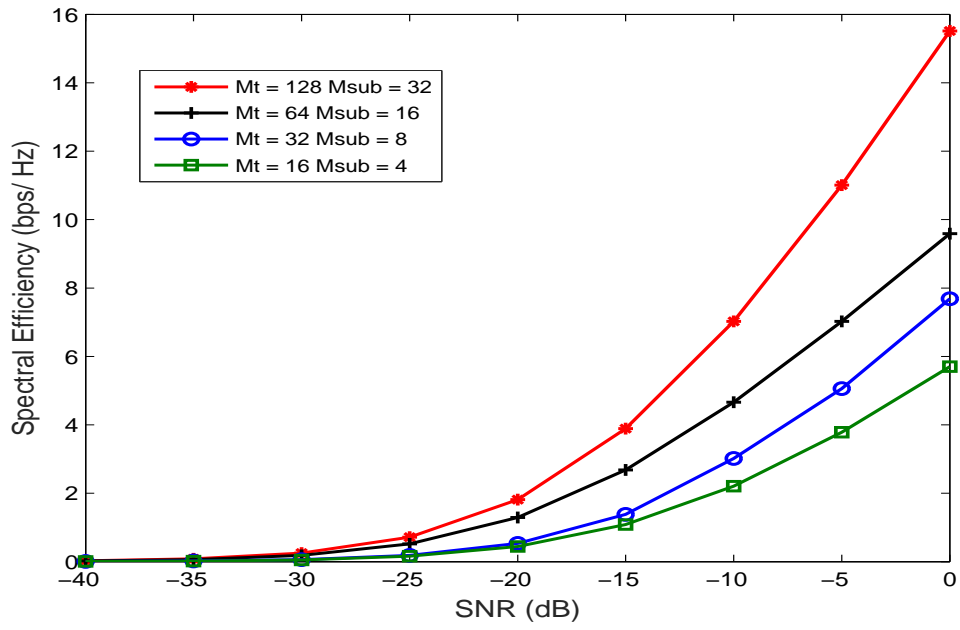


Figure V.9 — Spectral efficiency (SE) for different values of  $M_{sub}$  with a fixed ratio  $M_t/M_{sub} = 4$

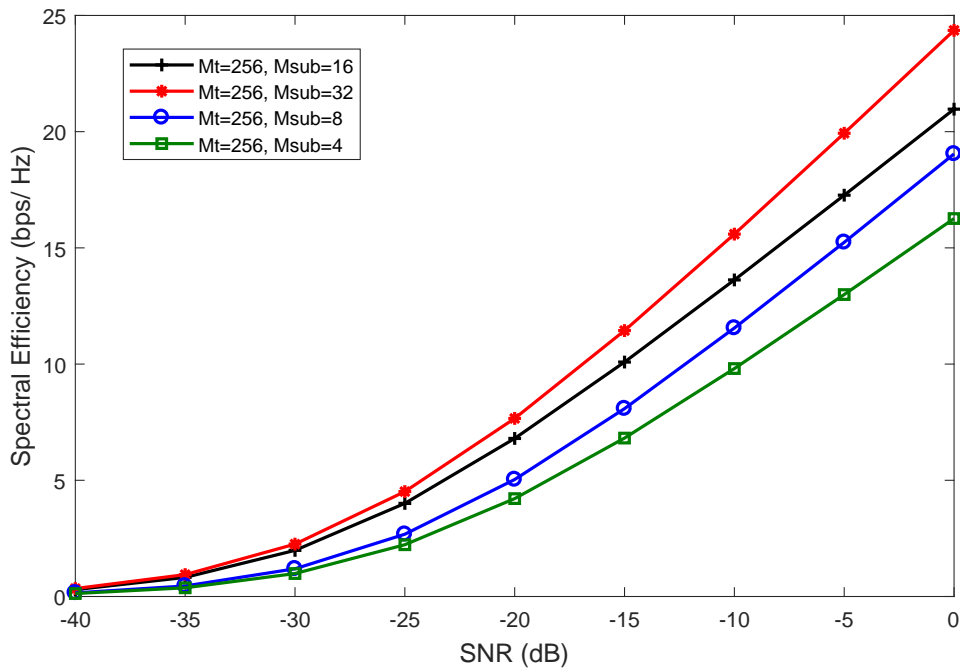


Figure V.10 — Spectral efficiency (SE) for different values of  $M_{sub}$  with a fixed value  $M_t$

# CONCLUSION



## CONCLUSION

Wireless communications plays an important role in our society and they are in constant progress to adjust to the increasing number of users and services. Several new techniques and technologies have been implemented along the years. In terms of cellular communications major advances were divided by the so called generations, the first one characterized by using analog voice communications, the second had digital voice communications, the third had multimedia data services and now with the introduction of 5G the concept anywhere, anything, any-time gains a complete new meaning with high data rates, great cell coverage and high mobility for the end user. The goal of this work was to develop a transmission channel estimation technique for mmWave cellular and Massive MIMO systems to combat pilot contamination problem.

- In first chapter of this thesis, we started with a quick overview of the evolution of cellular communications. then, we have retraced the history of the evolution of cellular networks. We justified the transition to 5G. Then we have described some possible architectures for a 5G cellular system and the multiple access and modulation techniques being developed for use in the next generation. We have listed some challenges and areas of research to be enriched before deploying a real mmWave cellular network.
- In chapter 2, we have proposed to incorporate the algorithm of source separation SOBI, and NOMA scheme in special case IDMA to ensure communication in the presence of RSI and MAI. The robustness of the novel scheme to the residual interference created by the BS, multipath and multiuser was highlighted. Moreover, a new scheme for baseband RSI cancellation stage in full-duplex Massive MIMO transceivers have been proposed. The SOBI algorithm is applied to find the residual SI channel and to compensate the SI distortion caused by the transmitter impairments. This proposed scheme performs estimation of residual SI channel blindly. Compared to the standard non-blind LS estimator, the proposed scheme does not require training blocks to find the residual SI channel. Furthermore, it is able to compensate the distorted SI and achieve nearly the same performance as the half-duplex (HD) case. Finally, simulation results have shown that the proposed algorithm improves the channel estimation accuracy and the cancellation performance. Furthermore, the impact of antenna configuration of SI signal is expressed. It is

shown, with both models, that FD-massive MIMO systems are more sensitive to the antenna configuration.

- In chapter 3, an oblique projection integrated inside zero forcing beamformer is proposed in massive MIMO downlink transmission to mitigate the interference coming from the neighboring cells. Compared with an MMSE and ZF beamforming, it is unnecessary that the desired signal and the interference are orthogonal. It has been shown that this system outperforms MMSE and ZF beamformer in terms of Achievable Rate to channel adverse effects. This is due to the additional protection offered by the OP projector. The simulation results show that the OP beamforming can enhance the desired signal while nulling the multiple interference components perfectly. Furthermore, our results show the superiority of our proposed algorithm to the reference schemes.
- In chapter 4, we have studied the impact of pilot contamination in multicell massive MIMO systems and investigate schemes to mitigate it. We evaluate the MSE of channel estimates in case of a BU-ESPRIT algorithm. Indeed, we incorporate a new approach channel parameter estimation based on BU-ESPRIT algorithm to combat the PC problem. Simulations have revealed that the results attained by adopting the BU-ESPRIT approach are close to the results of the system not expressing the PC issue, thus confirming the potential of the incorporated algorithm to mitigate the PC problem. Moreover, the obtained results approach the CRB bound.
- In chapter 5, we have proposed an approach to deal with PC issue in mmWave massive MIMO cellular system. The proposed precoder employs AST for mitigating the PC problem. Hence, the novelty of this work is based on distorting the sidelobes signal by generating a random sequence using Walsh codes and as result, it combines in a destructive manner in reception. To confirm our approach, simulation results indicate that the proposed precoder realizes SE gain that is close to the one of PC free system. Moreover, the adopted technique is of low cost as no hardware complexity is added compared to conventional systems.

This thesis has allowed us to deepen our knowledge of the basic concepts of cellular systems as well as the estimation techniques of the transmission channel. We also gained knowledge of the new 5G generation and the different estimation that can be used in its systems.

Author's papers

## Author's papers

### Publications

- [1] Nessrine Smaili, Mustapha Djeddou, Arab Azrar :”Pilot contamination mitigation based on antenna subset transmission for mmWave massive MIMO”. International journal of communication system (IJCS), Volume 32, Issue 14, 03 July 2018;e3768. <https://doi.org/10.1002/dac.3768>.
- [2] N.Smaili, M.Djeddou, K.Ghanem A.Azrar :”Effect of Oblique Projection Beamforming on the Achievable Rate in Massive MIMO System”. Journal of Communications Technology and Electronics, November 2018, Volume 63, Issue 11, pp 1296–1302.<https://doi.org/10.1134/S1064226918110128>.

### Conference communications

- [1] Nessrine Smaili, Mustapha Djeddou, Arab Azrar :”Beamspace Unitary ESPRIT Parameter Channel Estimation For Pilot Contamination Mitigation”. International Conference on Smart Communications in Network Technologies (SaCoNeT),27-31 October 2018, El Oued, Algeria.
- [2] Nessrine Smaili, Mustapha Djeddou, Arab Azrar :”Residual self-interference cancellation in NOMA-OFDM full duplex massive MIMO”. International Conference on Mathematics and Information Technology (ICMIT), 4-5 December 2017 , El Oued, Algeria.

# Bibliography

- [1] Zhongshan Zhang, Keping Long, Athanasios V Vasilakos, and Lajos Hanzo. Full-duplex wireless communications: Challenges, solutions, and future research directions. 2015.
- [2] Yang Liu, Gaofeng Pan, Hongtao Zhang, and Mei Song. On the capacity comparison between mimo-noma and mimo-oma. *IEEE Access*, 4:2123–2129, 2016.
- [3] Haifan Yin, David Gesbert, Miltiades Filippou, and Yingzhuang Liu. A coordinated approach to channel estimation in large-scale multiple-antenna systems. *IEEE Journal on Selected Areas in Communications*, 31(2):264–273, 2013.
- [4] Jubin Jose, Alexei Ashikhmin, Thomas L Marzetta, and Sriram Vishwanath. Pilot contamination and precoding in multi-cell tdd systems. *IEEE Transactions on Wireless Communications*, 10(8):2640–2651, 2011.
- [5] Moray Rumney et al. *LTE and the evolution to 4G wireless: Design and measurement challenges*. John Wiley & Sons, 2013.
- [6] Henrik Schulze and Christian Lüders. *Theory and applications of OFDM and CDMA: Wideband wireless communications*. John Wiley & Sons, 2005.
- [7] Saddam Hossain. 5g wireless communication systems. *American Journal of Engineering Research (AJER)*, 2(10):344–353, 2013.
- [8] Peter WC Chan, Ernest S Lo, Ray R Wang, Edward KS Au, Vincent KN Lau, Roger S Cheng, Wai Ho Mow, Ross D Murch, and Khaled Ben Letaief. The evolution path of 4g networks: Fdd or tdd? *IEEE Communications Magazine*, 44(12):42–50, 2006.

- [9] Thomas L Marzetta. Noncooperative cellular wireless with unlimited numbers of base station antennas. *IEEE Transactions on Wireless Communications*, 9(11):3590–3600, 2010.
- [10] Balasubramanian Gopalakrishnan and Nihar Jindal. An analysis of pilot contamination on multi-user mimo cellular systems with many antennas. In *Signal Processing Advances in Wireless Communications (SPAWC), 2011 IEEE 12th International Workshop on*, pages 381–385. IEEE, 2011.
- [11] Mamta Agiwal, Abhishek Roy, and Navrati Saxena. Next generation 5g wireless networks: A comprehensive survey. *IEEE Communications Surveys & Tutorials*, 18(3):1617–1655, 2016.
- [12] Thomas L Marzetta, Giuseppe Caire, Merouane Debbah, I Chih-Lin, and Saif K Mohammed. Special issue on massive mimo. *Journal of Communications and Networks*, 15(4):333–337, 2013.
- [13] Federico Boccardi, Robert W Heath, Aurelie Lozano, Thomas L Marzetta, and Petar Popovski. Five disruptive technology directions for 5g. *Communications Magazine, IEEE*, 52(2):74–80, 2014.
- [14] Theodore S Rappaport, Shu Sun, Rimma Mayzus, Hang Zhao, Yaniv Azar, Kangping Wang, George N Wong, Jocelyn K Schulz, Mathew Samimi, and Felix Gutierrez. Millimeter wave mobile communications for 5g cellular: It will work! *Access, IEEE*, 1:335–349, 2013.
- [15] Jeffrey G Andrews, Stefano Buzzi, Wan Choi, Stephen V Hanly, Aurelie Lozano, Anthony CK Soong, and Jianzhong Charlie Zhang. What will 5g be? *Selected Areas in Communications, IEEE Journal on*, 32(6):1065–1082, 2014.
- [16] Emil Björnson, Luca Sanguinetti, Jakob Hoydis, and Mérouane Debbah. Designing multi-user mimo for energy efficiency: When is massive mimo the answer? In *Wireless Communications and Networking Conference (WCNC), 2014 IEEE*, pages 242–247. IEEE, 2014.
- [17] Iyad Lahsen-Cherif. *Spectral and Energy Efficiency in 5G Wireless Networks*. PhD thesis, Université Paris-Saclay, 2016.

- [18] Jian Wang, Aixiang Jin, Dai Shi, Lei Wang, Hui Shen, Dan Wu, Liang Hu, Liang Gu, Lei Lu, Yan Chen, et al. Spectral efficiency improvement with 5g technologies: Results from field tests. *IEEE Journal on Selected Areas in Communications*, 35(8):1867–1875, 2017.
- [19] Thomas L Marzetta. How much training is required for multiuser mimo? In *Signals, Systems and Computers, 2006. ACSSC'06. Fortieth Asilomar Conference on*, pages 359–363. IEEE, 2006.
- [20] Fredrik Rusek, Daniel Persson, Buon Kiong Lau, Erik G Larsson, Thomas L Marzetta, Ove Edfors, and Fredrik Tufvesson. Scaling up mimo: Opportunities and challenges with very large arrays. *Signal Processing Magazine, IEEE*, 30(1):40–60, 2013.
- [21] Erik Larsson, Ove Edfors, Fredrik Tufvesson, and Thomas Marzetta. Massive mimo for next generation wireless systems. *Communications Magazine, IEEE*, 52(2):186–195, 2014.
- [22] Thomas L Marzetta. Massive mimo: An introduction. *Bell Labs Technical Journal*, 20:11–22, 2015.
- [23] Clayton Shepard, Hang Yu, Narendra Anand, Erran Li, Thomas Marzetta, Richard Yang, and Lin Zhong. Argos: Practical many-antenna base stations. In *Proceedings of the 18th annual international conference on Mobile computing and networking*, pages 53–64. ACM, 2012.
- [24] Zhongshan Zhang, Xiyuan Wang, Keping Long, Athanasios V Vasilakos, and Lajos Hanzo. Large-scale mimo-based wireless backhaul in 5g networks. *Wireless Communications, IEEE*, 22(5):58–66, 2015.
- [25] Kemal Davaslioglu and Richard D Gitlin. 5g green networking: Enabling technologies, potentials, and challenges. In *Proceedings of the 17th IEEE International Conference on Annual Wireless and Microwave Technology (WAMICON), Florida, FL, USA*, pages 11–13, 2016.
- [26] Erik G Larsson, Ove Edfors, Fredrik Tufvesson, and Thomas L Marzetta. Massive mimo for next generation wireless systems. *IEEE communications magazine*, 52(2):186–195, 2014.

- [27] Wenjia Liu, Shengqian Han, Chenyang Yang, and Chengjun Sun. Massive mimo or small cell network: Who is more energy efficient? In *Wireless Communications and Networking Conference Workshops (WCNCW), 2013 IEEE*, pages 24–29. IEEE, 2013.
- [28] Ian F Akyildiz, Won-Yeol Lee, Mehmet C Vuran, and Shantidev Mohanty. Next generation/dynamic spectrum access/cognitive radio wireless networks: A survey. *Computer networks*, 50(13):2127–2159, 2006.
- [29] Wenjia Liu, Shengqian Han, Chenyang Yang, and Chengjun Sun. Massive mimo or small cell network: Who is more energy efficient? In *Wireless Communications and Networking Conference Workshops (WCNCW), 2013 IEEE*, pages 24–29. IEEE, 2013.
- [30] Naga Bhushan, Junyi Li, Durga Malladi, Rob Gilmore, Dean Brenner, Aleksandar Damnjanovic, Ravi Sukhavasi, Chirag Patel, and Stefan Geirhofer. Network densification: the dominant theme for wireless evolution into 5g. *IEEE Communications Magazine*, 52(2):82–89, 2014.
- [31] Junyu Liu, Min Sheng, Lei Liu, and Jiandong Li. Network densification in 5g: From the short-range communications perspective. *IEEE Communications Magazine*, 55(12):96–102, 2017.
- [32] Massimo Condoluci, Mischa Dohler, Giuseppe Araniti, Antonella Molinaro, and Kan Zheng. Toward 5g densenets: architectural advances for effective machine-type communications over femtocells. *IEEE Communications Magazine*, 53(1):134–141, 2015.
- [33] Shanzhi Chen, Fei Qin, Bo Hu, Xi Li, and Zhonglin Chen. User-centric ultra-dense networks for 5g: challenges, methodologies, and directions. *IEEE Wireless Communications*, 23(2):78–85, 2016.
- [34] Xiaolin Hou, Xin Wang, Huiling Jiang, and Hidetoshi Kayama. Investigation of massive mimo in dense small cell deployment for 5g. In *Vehicular Technology Conference (VTC-Fall), 2016 IEEE 84th*, pages 1–6. IEEE, 2016.
- [35] S Sasipriya and R Vigneshram. An overview of cognitive radio in 5g wireless communications. In *Computational Intelligence and Computing Research (ICCIC), 2016 IEEE International Conference on*, pages 1–5. IEEE, 2016.



- [36] Olayinka Adigun, Mahdi Pirmoradian, and Christos Politis. Cognitive radio for 5g wireless networks. *Fundamentals of 5G Mobile Networks*, pages 149–163, 2015.
- [37] Ming Xiao, Shahid Mumtaz, Yongming Huang, Linglong Dai, Yonghui Li, Michail Matthaiou, George K Karagiannidis, Emil Björnson, Kai Yang, I Chih-Lin, et al. Millimeter wave communications for future mobile networks. *IEEE Journal on Selected Areas in Communications*, 35(9):1909–1935, 2017.
- [38] Jeffrey G Andrews, Stefano Buzzi, Wan Choi, Stephen V Hanly, Angel Lozano, Anthony CK Soong, and Jianzhong Charlie Zhang. What will 5g be? *IEEE Journal on selected areas in communications*, 32(6):1065–1082, 2014.
- [39] Chang-Soon Choi. Rf impairment models for 60ghz-band sys/phy simulation. *IEEE 802.15-06-0477-01-003c*, 2006.
- [40] Zhouyue Pi and Farooq Khan. System design and network architecture for a millimeter-wave mobile broadband (mmb) system. In *Sarnoff Symposium, 2011 34th IEEE*, pages 1–6. IEEE, 2011.
- [41] Sridhar Rajagopal. Beam broadening for phased antenna arrays using multi beam subarrays. In *Communications (ICC), 2012 IEEE International Conference on*, pages 3637–3642. IEEE, 2012.
- [42] Fouad Gholam, Javier Vía, and Ignacio Santamaría. Beamforming design for simplified analog antenna combining architectures. *Vehicular Technology, IEEE Transactions on*, 60(5):2373–2378, 2011.
- [43] Wei Xiang, Kan Zheng, and Xuemin Sherman Shen. *5G mobile communications*. Springer, 2016.
- [44] Akhil Gupta and Rakesh Kumar Jha. A survey of 5g network: Architecture and emerging technologies. *IEEE access*, 3:1206–1232, 2015.
- [45] Ertugrul Basar. Index modulation techniques for 5g wireless networks. *IEEE Communications Magazine*, 54(7):168–175, 2016.
- [46] Gerhard Wunder, Peter Jung, Martin Kasparick, Thorsten Wild, Frank Schaich, Yejian Chen, Stephen Brink, Ivan Gaspar, Nicola Michailow, Andreas Festag, et al.

- 5gnow: non orthogonal, asynchronous waveforms for future mobile applications. *Communications Magazine, IEEE*, 52(2):97–105, 2014.
- [47] Nicola Michailow, Ivan Gaspar, Stefan Krone, Michael Lentmaier, and Gerhard Fettweis. Generalized frequency division multiplexing: Analysis of an alternative multi carrier technique for next generation cellular systems. In *Wireless Communication Systems (ISWCS), 2012 International Symposium on*, pages 171–175. IEEE, 2012.
- [48] Mamta Agiwal, Abhishek Roy, and Navrati Saxena. Next generation 5g wireless networks: A comprehensive survey.
- [49] F O’Hara and G Moore. A high performance cw receiver using feedthru nulling. *Microwave Journal*, 6(9):63–71, 1963.
- [50] Taneli Riihonen, Stefan Werner, and Risto Wichman. Mitigation of loopback self-interference in full-duplex mimo relays. *IEEE Transactions on Signal Processing*, 59(12):5983–5993, 2011.
- [51] Mayank Jain, Jung Il Choi, Taemin Kim, Dinesh Bharadia, Siddharth Seth, Kannan Srinivasan, Philip Levis, Sachin Katti, and Prasun Sinha. Practical, real-time, full duplex wireless. In *Proceedings of the 17th annual international conference on Mobile computing and networking*, pages 301–312. ACM, 2011.
- [52] Ehsan Aryafar, Mohammad Amir Khojastepour, Karthikeyan Sundaresan, Sampath Rangarajan, and Mung Chiang. Midu: Enabling mimo full duplex. In *Proceedings of the 18th annual international conference on Mobile computing and networking*, pages 257–268. ACM, 2012.
- [53] Melissa Duarte, Ashutosh Sabharwal, Vaneet Aggarwal, Rittwik Jana, KK Ramakrishnan, Christopher W Rice, and NK Shankaranarayanan. Design and characterization of a full-duplex multiantenna system for wifi networks. *IEEE Transactions on Vehicular Technology*, 63(3):1160–1177, 2014.
- [54] Dan Nguyen, Le-Nam Tran, Pekka Pirinen, and Matti Latva-aho. Precoding for full duplex multiuser mimo systems: Spectral and energy efficiency maximization. *IEEE Transactions on Signal Processing*, 61(16):4038–4050, 2013.

- [55] Dan Nguyen, Le-Nam Tran, Pekka Pirinen, and Matti Latva-aho. On the spectral efficiency of full-duplex small cell wireless systems. *IEEE Transactions on wireless communications*, 13(9):4896–4910, 2014.
- [56] Dongkyu Kim, Hyungsik Ju, Sungsoo Park, and Daesik Hong. Effects of channel estimation error on full-duplex two-way networks. *IEEE Transactions on Vehicular Technology*, 62(9):4666–4672, 2013.
- [57] Elsayed Ahmed and Ahmed M Eltawil. All-digital self-interference cancellation technique for full-duplex systems. *IEEE Transactions on Wireless Communications*, 14(7):3519–3532, 2015.
- [58] Taneli Riihonen, Stefan Werner, and Risto Wichman. Residual self-interference in full-duplex mimo relays after null-space projection and cancellation. In *Signals, Systems and Computers (ASILOMAR), 2010 Conference Record of the Forty Fourth Asilomar Conference on*, pages 653–657. IEEE, 2010.
- [59] Leonardo Jiménez Rodríguez, Nghi H Tran, and Tho Le-Ngoc. Performance of full-duplex af relaying in the presence of residual self-interference. *IEEE Journal on Selected Areas in Communications*, 32(9):1752–1764, 2014.
- [60] Tae Min Kim and Arogyaswami Paulraj. Outage probability of amplify-and-forward cooperation with full duplex relay. In *Wireless Communications and Networking Conference (WCNC), 2012 IEEE*, pages 75–79. IEEE, 2012.
- [61] Brian P Day, Adam R Margetts, Daniel W Bliss, and Philip Schniter. Full-duplex bidirectional mimo: Achievable rates under limited dynamic range. *IEEE Transactions on Signal Processing*, 60(7):3702–3713, 2012.
- [62] Adel Belouchrani, Karim Abed-Meraim, J-F Cardoso, and Eric Moulines. A blind source separation technique using second-order statistics. *IEEE Transactions on signal processing*, 45(2):434–444, 1997.
- [63] Daniel C Araújo, Taras Maksymyuk, André LF de Almeida, Tarcisio Maciel, João CM Mota, and Minho Jo. Massive mimo: survey and future research topics. *Iet Communications*, 10(15):1938–1946, 2016.

- [64] Raziieh Razavi, Reza Hoshyar, Muhammad Ali Imran, and Yi Wang. Information theoretic analysis of lds scheme. *IEEE Communications Letters*, 15(8):798–800, 2011.
- [65] Mohammed Al-Imari, Pei Xiao, Muhammad Ali Imran, and Rahim Tafazolli. Uplink non-orthogonal multiple access for 5g wireless networks. In *Wireless Communications Systems (ISWCS), 2014 11th International Symposium on*, pages 781–785. IEEE, 2014.
- [66] Hosein Nikopour and Hadi Baligh. Sparse code multiple access. In *Personal Indoor and Mobile Radio Communications (PIMRC), 2013 IEEE 24th International Symposium on*, pages 332–336. IEEE, 2013.
- [67] Kelvin Au, Liqing Zhang, Hosein Nikopour, Eric Yi, Alireza Bayesteh, Usa Vilaipornsawai, Jianglei Ma, and Peiying Zhu. Uplink contention based scma for 5g radio access. In *2014 IEEE Globecom Workshops (GC Wkshps)*, pages 900–905. IEEE, 2014.
- [68] Linglong Dai, Bichai Wang, Yifei Yuan, Shuangfeng Han, I Chih-Lin, and Zhaocheng Wang. Non-orthogonal multiple access for 5g: solutions, challenges, opportunities, and future research trends. *IEEE Communications Magazine*, 53(9):74–81, 2015.
- [69] Xiaoming Dai, Shanzhi Chen, Shaohui Sun, Shaoli Kang, Yinmin Wang, Zukang Shen, and Jin Xu. Successive interference cancelation amenable multiple access (sama) for future wireless communications. In *Communication Systems (ICCS), 2014 IEEE International Conference on*, pages 222–226. IEEE, 2014.
- [70] Jiankang Zhang, Sheng Chen, Xiaomin Mu, and Lajos Hanzo. Evolutionary-algorithm-assisted joint channel estimation and turbo multiuser detection/decoding for ofdm/sdma. *IEEE Trans. Vehicular Technology*, 63(3):1204–1222, 2014.
- [71] I Chih-Lin, Shuangfeng Han, Zhikun Xu, Qi Sun, and Zhengang Pan. 5g: rethink mobile communications for 2020+. *Phil. Trans. R. Soc. A*, 374(2062):20140432, 2016.
- [72] Jiachen Huang, Kewu Peng, Changyong Pan, Fang Yang, and Huangping Jin. Scalable video broadcasting using bit division multiplexing. *IEEE Transactions on Broadcasting*, 60(4):701–706, 2014.

- [73] Kenichi Higuchi and Anass Benjebbour. Non-orthogonal multiple access (noma) with successive interference cancellation for future radio access. *IEICE Transactions on Communications*, 98(3):403–414, 2015.
- [74] SM Riazul Islam, Nurilla Avazov, Octavia A Dobre, and Kyung-Sup Kwak. Power-domain non-orthogonal multiple access (noma) in 5g systems: Potentials and challenges. *IEEE Communications Surveys & Tutorials*, 19(2):721–742, 2017.
- [75] Zhiqiang Wei, Jinhong Yuan, Derrick Wing Kwan Ng, Maged ElKashlan, and Zhiguo Ding. A survey of downlink non-orthogonal multiple access for 5g wireless communication networks. *arXiv preprint arXiv:1609.01856*, 2016.
- [76] Shipon Ali, Ekram Hossain, and Dong In Kim. Non-orthogonal multiple access (noma) for downlink multiuser mimo systems: User clustering, beamforming, and power allocation. *IEEE Access*, 5:565–577, 2017.
- [77] Yunlong Cai, Zhijin Qin, Fangyu Cui, Geoffrey Ye Li, and Julie A McCann. Modulation and multiple access for 5g networks. *IEEE Communications Surveys & Tutorials*, 20(1):629–646, 2018.
- [78] Linglong Dai, Bichai Wang, Yifei Yuan, Shuangfeng Han, I Chih-Lin, and Zhaocheng Wang. Non-orthogonal multiple access for 5g: solutions, challenges, opportunities, and future research trends. *IEEE Communications Magazine*, 53(9):74–81, 2015.
- [79] Li Ping, Lihai Liu, Keying Wu, and Wai Kong Leung. Interleave division multiple-access. *IEEE transactions on wireless communications*, 5(4):938–947, 2006.
- [80] Li Ping, Qinghua Guo, and Jun Tong. The ofdm-idma approach to wireless communication systems. *IEEE Wireless Communications*, 14(3), 2007.
- [81] Bei Yin, Michael Wu, Christoph Studer, Joseph R Cavallaro, and Jorma Lilleberg. Full-duplex in large-scale wireless systems. In *2013 Asilomar Conference on Signals, Systems and Computers*, pages 1623–1627. IEEE, 2013.
- [82] Arman Shojaeifard, Kai-Kit Wong, Marco Di Renzo, Gan Zheng, Khairi Ashour Hamdi, and Jie Tang. Self-interference in full-duplex multi-user mimo channels. *arXiv preprint arXiv:1701.00277*, 2017.

- [83] Andrew LC Hui and K Ben Letaief. Successive interference cancellation for multiuser asynchronous ds/cdma detectors in multipath fading links. *IEEE Transactions on Communications*, 46(3):384–391, 1998.
- [84] Sang Wu Kim. Log-likelihood ratio based detection ordering for the v-blast. In *Global Telecommunications Conference, 2003. GLOBECOM'03. IEEE*, volume 1, pages 292–296. IEEE, 2003.
- [85] Nessrine Smaili, Khalida Ghanem, and Mustapha Djeddou. Performance of lte communication system in correlated rayleigh channel with different antenna configurations. In *Antennas and Propagation & USNC/URSI National Radio Science Meeting, 2015 IEEE International Symposium on*, pages 306–307. IEEE, 2015.
- [86] Rodrigo C de Lamare, Raimundo Sampaio-Neto, and Are Hjorungnes. Joint iterative interference cancellation and parameter estimation for cdma systems. *Communications Letters, IEEE*, 11(12):916–918, 2007.
- [87] Rohit et Gore Dhananjay Paulraj, Arogyaswami et Nabar. *Introduction à la communication sans fil espace-temps*.
- [88] Peter W Wolniansky, Gerard J Foschini, GD Golden, and R Valenzuela. V-blast: An architecture for realizing very high data rates over the rich-scattering wireless channel. In *Signals, Systems, and Electronics, 1998. ISSSE 98. 1998 URSI International Symposium on*, pages 295–300. IEEE, 1998.
- [89] Dirk Wubben, Ronald Bohnke, Volker Kuhn, and K-D Kammeyer. Mmse extension of v-blast based on sorted qr decomposition. In *Vehicular technology conference, 2003. VTC 2003-Fall. 2003 IEEE 58th*, volume 1, pages 508–512. IEEE, 2003.
- [90] D Wübben, J Rinas, R Böhnke, V Kühn, and KD Kammeyer. Efficient algorithm for detecting layered space-time codes. In *Proceedings of the 4th International ITG Conference on Source and Channel Coding (SCC)*, pages 1–7, 2002.
- [91] Jean-Francois Cardoso and Antoine Souloumiac. Jacobi angles for simultaneous diagonalization. *SIAM journal on matrix analysis and applications*, 17(1):161–164, 1996.

- [92] Jakob Hoydis, Stephan Ten Brink, and Mérouane Debbah. Massive mimo: How many antennas do we need? In *Communication, Control, and Computing (Allerton), 2011 49th Annual Allerton Conference on*, pages 545–550. IEEE, 2011.
- [93] Mamta Agiwal, Abhishek Roy, and Navrati Saxena. Next generation 5g wireless networks: A comprehensive survey. *IEEE Communications Surveys & Tutorials*, 18(3):1617–1655, 2016.
- [94] Hong Yang and Thomas L Marzetta. Performance of conjugate and zero-forcing beamforming in large-scale antenna systems. *IEEE Journal on Selected Areas in Communications*, 31(2):172–179, 2013.
- [95] Selahattin Kayalar and Howard L Weinert. Oblique projections: Formulas, algorithms, and error bounds. *Mathematics of Control, Signals and Systems*, 2(1):33–45, 1989.
- [96] Richard T Behrens and Louis L Scharf. Signal processing applications of oblique projection operators. *Signal Processing, IEEE Transactions on*, 42(6):1413–1424, 1994.
- [97] Piet Vandaele and Marc Moonen. Two deterministic blind channel estimation algorithms based on oblique projections. *Signal processing*, 80(3):481–495, 2000.
- [98] Xiang Yu and Lang Tong. Joint channel and symbol estimation by oblique projections. *Signal Processing, IEEE Transactions on*, 49(12):3074–3083, 2001.
- [99] KA Meraim, Henri Maitre, Pierre Duhamel, et al. Blind multichannel image restoration using oblique projections. In *Sensor Array and Multichannel Signal Processing Workshop Proceedings, 2002*, pages 125–129. IEEE, 2002.
- [100] Per Christian Hansen and Søren Holdt Jensen. Prewhitening for rank-deficient noise in subspace methods for noise reduction. *Signal Processing, IEEE Transactions on*, 53(10):3718–3726, 2005.
- [101] Rémy Boyer and Guillaume Bouleux. Oblique projections for direction-of-arrival estimation with prior knowledge. *Signal Processing, IEEE Transactions on*, 56(4):1374–1387, 2008.

- [102] Hien Quoc Ngo, Erik G Larsson, and Thomas L Marzetta. Aspects of favorable propagation in massive mimo. In *Signal Processing Conference (EUSIPCO), 2014 Proceedings of the 22nd European*, pages 76–80. IEEE, 2014.
- [103] David Gesbert, Stephen Hanly, Howard Huang, Shlomo Shamai Shitz, Osvaldo Simeone, and Wei Yu. Multi-cell mimo cooperative networks: A new look at interference. *IEEE Journal on Selected Areas in Communications*, 28(9):1380–1408, 2010.
- [104] Hayssam Dahrouj and Wei Yu. Coordinated beamforming for the multicell multi-antenna wireless system. *IEEE transactions on wireless communications*, 9(5), 2010.
- [105] Luca Venturino, Narayan Prasad, and Xiaodong Wang. Coordinated linear beamforming in downlink multi-cell wireless networks. *IEEE Transactions on Wireless Communications*, 9(4), 2010.
- [106] David Gesbert, Saad Ghazanfar Kiani, Anders Gjendemsjo, and Geir Egil Oien. Adaptation, coordination, and distributed resource allocation in interference-limited wireless networks. *Proceedings of the IEEE*, 95(12):2393–2409, 2007.
- [107] Louis L Scharf and Michael L McCloud. Blind adaptation of zero forcing projections and oblique pseudo-inverses for subspace detection and estimation when interference dominates noise. *Signal Processing, IEEE Transactions on*, 50(12):2938–2946, 2002.
- [108] Tapan Bhandari, Sachin Nagarajan, et al. Oblique projection based equalization for ofdm in presence of in-device coexistence interference. In *Emerging Trends in Communication, Control, Signal Processing & Computing Applications (C2SPCA), 2013 International Conference on*, pages 1–5. IEEE, 2013.
- [109] Chun-Hsien Wu and Shiunn-Jang Chern. Minimum ber block-based precoder design for zero-forcing equalization: An oblique projection framework. *Signal Processing, IEEE Transactions on*, 55(12):5630–5642, 2007.
- [110] Emil Bjornson, Mats Bengtsson, and Björn Ottersten. Optimal multiuser transmit beamforming: A difficult problem with a simple solution structure [lecture notes]. *Signal Processing Magazine, IEEE*, 31(4):142–148, 2014.
- [111] Jubin Jose, Alexei Ashikhmin, Thomas L Marzetta, and Sriram Vishwanath. Pilot contamination problem in multi-cell tdd systems. In *Information Theory, 2009. ISIT 2009. IEEE International Symposium on*, pages 2184–2188. IEEE, 2009.



- [112] Jubin Jose, Alexei Ashikhmin, Thomas L Marzetta, and Sriram Vishwanath. Pilot contamination problem in multi-cell tdd systems. In *Information Theory, 2009. ISIT 2009. IEEE International Symposium on*, pages 2184–2188. IEEE, 2009.
- [113] Honglei Miao, Markku Juntti, and Kegen Yu. 2d-unitary esprit based joint aoa and aod estimation for mimo system. In *Personal, Indoor and Mobile Radio Communications, 2006 IEEE 17th International Symposium on*, pages 1–5. IEEE, 2006.
- [114] Honglei Miao and Markku J Juntti. Space time channel estimation and performance analysis for wireless mimo ofdm systems with spatial correlation. *Vehicular Technology, IEEE Transactions on*, 54(6):2003–2016, 2005.
- [115] Alle Jan Van Der Veen, Michaela C Vanderveen, and Arogyaswami Paulraj. Joint angle and delay estimation using shift invariance techniques. *Signal Processing, IEEE Transactions on*, 46(2):405–418, 1998.
- [116] Tie Jun Shan, Mati Wax, and Thomas Kailath. On spatial smoothing for direction of arrival estimation of coherent signals. *IEEE Transactions on Acoustics, Speech, and Signal Processing*, 33(4):806–811, 1985.
- [117] J.Lacoume I.tas, C.Latombe. Localisation de sources corrélées par traitement d’antenne en utilisant le lissage spatial. 5(5), 1988.
- [118] Ji Li, Jean Conan, and Samuel Pierre. Joint estimation of channel parameters for mimo communication systems. In *Wireless Communication Systems, 2005. 2nd International Symposium on*, pages 22–26. IEEE, 2005.
- [119] Petre Stoica, Andreas Jakobsson, and Jian Li. Cisoid parameter estimation in the colored noise case: asymptotic cramer-rao bound, maximum likelihood, and nonlinear least-squares. *IEEE Transactions on Signal Processing*, 45(8):2048–2059, 1997.
- [120] Petre Stoica and Arye Nehorai. Performance study of conditional and unconditional direction-of-arrival estimation. *IEEE Transactions on Acoustics, Speech, and Signal Processing*, 38(10):1783–1795, 1990.
- [121] Bin Li, Jia Hou, Xiaofan Li, Yijiang Nan, Arumugam Nallanathan, and Chenglin Zhao. Deep sensing for space-time doubly selective channels: when a primary user is mobile and the channel is flat rayleigh fading. *IEEE Transactions on Signal Processing*, 64(13):3362–3375, 2016.

- [122] Petre Stoica and Arye Nehorai. Music, maximum likelihood and cramer-rao bound. In *ICASSP-88., International Conference on Acoustics, Speech, and Signal Processing*, pages 2296–2299. IEEE, 1988.
- [123] Eakkamol Pakdeejit. Linear precoding performance of massive mu-mimo downlink system. 2013.
- [124] Thomas L Marzetta. Noncooperative cellular wireless with unlimited numbers of base station antennas. *Wireless Communications, IEEE Transactions on*, 9(11):3590–3600, 2010.
- [125] Hien Quoc Ngo, Erik G Larsson, and Thomas L Marzetta. Energy and spectral efficiency of very large multiuser mimo systems. *IEEE Transactions on Communications*, 61(4):1436–1449, 2013.
- [126] Balasubramanian Gopalakrishnan and Nihar Jindal. An analysis of pilot contamination on multi-user mimo cellular systems with many antennas. In *Signal Processing Advances in Wireless Communications (SPAWC), 2011 IEEE 12th International Workshop on*, pages 381–385. IEEE, 2011.
- [127] YD Guo, Yu Shrike Zhang, and NN Tong. Beamspace esprit algorithm for bistatic mimo radar. *Electronics letters*, 47(15):876–878, 2011.
- [128] Dang Xiaofang, Chen Baixiao, Yang Minglei, and Zheng Guimei. Beamspace unitary esprit algorithm for angle estimation in bistatic mimo radar. *International Journal of Antennas and Propagation*, 2015, 2015.
- [129] Dang Xiaofang, Chen Baixiao, Yang Minglei, and Zheng Guimei. Beamspace unitary esprit algorithm for angle estimation in bistatic mimo radar. *International Journal of Antennas and Propagation*, 2015, 2015.
- [130] Michael D Zoltowski, Martin Haardt, and Cherian P Mathews. Closed-form 2d angle estimation with rectangular arrays in element space or beamspace via unitary esprit. *Signal Processing, IEEE Transactions on*, 44(2):316–328, 1996.
- [131] R. H. Roy III G. Xu and T. Kailath. Detection of number of sources via exploitation of centro-symmetry property. *International Journal of Antennas and Propagation*, 42(1):102–112, 1994.

- [132] Shuangfeng Han, I Chih-Lin, Zhikun Xu, and Corbett Rowell. Large-scale antenna systems with hybrid analog and digital beamforming for millimeter wave 5g. *IEEE Communications Magazine*, 53(1):186–194, 2015.
- [133] Ahmed Alkhateeb, Omar El Ayach, Geert Leus, and Robert W Heath. Channel estimation and hybrid precoding for millimeter wave cellular systems. *IEEE Journal of Selected Topics in Signal Processing*, 8(5):831–846, 2014.
- [134] Zhouyue Pi and Farooq Khan. An introduction to millimeter wave mobile broadband systems. *Communications Magazine, IEEE*, 49(6):101–107, 2011.
- [135] Theodore S Rappaport, Shu Sun, Rimma Mayzus, Hang Zhao, Yaniv Azar, Kangping Wang, George N Wong, Jocelyn K Schulz, Mathew Samimi, and Felix Gutierrez. Millimeter wave mobile communications for 5g cellular: It will work! *Access, IEEE*, 1:335–349, 2013.
- [136] Abbas Abbaspour Tamijani and Kamal Sarabandi. An affordable millimeter wave beam steerable antenna using interleaved planar subarrays. *Antennas and Propagation, IEEE Transactions on*, 51(9):2193–2202, 2003.
- [137] Behzad Biglarbegan, Mohammad Fakharzadeh, Dan Busuioc, Mohammad Reza Nezhad-Ahmadi, and Safieddin Safavi Naeini. Optimized microstrip antenna arrays for emerging millimeter ave wireless applications. *Antennas and Propagation, IEEE Transactions on*, 59(5):1742–1747, 2011.
- [138] Junyi Wang, Zhou Lan, Chang Woo Pyo, Tuncer Baykas, Chin Sean Sum, Md Arifur Rahman, Jing Gao, Riku Funada, Fumihide Kojima, Hiroshi Harada, et al. Beam codebook based beamforming protocol for multi gbps millimeter-wave wpan systems. *Selected Areas in Communications, IEEE Journal on*, 27(8):1390–1399, 2009.
- [139] Y Ming Tsang, Ada SY Poon, and Sateesh Addepalli. Coding the beams: Improving beamforming training in mmwave communication system. In *Global Telecommunications Conference (GLOBECOM 2011), 2011 IEEE*, pages 1–6. IEEE, 2011.
- [140] Sooyoung Hur, Taejoon Kim, David J Love, James V Krogmeier, Timothy A Thomas, and Amitava Ghosh. Millimeter wave beamforming for wireless back-

- haul and access in small cell networks. *Communications, IEEE Transactions on*, 61(10):4391–4403, 2013.
- [141] Xinying Zhang, Andreas F Molisch, and Sun Yuan Kung. Variable phase shift based rf baseband codesign for mimo antenna selection. *Signal Processing, IEEE Transactions on*, 53(11):4091–4103, 2005.
- [142] Omar El Ayach, Sridhar Rajagopal, Shadi Abu Surra, Zhouyue Pi, and Robert W Heath. Spatially sparse precoding in millimeter wave mimo systems. *Wireless Communications, IEEE Transactions on*, 13(3):1499–1513, 2014.
- [143] Vijay Venkateswaran and Alle Jan Van der Veen. Analog beamforming in mimo communications with phase shift networks and online channel estimation. *Signal Processing, IEEE Transactions on*, 58(8):4131–4143, 2010.
- [144] Ahmed Alkhateeb, Omar El Ayach, Geert Leus, and Robert W Heath. Hybrid precoding for millimeter wave cellular systems with partial channel knowledge. In *Information Theory and Applications Workshop (ITA), 2013*, pages 1–5. IEEE, 2013.
- [145] Ahmed Alkhateeb, Omar El Ayach, Geert Leus, and Robert W Heath. Channel estimation and hybrid precoding for millimeter wave cellular systems. *Selected Topics in Signal Processing, IEEE Journal of*, 8(5):831–846, 2014.
- [146] Jakob Hoydis, Stephan Ten Brink, and Mérouane Debbah. Massive mimo: How many antennas do we need? In *Communication, Control, and Computing (Allerton), 2011 49th Annual Allerton Conference on*, pages 545–550. IEEE, 2011.
- [147] Olakunle Elijah, Chee Yen Leow, Tharek Abdul Rahman, Solomon Nunoo, and Solomon Zakwoi Iliya. A comprehensive survey of pilot contamination in massive mimo—5g system. *IEEE Communications Surveys & Tutorials*, 18(2):905–923, 2016.
- [148] Jiankang Zhang, Bo Zhang, Sheng Chen, Xiaomin Mu, Mohammed El-Hajjar, and Lajos Hanzo. Pilot contamination elimination for large-scale multiple-antenna aided ofdm systems. *IEEE Journal of Selected Topics in Signal Processing*, 8(5):759–772, 2014.

- [149] Guangxu Zhu, Kaibin Huang, Vincent KN Lau, Bin Xia, Xiaofan Li, and Sha Zhang. Hybrid beamforming via the kronecker decomposition for the millimeter-wave massive mimo systems. *arXiv preprint arXiv:1704.03611*, 2017.
- [150] Rubayet Shafin and Lingjia Liu. Doa estimation and performance analysis for multi-cell multi-user 3d mmwave massive-mimo ofdm system. In *Wireless Communications and Networking Conference (WCNC), 2017 IEEE*, pages 1–6. IEEE, 2017.
- [151] Syed Ahsan Raza Naqvi, Syed Ali Hassan, and Zaka ul Mulk. Pilot reuse and sum rate analysis of mmwave and uhf-based massive mimo systems. In *Vehicular Technology Conference (VTC Spring), 2016 IEEE 83rd*, pages 1–5. IEEE, 2016.
- [152] A Lee Swindlehurst, Ender Ayanoglu, Payam Heydari, and Filippo Capolino. Millimeter-wave massive mimo: The next wireless revolution? *IEEE Communications Magazine*, 52(9):56–62, 2014.
- [153] Shu Sun, Theodore S Rappaport, Robert W Heath, Andrew Nix, and Sundeep Rangan. Mimo for millimeter-wave wireless communications: beamforming, spatial multiplexing, or both? *IEEE Communications Magazine*, 52(12):110–121, 2014.
- [154] Mandar N Kulkarni, Amitava Ghosh, and Jeffrey G Andrews. A comparison of mimo techniques in downlink millimeter wave cellular networks with hybrid beamforming. *IEEE Transactions on Communications*, 64(5):1952–1967, 2016.
- [155] Nachiappan Valliappan, Angel Lozano, and Robert W Heath. Antenna subset modulation for secure millimeter-wave wireless communication. *IEEE Transactions on Communications*, 61(8):3231–3245, 2013.
- [156] Flavio Maschietti, David Gesbert, Paul de Kerret, and Henk Wymeersch. Robust location-aided beam alignment in millimeter wave massive mimo. *arXiv preprint arXiv:1705.01002*, 2017.
- [157] Morteza Hashemi, Ashu Sabharwal, C Emre Koksall, and Ness B Shroff. Efficient beam alignment in millimeter wave systems using contextual bandits. *arXiv preprint arXiv:1712.00702*, 2017.
- [158] Joseph L Walsh. A closed set of normal orthogonal functions. *American Journal of Mathematics*, 45(1):5–24, 1923.

- [159] Andrea Goldsmith, Syed Ali Jafar, Nihar Jindal, and Sriram Vishwanath. Capacity limits of mimo channels. *IEEE Journal on selected areas in Communications*, 21(5):684–702, 2003.
- [160] Jose Pablo Gonzalez-Coma, Javier Rodriguez-Fernandez, Nuria Gonzalez-Prelcic, Luis Castedo, and Robert W Heath. Channel estimation and hybrid precoding for frequency selective multiuser mmwave mimo systems. *IEEE Journal of Selected Topics in Signal Processing*, 2018.
- [161] Shiwen He, Jiaheng Wang, Yongming Huang, Björn Ottersten, and Wei Hong. Codebook-based hybrid precoding for millimeter wave multiuser systems. *IEEE Transactions on Signal Processing*, 65(20):5289–5304, 2017.